JCEEA

Czasopismo Inżynierii Lądowej, Środowiska i Architektury

Journal of Civil Engineering, Environment and Architecture

Kwartalnik
tom XXXV
zeszyt 65 (nr 3/2018)
lipiec-wrzesień

(e-ISSN 2300-8903)

Czasopismo Inżynierii Lądowej, Środowiska i Architektury jest kontynuacją
Zeszytów Naukowych Politechniki Rzeszowskiej - Budownictwo i Inżynieria Środowiska.

Issued with the consent of the Rector

Editor in Chief Publishing House of Rzeszow University of Technology
Professor Grzegorz OSTASZ, DSc, PhD

e-ISSN 2300-8903
p-ISSN 2300-5130

The electronic version of the Journal is an original version.

Editorial Office: Rzeszow University of Technology, Faculty of Civil and Environmental Engineering and Architecture, St. Poznańska, 35-084 Rzeszów, Poland, www.oficyna.prz.edu.pl//pl/zeszyty-naukowe/czasopismo-inzynierii-ladowej-s/ (e-mail: jceea_bud@prz.edu.pl)

Publisher: Publishing House of Rzeszow University of Technology, 12 Powstanców Warszawy Ave., 35-959 Rzeszow, www.oficyna.prz.edu.pl (e-mail: oficyna@prz.edu.pl)

Additional information and an imprint – p. 135

Table of Contents

CZASOPISMO INŻYNIERII LĄDOWEJ, ŚRODOWISKA I ARCHITEKTURY
JOURNAL OF CIVIL ENGINEERING, ENVIRONMENT AND ARCHITECTURE
JCEEA, t. XXXV, z. 65 (3/18), lipiec-wrzesień 2018, s. 5-24, DOI:10.7862/rb.2018.38

Roman KADAJ[1]

TRANSFORMATIONS BETWEEN THE HEIGHT REFERENCE FRAMES: Kronsztadt'60, PL-KRON86-NH, PL-EVRF2007-NH

The State Spatial Reference System in Poland currently includes two height reference frames: the first, PL-KRON86-NH, with the old name Kronsztadt'86, and the second, called PL-EVRF2007-NH, as a Polish implementation of the European Vertical Reference Frame (EVRF), named also NAP (Normal Amsterdams Peil). Kronsztadt'86 was supposed to replace the earlier reference system called Kronsztadt'60, but the intentions were not fully in line with reality. Kronsztadt'60 has been implemented in all geodetic and cartographic elaborations even before the computer era and will probably exist until the use of analogue maps or their duplicates in the form of raster maps. For practical purposes, transformation formulas have been developed between all three reference frames mentioned in the title of work. For this purpose, about 16,000 points of the base height network in the PL-EVRF2007-NH and PL-KRON86-NH were used and more than 7,000 points in the Kronsztadt'60. Transformational formulas were developed in two variants: in the form of polynomials approximated by the least squares method and in the form of an interpolative grid. Basic empirical relationships were implemented among others in the program TRANSPOL v. 2.06 [8], elaborated according to the assumptions of the Head Office of Geodesy and Cartography.

Keywords: height transformations, reference frames, Kronsztadt'60, Kronsztadt'86, Kronsztadt'2006, PL-KRON86-NH, PL-EVRF2007-NH

1. Historical review of Polish height reference frames and general relations between them

In the time of the Second Polish Republic, a uniform height reference frame was created, using the heights data inherited from the partitioning countries. These data referred to the average levels of the three seas: the North Sea with the mareograph in Amsterdam (the Netherlands), the Baltic Sea with the mareograph in Kronstadt (Russia) (see eg. [12]), and the Adriatic Sea with the mareograph in Trieste. Finally, after the creation of a uniform leveling network in the 1930s (Fig.1), the "Amsterdam" reference system was adopted, also known as the NAP (Normal Amsterdams Peil). A fixed point in the network was a benchmark at the town hall in Toruń, which was previously associated with the NAP system.

[1] Roman Kadaj, Rzeszow University of Technology, Department of Geodesy and Geotechnics, 35-959 Rzeszów, ul. Poznańska 2, kadaj@prz.edu.pl

Fig. 1. Sketch of the basic height network during the times of the Second Polish Republic. According to the then naming, the network consisted of lines I and II order. Traverses closed numbered with Roman numerals. The age points (in the legend named as "basic") and a mareograph in Gdynia are marked by big circles. Source: Archive WIG [25]

After the World War II, as part of the post-war measurement campaign of 1946–1955, the first class height networks were established in the areas recovered. The new areas were the Western Lands and the Northern Lands, which were part of the area of former East Prussia. In 1951 these networks were calculated in reference to the existing height network in the area of the Second Polish Republic,

that is in the "Amsterdam" (NAP) system. After only two years (1953–1955) was designed and a uniform height network was established, linking with the basic heights network of neighboring countries. The average level of the Baltic Sea, measured by a mareograph in the town of Kronstadt in the Gulf of Finland (now the Russian Federation) was used as the reference level. The new heights reference frame in Poland was called the "Kronsztadt" (as the Polonized name of the town). The whole measurement-computation operation in the years (1946–1955) is called the second measurement campaign of the national height network. In the new system, the height ordinate of the benchmark on the town hall in Toruń was also designated. The difference in the heights between the "Amsterdam" and "Kronsztadt" reference frames for the benchmark in Toruń was 84 mm.

The "Kronsztadt" reference frame was introduced throughout the entire territory of Poland as the obligatory height system. The heights in this reference frame appeared in all classic (paper) cartographic elaborations, including the engineering maps and in the information bases of geodetic points. In later years, to distinguish it from other definitions, this reference frame adopted the name "Kronsztadt'60" (probably marking the epoch of its implementation).

In the years (1974–1982), another third measurement campaign was designed and implemented. After about 20 years, it was found that a significant part of the benchmarks was destroyed or not found, so the necessary supplements and modernization of its structure were carried out in the network. Connections to neighboring countries' networks have been taken into account again. The adjustment and computing of the I class network was done using the NOVA 840 digital machine. As a result, the new heights of all benchmark were obtained. This was the basis for establishing a new height system in Poland, which was called "Kronsztadt'86" (see eg: [1], [16], [17], [18]). Comparing the heights of 7679 benchmarks (surviving common points in the networks of the second and third measurement campaigns), the average difference was 48 mm ($H_{Kronsztadt'60} - H_{Kronsztadt'86}$) with a spread in the range from -10 mm to +139 mm. Wyrzykowski in [17] interprets this effect as a result of vertical movements of the Earth's crust at 1.8 mm / year. Such a conclusion would be justified, provided that the same reference level adopted in both campaigns was independent of the vertical movements of the earth's crust in the studied area of Poland (analogously to the local tasks of displacement analysis, where a stable reference system is required). It is difficult to say how the above condition was realized, for example by referring to the average level of the Baltic Sea indicated by mareograph, or by uniform alignment of the main polygons of the former Eastern bloc countries network, in reference to the mereograph in Kronsztadt. The effect analyzed by Wyrzykowski may also have been partly a result of erroneous measurement and calculation processes, including reduction of observations, and changes in the geometric structure of the network. It seems, however, that inference about the vertical movements of the Earth's crust on the territory of Poland, based on the results of all measurement campaigns, despite

many efforts to obtain archival materials (see: [11]), will not be fully possible due to failure to comply particular condition, maintaining a common and stable frame of reference. If it were only for local displacements, for example in the area of the Upper Silesian Industrial District, a sufficiently stable frame of reference can create external points of this area, especially points with observation of mutual constancy confirmed.

The new height reference frame (Kronsztadt'86) was used only in geodetic elaborations of the post-analogue (computer) era, while height data related to classic (paper) geodetic elaborations remained unchanged in the Kronsztadt'60. Currently we have already the basic economic maps made as vector maps in all major cities and industrial areas. Such maps can be easily updated or transformed in computer technology. This applies in particular to the height reference system.

In the years 1999–2002, IV measurement campaign of the basic height network was carried out. In the calculations of this network (see [4]) it was assumed that the average height in the set of 15 age points (Fig. 2) in relation to the previous measurement campaign should not change. The author of the calculations (Gajderowicz) first made the observational adjustment of the network, based on a single point of Warsaw-Wola, and then corrected all ordinates by a fixed value so that the above condition for 15 age points was met (see Fig. 2). It can be said that the described approach does not allow to identify the vertical displacement of the Earth's crust between Campaigns II and III, because the reference level "flows" along with the network. As a result of

Fig. 2. Sketch of the I class leveling network in the IV campaign (1999–2002), with 15 age points (appointed with black quadrate) and 64 points of the Polish part of EUVN network , appointed on red (information sources: [4], [8], [10], [22])

leveling the first class network, a new reference frame was created, which called "Kronsztadt'2006". This reference frame, although internally well proven in terms of observational reducing and close network adjustment with accuracy characteristics, was not formally adopted for practical applications. The reasons, it seems, were simple. First, geodetic practice, does not tolerate too frequent changes of spatial reference systems, because it always entails significant costs and introduces, at least in transition periods, a certain disorder. The second reason was that in the near future a return to a uniform, European, height system was planned with reference to the average level of the North Sea with a mareograph in Amsterdam.

Comparing the point heights between Campaign III and IV for 16,222 points of the basic height network, we get an average difference of 5 mm (see Fig. 3), with a distribution from -27 to + 42 mm. The reference frame Kronsztad'2006 was used only as an auxiliary (indirect) object in the conversion between various height reference frames ([8], [9], [10]). In addition, the data in Kronsztad'2006 were used to determine the heights in the new PL-EVRF2007-NH reference frame, which is the Polish implementation of the European height reference frame EVRF2007, related to the average sea level measured on the Amsterdam maretograph (NAP – Normal Amsterdam Peil). According to the information received from the Central Geodetic and Cartographic Documentation Center, the results obtained from the fourth measurement campaign were also used for local updates of heights in the reference frame Kronsztad'86, which after this modification adopted the name PL-KRON86-NH. In the last years in Poland another measurement and calculation campaign of the basic height network was carried out, but the results of studies are not ready for use yet [23].

The issues of height reference frames, as elements of the spatial reference system in Poland, are regulated by the Regulation of the Council of Ministers (see [20], [21]). In the light of this regulation, there are currently two height reference frames assigned special names (see [5], [6], [21]):

a) A height reference frame called PL-KRON86-NH, which is basically a Kronsztadt'86, but locally modified by including some observation lines from the newer (IV) measurement campaign to class 1 network.
b) The height reference frame called PL-EVRF2007-NH, which is the implementation of the European reference frame EVRF2007 in Amsterdam (NAP system - Normal Amsterdams Peil). The heights of the points of the basic height network in the European system was determined on the basis of a subset of the points of this network, which is part of the EUVN European network. It is assumed to be a system of Mołodenski's normal heights, with zero tide (see [6] and in the theoretical sense: [3], [7], [13], [14], [15], [16]). The average height difference between the PL-EVRF2007-NH and PL-KRON86-NH reference frames, determined based on over 15999 points, is 166 mm, with a dispersion from 123 to 223 mm.

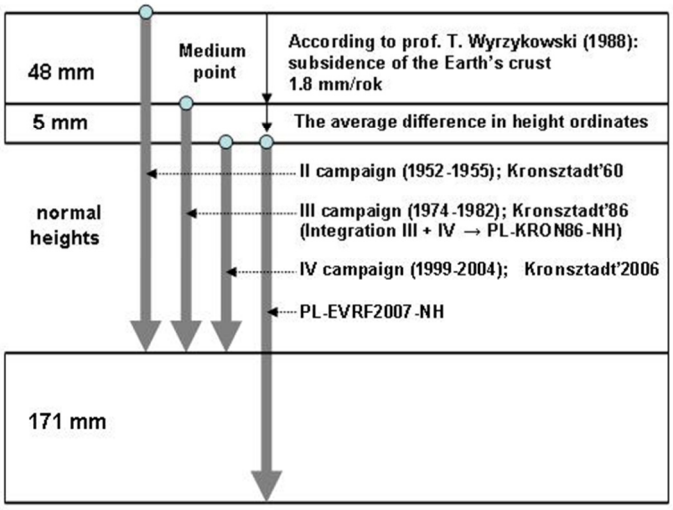

Fig. 3. Average relations between the reference frames

2. General principles of transformation between height reference frames

Fig. 4 shows symbolically the transition paths (transformations) between the previously mentioned height systems. In addition to the direct transformation between the PL-KRON86-NH and PL-EVRF2007-NH reference frames, alternative transition paths may be also by the Kronsztadt'2006. The indirect

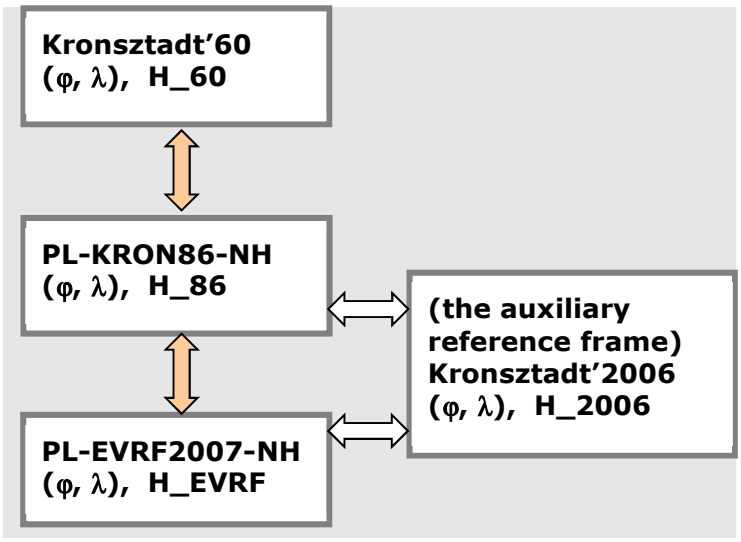

Fig. 4. Schema of transformations between the height reference frames

transition through the Kronsztadt'2006 reference frame was used in the new version of the TRANSPOL program in the height transformation module [8]. Although the "Kronsztad'2006" reference frame was not officially introduced for applications, it was the basis for determining of point heights in the PL-EVRF2007-NH reference frame for I class network.

The general formula realizing the transformation between two height reference frames can be presented in the form of:

$$H_{II} = H_I + \delta H_o + \delta H_{I\text{-}II}\,(u,v) \tag{1}$$

where: I, II – example markings of height reference frames (reference systems),
H_I – a height in a reference frame I,
H_{II} – a height in a reference frame II,
δH_o – average height difference between reference frames, calculated on a given set of reference points,
$\delta H(u, v)$ – local correction relative to average height increment, depended on the position of the point specified by the parameters u, v.

In particular, the parameters of position may be coordinates in any two-dimensional system, for example the Cartesian x, y or geodetic B, L coordinates. To determine the local correction $\delta H(u, v)$ we apply two alternative methods, described in detail in the following sections. One of them, called the interpolative or empirical method, based on interpolative grid. The second method, called polynomial or analytical method, expresses the local correction in the form of a polynomial of two variables, whereby polynomial coefficients are estimated based on reference points (points having heights in both reference frames). The interpolative grid, as a fixed element of the interpolation algorithm, is created on the basis of a given set of reference points. The methodological details of both methods are described in the following sections.

The general formula (1), in relation to the national height systems that we are interested in, will adopt the following detailed forms:

$$\begin{aligned} &H_{Kronsztadt'60} = H_{PL\text{-}KRON86\text{-}NH} + 0.048\text{m} + dH1(B,L), \\ &dH1(B,L) \in \langle -0.010,\ 0.139 \rangle \end{aligned} \tag{2}$$

(7679 common benchmarks were used in both reference frames)

$$\begin{aligned} &H_{Kronsztadt'2006} = H_{PL\text{-}KRON86\text{-}NH} - 0.005\text{m} + dH2(B, L), \\ &dH2(B,L) \in \langle -0.037,\ 0.062 \rangle \end{aligned} \tag{3}$$

$$H_{PL\text{-}EVRF2007\text{-}NH} = H_{Kronsztadt'2006} + 0.171\text{m} + dH3(B,L)$$

$$dH3(B,L) \in \langle -0.017,\ 0.016 \rangle \tag{4}$$

(16222 common benchmarks were used in the following reference frames: PL-KRON86-NH, Kronsztadt'2006, PL-EVRF2007-NH) where $dH1(B,L)$, $dH2(B,L)$, $dH3(B,L)$ represent local corrections depending on the location specified by B, L coordinates. To determine these corrections both the interpolation method was used (see section 3) as well as the polynomial method (see section 4). Both methods were the subject of computer implementations ([8], [9], [10]).

3. Construction of interpolative grids for height transformations using the empirical method

The basic grid is a set of points (nodes), located regularly in a certain conventional area. In our case, we assume that the grid nodes have the geodetic coordinates B, L with the resolution of $0.01^{o} \times 0.01^{o}$. Such a base grid on the area of Poland we call PL-grid-001.

The basic grid PL-grid-001 (Fig. 5), which is the basis for creating interpolative grids (featured grids) for various transformations, will contain a total of 613,621 nodes, arranged on 601 parallel lines in the range of latitude from 49^{o} to 55^{o} and 1021 meridians in the geodetic length range from 14^{o} to 24.2^{o}

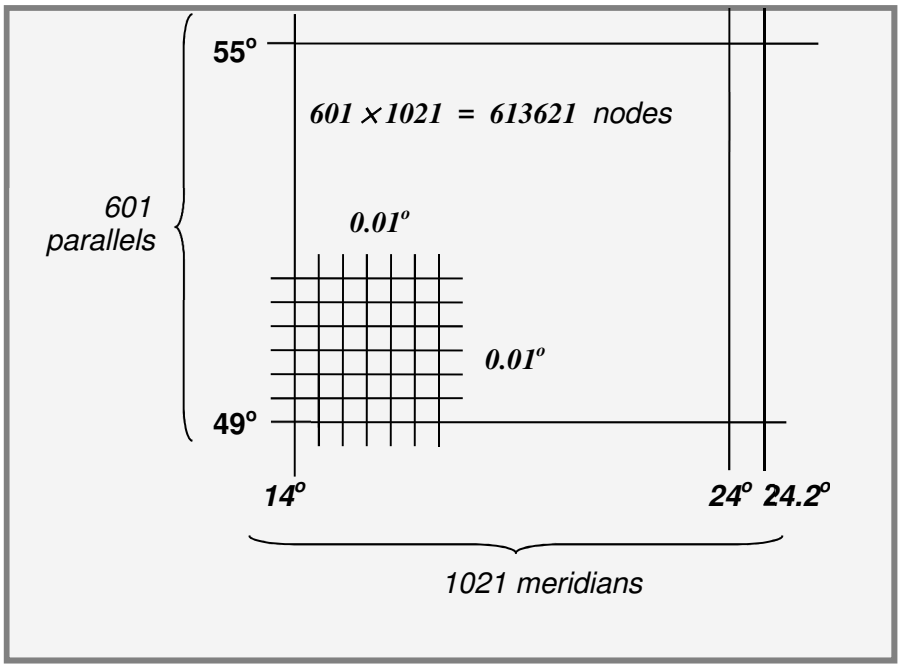

Fig. 5. Structure of the basic grid PL-grid-001

With the above definition, the PL-grid-001 basic grid covers the area of Poland with a certain margin that meets the technical requirements of the application. For each mesh node, we can specify the i and j indices of a rectangular array as follows:

$$i = (B_i - 49.00) \cdot 100; j = (L_j - 14.00) \cdot 100 \quad (5)$$

where B_i, L_i are the geodesic coordinates of grid nodes in degrees, $i = 0,1,2, \ldots ,600$; $j = 0,1, 2, \ldots ,1020$.

Conversely, if the indicators (i, j) of a given node are known, then its coordinates are given by the formulas:

$$B_i = i \cdot 0.01 + 49.00; L_j = j \cdot 0.01 + 14.00^{o} \quad (6)$$

Assigning a feature of some kind for each node of the grid, we obtain the appropriate interpolative grid (featured grid).

An interpolative grid in general is a set of certain features (for example height differences between two systems) assigned to points (nodes) of the basic grid. Of course, when transforming the height of a point that is not the node of the basic grid, we interpolate the appropriate feature (a height difference) based on the features of the four nearest nodes.

We create an interpolative grid for a given pair of height reference frames, based on a given basic grid and a given set of network points (in our case it will be the basic height network from the entire country) having heights in both systems. For each point, we create the appropriate difference (increases) in height between the reference frames. The next step is to transfer the these differences to the grid nodes. For this purpose, we have a choice of a whole range of so called geostatic methods, used to interpolate the grid nodes by a discrete set of points (see eg. [19]). Especially popular in geodesy (used, among others, in the so-called "post-transformative correction") is the method of inverse distances as weights, in short: IDW (Inverse Distance Weighting), with the exponent of the power $q \in <1, 5>$. Other methods are: triangle (triangulation) method, Thiessen's traverses, minimum curvature, polynomial interpolation, and kriging including also correlations between given points. Taking into account the geodetic applications already tested, in the creation of interpolation grids as spatial data models ([10]) the IDW method with the exponent of the power $q = 2$ was used.

Fig. 6 shows the use of the IDW method to create an interpolative grid based on distributed geodetic reference points. We assume that for interpolation of each grid node, only points located in a certain neighborhood of a given node with a radius guaranteeing correct interpolation task execution are selected. The radius length is determined numerically depending on the local density of the reference points (according to the IDW principle, points located further away from the node should not affect the value of the interpolated feature). We define the feature of the grid node as a weighted average:

$$C_{ij} = (\Sigma C_k \cdot w_k) / (\Sigma w_k),\ w_k = 1/\rho_k^{\,2} = weight \tag{7}$$

(summation only for points in the interpolation area).
where: i, j – mesh node indicators,

w_k – weight for the k-th geodetic point (benchmark) in the interpolation area relative to the grid node (i, j),

ρ_k – distance of the k-th geodetic point from the interpolated node,

C_k – a feature of the k-th point (the height increase dH between two systems),

C_{ij} – the interpolated feature (the height increase) of the mesh node.

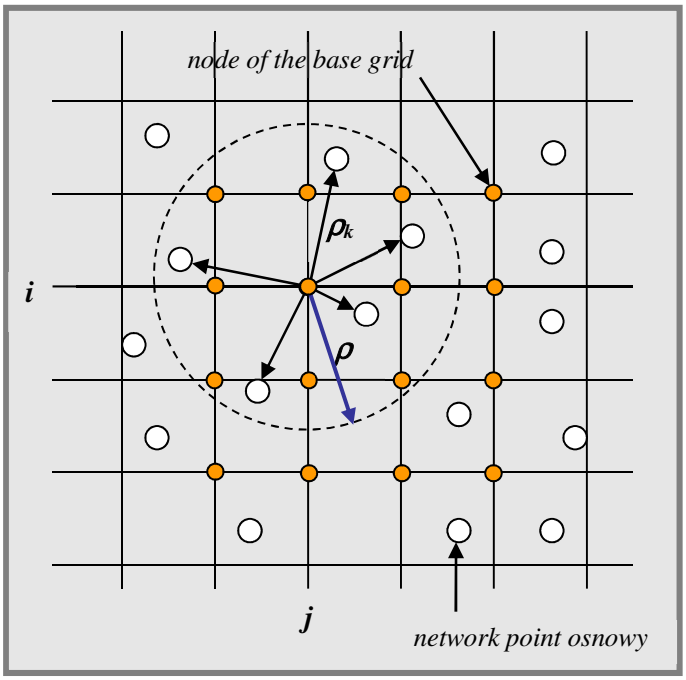

Fig. 6. Interpolation of grid nodes based on the close points of the geodetic network, by means of the weighted average method; ρ – radius of searching of points for node interpolation, ρk – distance of the network point from the interpolated node

The described empirical method, based on the interpolative grid, has been implemented in the TRANSPOL v. 2.06 program and in the national base of basic geodetic networks at GUGiK ([8], [10]). Interpolative grids saved in the form of discrete text files are published also at the address indicated. The file concerning our transformation tasks contains differences between normal heights in PL-KRON86-NH and PL-EVRF2007-NH reference frames, for all nodes of base grid with increments of 0.01° in latitude and longitude, for the whole area of Poland. In the published (in [10]) sets lack the old reference

system Kronsztadt'60 but this reference frame has been included in another database software (in [9]). The polynomial transformation method presented below includes all considered reference frames in the given numerical formulas.

4. Polynomial transformations

4.1. Conversions between the reference frames: Kronsztad'60 and PL-KRON86-NH

The polynomial transformation between these reference frames have been carried out, for example, for the Cracow district [2]. The polynomial of the second degree turned out to be adequate for such an area. For larger areas, especially covering the whole of Poland, it becomes a necessity to take into account mutual inconsistencies of the reference frames represented by the corresponding heights of leveling networks. These inconsistencies may also result from vertical displacements of some benchmarks, given that the period between measurement campaigns measures about two decades. Of course, a polynomial approximation can be not define all local deviations because they are accidental. In contrast to the interpolative grid, the polynomial approximation smooths the appropriate empirical relationship. In practical applications, this may be an undesirable effect, but a smoothed transformation formula allows detection of possible gross errors (outliers phenomena) in height values of the reference points. In addition, post-transformative corrections resulting from deviations at reference points can be introduced to the result of the polynomial transformation, approaching the result of the empirical (interpolative) method.

In our case, however, there are no physical reasons to assume any particular form of the height change model. Therefore, we use the general form of the algebraic polynomial of two variables as a standard. Parameters of polynomials are estimated using the least squares method, taking into account given sets of reference points. The calculations were carried out with GEONET 2006 system programs (see: www.geonet.net.pl).

We assume that the arguments of polynomials are the flat coordinates x, y of points in the uniform PL-1992 system for whole Poland. The adoption of the PL-1992 system as a positioning platform for points is convenient, because this system is not divided into zones. Of course, it would also be possible to adopt coordinates in other systems, for example in the B, L geodetic coordinate system. The position coordinates of the point can be approximate, because the big change of a horizontal position does not cause a significant change in height. In practice, the flat coordinates of the benchmarks are usually rounded to full meters.

The following formula express the polynomial transformation of height between the reference frames PL-KRON86-NH and Kronsztad'60 estimated by 7,679 reference points:

$$H_{(Kronsztad'60)} = H_{(PL\text{-}KRON86\text{-}NH)} + \delta H_o + \delta H + \varepsilon \tag{8}$$

H_o=0.0485 *m* = average height offset,

$H = a_{00} + a_{01} \cdot v + a_{10} \cdot u + a_{02} \cdot v^2 + a_{11} \cdot u \cdot v + a_{20} \cdot u^2 + a_{03} \cdot v^3 + a_{12} \cdot u \cdot v^2 + a_{21} \cdot u^2 \cdot v + a_{30} \cdot u^3 + a_{04} \cdot v^4 + a_{13} \cdot u \cdot v^3 + a_{22} \cdot u^2 \cdot v^2 + a_{31} \cdot u^3 \cdot v + a_{40} \cdot u^4$,

$u = (x - x_o) \cdot s$, $v = (y - y_o) \cdot s$ – arguments normalized so that $|u| < 1$ and $|v| < 1$,

x, y – point coordinates (in meters) in the Polish system PL-1992,

x_o =466,458 *m*, y_o =514,429 *m* – components of the translation vector (centering coordinates),

$s = 2.51510 \cdot 10^{-06}$ = standarizing scale,

a_{ij} $(i, j = 0,1,2,4,\ i+j \le 4)$ – polynomial coefficients of degree n = 4 (the values in Table 1), estimated by using of Least Squares (LSQ) method,

ε – random error (the Fig. 7 shows the characteristic estimates of errors as point deviations from polynomial model).

Of course, the inverse transformation results directly from (8):

$$H_{(PL\text{-}KRON86\text{-}NH0)} = H_{(Kronsztadt'60)} - \delta H_o - \delta H - \varepsilon \tag{9}$$

Table 1. Polynomial coefficients for transformations between the reference frames Kronsztad'60 and PL-KRON86-NH

POLYNOMIAL COEFFICIENTS AND STANDARD DEVIATIONS

a_{00} :=	1.88044E-02	3.905E-04
a_{01} :=	3.72458E-02	9.623E-04
a_{02} :=	-8.88262E-02	3.142E-03
a_{03} :=	-3.62611E-03	2.145E-03
a_{04} :=	5.11118E-02	5.261E-03
a_{10} :=	3.36639E-02	1.068E-03
a_{11} :=	9.78759E-02	3.469E-03
a_{12} :=	-1.61254E-02	3.178E-03
a_{13} :=	-1.22407E-01	7.141E-03
a_{20} :=	-6.57799E-02	3.660E-03
a_{21} :=	8.81326E-03	3.794E-03
a_{22} :=	1.42289E-01	9.288E-03
a_{30} :=	-3.09316E-02	2.893E-03
a_{31} :=	-2.52344E-02	9.762E-03
a_{40} :=	4.86396E-02	7.374E-03

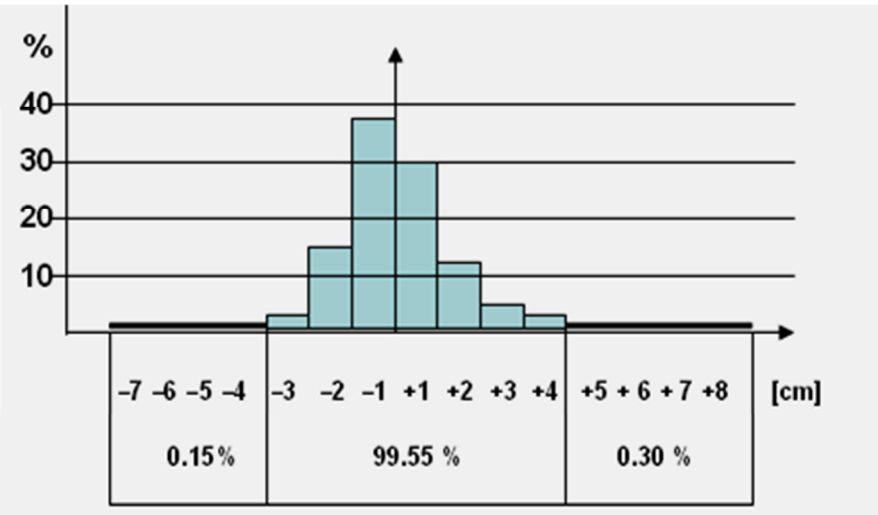

Fig. 7. Distribution of transformation deviations for 7679 reference points between the Kronsztadt-60 and PL-KRON86-NH reference frames

4.2. Conversions between PL-KRON86-NH and PL-EVRF2007-NH reference frames

The formula of the polynomial transformation between PL-KRON86-NH and PL-EVRF2007-NH reference frames, estimated by 15999 reference points, is expressed as follows:

$$H_{(PL\text{-}EVRF2007\text{-}NH)} = H_{(PL\text{-}KRON86\text{-}NH)} + \delta H_o + \delta H + \varepsilon \tag{10}$$

$\delta H_o = 0.1659$ = the average height offset,

$\delta H = a_{00} + a_{01} \cdot v + a_{10} \cdot u + a_{02} \cdot v^2 + a_{11} \cdot u \cdot v + a_{20} \cdot u^2 + a_{03} \cdot v^3 + a_{12} \cdot u \cdot v^2 + a_{21} \cdot u^2 \cdot v + a_{30} \cdot u^3$,

$u = (x - x_o) \cdot s$, $v = (y - y_o) \cdot s$ – arguments normalized so that $|u| < 1$ and $|v| < 1$,

x, y – point coordinates (in meters) in the Polish system PL-1992,

$x_o = 469{,}175\ m$, $y_o = 513{,}591\ m$ – components of the translation vector (centering coordinates),

$s = 2.55611 \cdot 10^{-06}$ = standardizing scale,

a_{ij} $(i, j = 0,1,2,3,\ i+j \le 3)$ – polynomial coefficients of degree n =3 (the values in Table 2),estimated by using of Least Squares (LSQ) method,

ε – random error (the Fig. 8 shows the characteristic estimates of errors as point deviations from polynomial model).

Of course, the inverse transformation results directly from (10):

$$H_{(PL\text{-}KRON86\text{-}NH)} = H_{(PL\text{-}EVRF2007\text{-}NH)} - \delta H_o - \delta H - \varepsilon \tag{11}$$

Table 2. Polynomial coefficients for transformations between the reference frames PL-KRON89-NH and PL-EVRF2007-NH

POLYNOMIAL COEFFICIENTS AND STANDARD DEVIATIONS

a_{00}:=	1.29208E-04	1.159E-04
a_{01}:=	1.20768E-02	3.876E-04
a_{10}:=	-1.94601E-02	4.356E-04
a_{02}:=	-3.40115E-03	3.678E-04
a_{11}:=	-1.20758E-02	4.766E-04
a_{20}:=	-1.38555E-04	4.440E-04
a_{03}:=	-4.63454E-03	8.677E-04
a_{12}:=	5.73956E-02	1.144E-03
a_{21}:=	-2.98559E-02	1.364E-03
a_{30}:=	1.68069E-02	1.149E-03

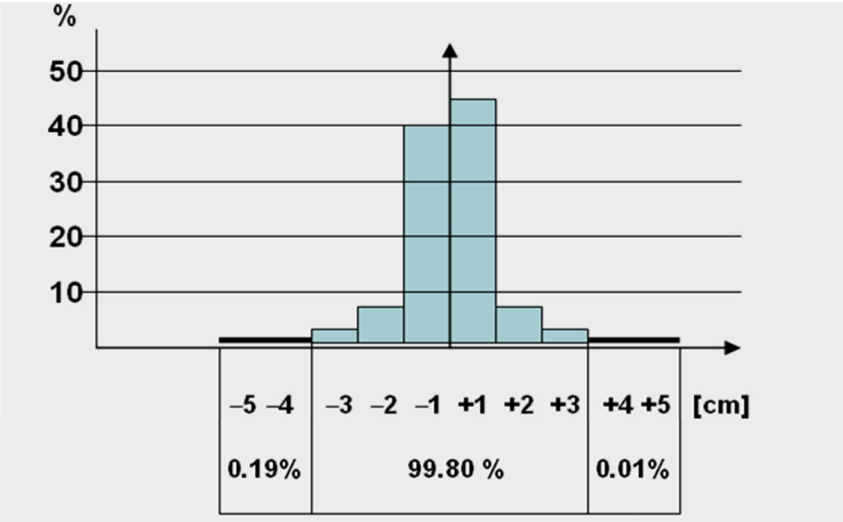

Fig. 8. Distribution of transformation deviations for 15999 reference points between the reference frames PL-KRON86-NH and PL-EVRF2007-NH

5. Illustration of differences between reference frames in the area of Poland

The Figures 9–11 show the contour line of constant differences between height reference frames in the Polish area. It seems very likely to say that in every newer measuring era there is a qualitative improvement in measurement methods and calculation techniques. In this sense, there are several conclusions (interpretations) that we note below.

In the Fig. 9, we note that deviations between the Kronsztad'60 and PL-KRON86-NH reference frames increase towards the north-east and are the smallest in the western areas. In the interpretation of these differences, it is important to note that in the measurement campaigns, which resulted in the Kronsztadt-60 system, three independent networks have been integrated: from the area of the Second Republic of Poland, newly connected western and northern territories. Of course, the cause-and-effect aspects of the differences between the reference frames may be the subject of separate studies. Meanwhile, according to the purpose of this work, the subject of our research was specific metric compounds that can be practically used to transform heights between systems (polynomials, interpolative grids).

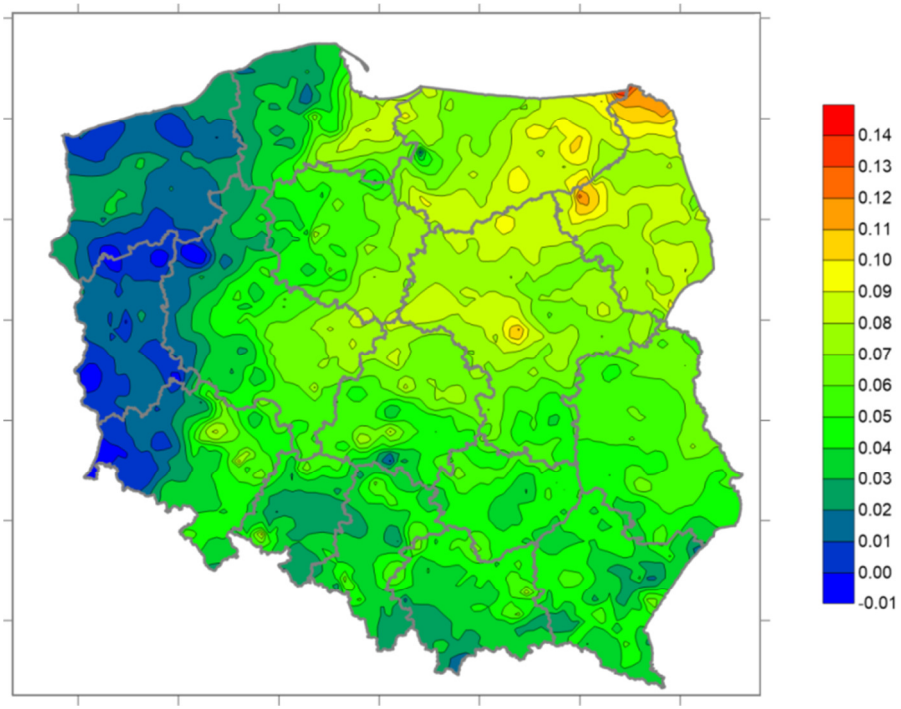

Fig. 9. Image of height differences δ = HKronsztad'60 – HPL-KRON86-NH (in meters)

In turn, the Fig. 10 shows analogous contour lines of equal spacing between the PL-KRON86-NH and Kronsztad'2006 reference frames. We see, first of all, that the differences between normal heights of both frames in the whole area of Poland are already small, however small areas appear with the absolute maximum values of these differences reaching 3.5 cm.

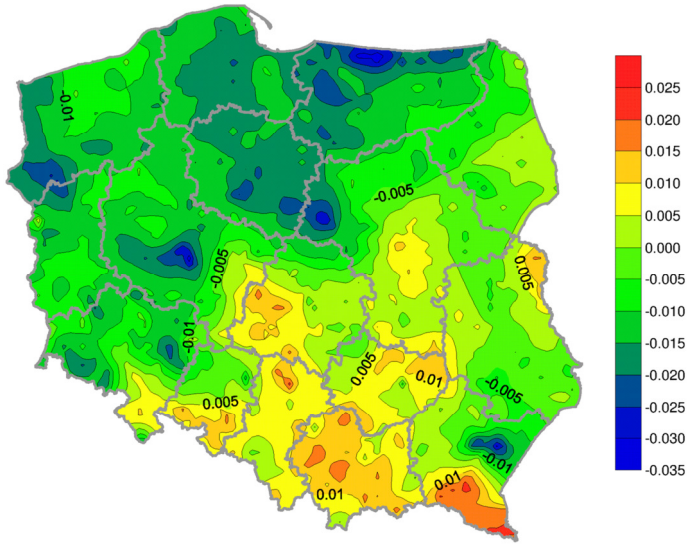

Fig. 10. Image of height differences δ = H Kronsztad'2006 – HPL-KRON86-NH in meters (source: [8])

In the Fig. 11 we have an image of contour lines of equal height differences between the Kronsztadt'2006 and PL-EVRF2007-NH reference frames. The regularity of this dependence in comparison to the previous ones, shown in Figures 9 and 10, results from the fact that the heights in the PL-EVRF2007-NH system come from the direct conversion of heights in the Kronsztadt'2006 (computed by Gajderowicz [4]), i.e. from the same leveling network.

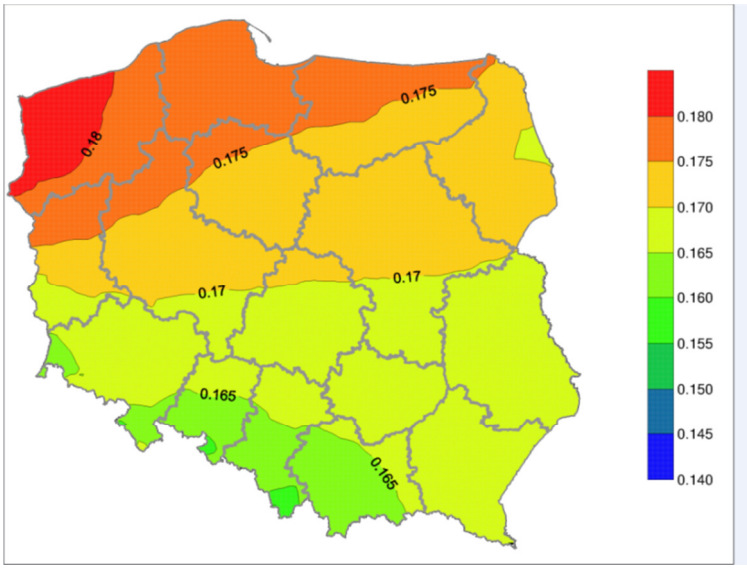

Fig. 11. Image of height differences $\delta = H_{\text{PL-EVRF2007-NH}} - H_{\text{Kronsztadt'2006}}$ in meters (source: [8])

If we add the height differences from Fig. 9 and 10, then according to their definitions given in the description of drawings, we get the deviations between two currently applicable state reference frames: PL-EVRF2007-NH (new "Amsterdam" reference frame), PL-KRON86-NH (Fig. 12). Local irregularities are the result of differences in normal heights determined independently in the framework of the 3rd and 4th measurement campaign.

It is known that the next 5th measurement campaign of the basic height network was already carried out along with the necessary epochal modernization of the network. Unfortunately, the results have not yet been practically used, as some network inconsistencies have been identified in the areas south-eastern of Poland.

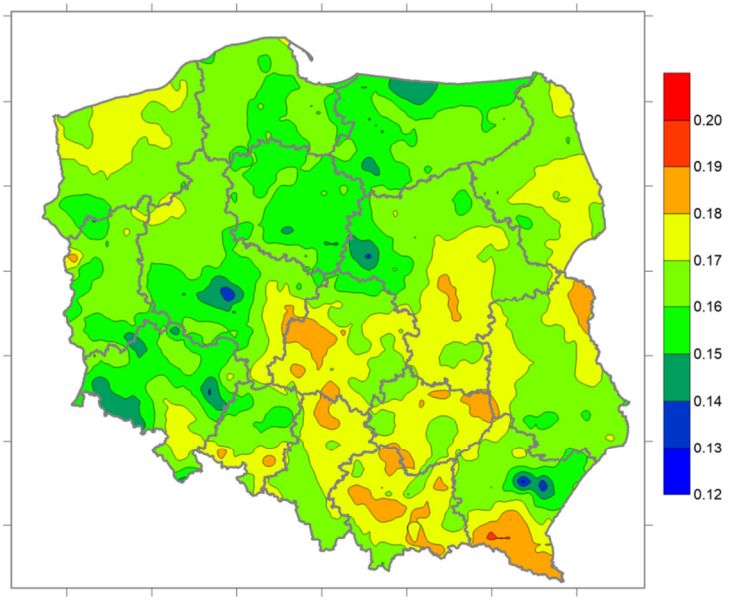

Fig. 12. Image of height differences δ = HPL-EVRF2007-NH – HPL-KRON86-NH (in meters)

6. Conclusions

Now in Poland normal heights in two reference frames: PL-KRON86-NH (modernized Kronsztadt '86) and the PL-EVRF2007-NH (the Polish implementation of the European height reference frame EVRF2007) are used. Regardless of official legal regulations (see: [20], [21]), there is also (materially, in various geodetic and cartographic documents) the former Kronsztad'60 reference frame. In addition, a certain theoretical significance has the Kronsztad'2006 reference frame, which was the original object for the calculation of the heights in PL-EVRF2007-NH reference frame. Kronsztad'2006 is also present in the height transformation module in the

TRANSPOL 2.06 program [8]. This publication considers transformations between all the mentioned height reference frames, describing methods and algorithms adopted in the special elaborations for the Central Office of Geodesy and Cartography (including: [8], [9], [10]).

The basic method of transformation between height reference frames, recommended for use in geodetic practice is the empirical (interpolative) method using interpolative grids. For a given pair of reference frames, grid nodes have features (increases in height between two reference frames) determined on the basis of known values of features in the network points, by the weighted average method. The weight is defined as a number inversely proportional to the square of the distance of the node from a given point of the network. In order to interpolate a given grid node, only network points located in a circular area around the node are selected (see Fig. 6). The radius of the area depends on the local density of reference points. For any transformed point, which is not a grid node, the determination of the feature (the corresponding increase in height) boils down to the known bi-linear interpolation in a single cell of the grid.

In addition to the empirical method, the possibility of height transformation is presented using polynomials describing the "smoothed" relationship between height reference frames used in Poland. The polynomial transformation does not accurately fit into the local leveling network, but may have special applications. For example, it can be used to detect local warp errors in the original or current system. The signal of the large local error will be the deviation of the polynomial transformation from the known from the measurement of the height of a given control point. Of course, between empirical and polynomial transformation there will be differences, which a distribution in area of Poland can be identified in Fig. 9–12.

Acknowledgments: *The publication was made in 2017 as part of statutory research at the Department of Geodesy and Geotechnics of Rzeszów University of Technology and was presented in the form of a report at the 6th National Scientific and Technical Conference p. "Numerical Cartography and Geodetic Computer Science", Iwonicz-Zdrój, 6-8 September 2017.*

References

[1] Alexandrowicz L.: Realizacja zmodernizowanych wysokościowych osnów geodezyjnych kraju [Engl.: *Implementation of modernized height geodetic networks of the country*]. Przegląd Geodezyjny, nr 9–10 / 1986.

[2] Banasik P., Ligas M., Kudrys J., Skorupa B., Bujakowski K.: Transformacja wysokości z układu Kronsztadt'60 do układu Kronsztadt'86 na przykładzie powiatu krakowskiego [Engl.: *Transformation of heights from the Kronsztadt'60 system to the Kronsztadt'86 system on the example of the Cracow poviat*]. Przegląd Geodezyjny, nr 4/2012, 6–13.

[3] Barlik M.: Wpływ deformacji pływowych na niwelację satelitarną metodą GPS [Engl.: *Influence of tidal deformations on satellite leveling using the GPS method*]. Przegląd Geodezyjny nr 2/1992, 8–11.

[4] Gajderowicz I.: Propozycja nowego polskiego układu wysokościowego [Engl.: *Proposal of new Polish vertical reference frame*]. Geomatics and Environmental Engineering 2007, Vol. 1, No. 1/1, 125–132.

[5] Graszka W.: Definicja i realizacja europejskiego systemu wysokościowego EVRS w Polsce [Engl.: *Definition and implementation of the European Vertical Reference System* (*EVRS*) *in Poland*]. Sympozjum KG PAN: Realizacja osnów geodezyjnych a problemy geodynamiki. Grybów, 25–27.09.2014.

[6] Graszka W., Pielasa E., Wajda S., Piętka D.: Podstawowa osnowa wysokościowa, grawimetryczna i magnetyczna – ocena stanu i prognozy rozwoju [Engl.: *Basic networks: heights, gravimetric and magnetic - evaluation of the state and prognosis of development*]. Sympozjum KG PAN: „Współczesne problemy podstawowych osnów geodezyjnych w Polsce", Grybów, 14–16.09.2016.

[7] Hermanowski A., Kamela Cz., Stańczyk Z., Warchałowski E., Włoczewski F., Wyrzykowski T.: Niwelacja Precyzyjna [Engl.: *Precise Leveling*]. PPWK Warszawa 1971.

[8] Kadaj R., Świętoń T.: TRANSPOL v. 2.06: Program transformacji pomiędzy różnymi układami w państwowym systemie odniesień przestrzennych [Engl.: *TRANSPOL v. 2.06: Program of transformation between various reference frames in the state spatial reference system*]. GUGiK – Warszawa, 17.12.2012 (contract No.BO-4-2503-183/GI-2500-610-83/2012), www.gugik.gov.pl/bip/prawo/modele-danych.

[9] Kadaj R., Świętoń T.: Biblioteka programistyczna .dll do transformacji pomiędzy układami współrzędnych w obszarze Polski. Wykonano dla Centralnego Banku Osnów Geodezyjnych w GUGiK przez firmę GEOMAR S.A. Szczecin, umowa z dnia 24.05.2013 r [Engl.: *Programming library .dll for transformation between coordinate systems in the area of Poland. Made for the Central Bank of Geodesic Surveys in GUGiK by GEOMAR S.A. Szczecin, contract of 24/05/2013*].

[10] Kadaj R., Świętoń T.: Model różnic wysokości pomiędzy układami wysokościowymi PL-EVRF2007-NH i PL-KRON86-NH [Engl.: *Model of height differences between PL-EVRF2007-NH and PL-KRON86-NH reference frames*]. GUGiK, 2012, www.gugik.gov.pl/bip/prawo/modele-danych.

[11] Kowalczyk K.: Dane niwelacyjne w badaniu ruchów skorupy ziemskiej na obszarze Polski [Engl.: *Leveling data in the study of the movements of the Earth's crust on the territory of Poland*]. Acta Sci. Pol., Geodesia et Descriptio Terrarum 8(1), 2009, 31–43.

[12] Kurałowicz Z., Słomska A.: Powierzchnie i wysokościowe układy odniesienia – obserwacje na stacjach mareograficznych Kronsztad i Amsterdam [Engl.: *Surfaces and height reference systems - observations at the Kronstadt and Amsterdam mareographic stations*]. Inżynieria Morska i Geotechnika, nr 5/2014, 377–384.

[13] Łyszkowicz A.: Nowy układ wysokościowy [Engl.: *A new height system*] Geodeta, 2 (33) luty 1998, 35–38.

[14] Łyszkowicz A.: Jednoetapowo-lepiej. Uwagi dotyczące wyrównania sieci niwelacji precyzyjnej w Polsce [Engl.: *One step-better. Comments on the precise leveling network in Poland*]. Geodeta nr 10(113), 2004, 26–30.

[15] Łyszkowicz A.: Geodezja Fizyczna [Engl.: *Physical Geodesy*]. Wydawnictwo UWM w Olsztynie. Olsztyn 2012. ISBN 978-83-7299-771-5.

[16] Łyszkowicz A., Kuczyńska-Siehień A., Biryło M.: Preliminary unification of Kronsztad86 local vertical datum with global vertical datum. Reports on Geodesy and Geoinformatics, vol. 97 /2014; pages 103-111, DOI: 10.2478/rgg-2014-0015.

[17] Wyrzykowski T.: Nowy pomiar państwowej sieci niwelacji precyzyjnej I klasy (1974–1979) [Engl.: *New measurement of the state I class precision leveling network* (*1974–1979*)]. II Sympozjum „Współczesne problemy podstawowych sieci geodezyjnych". Komitet Geodezji PAN, Warszawa, 1980.

[18] Wyrzykowski T.: Charakterystyka nowej krajowej sieci niwelacji I klasy (pomiary z lat 1974–82) [Engl.: *Characteristics of the new national I class leveling network* (*measurements from 1974-82*)]. IV Sympozjum „Współczesne problemy podstawowych sieci geodezyjnych". Komitet Geodezji PAN, Sekcja Sieci Geodezyjnych, Warszawa, 1988.

[19] Zawadzki J.: Metody geostatyczne dla kierunków przyrodniczych i technicznych [Engl.: *Geostatic methods for natural and technical faculty*]. Oficyna Wydawnicza Politechniki Warszawskiej, 2011. ISBN: 978-83-7207-953-4.

[20] Rozporządzenie Rady Ministrów z dnia 15 października 2012 r. w sprawie państwowego systemu odniesień przestrzennych [Engl.: *Regulation of the Council of Ministers of October 15, 2012 on the state spatial reference system*]. Dz.U. Nr 0, poz. 1247, 2012.

[21] Rozporządzenie Ministra Administracji i Cyfryzacji z dnia 14 lutego 2012 r. w sprawie osnów geodezyjnych, grawimetrycznych i magnetycznych [Engl.: *Regulation of the Minister of Administration and Digitization of February 14, 2012 on geodetic, gravimetric and magnetic control networks*] (Dz.U. Nr 0, poz. 352, 2012).

[22] Podzbiory bazy danych CODGiK / GUGiK na podstawie zamówień z dnia 25.01.2007 oraz z dnia 28.05.2012 [Engl.: *Subsets of the CODGiK / GUGiK database based on orders from January 25, 2007 and from May 28, 2012*].

[23] Wyrównanie podstawowej osnowy wysokościowej I i II klasy na obszarze kraju w europejskim układzie odniesienia PL-EVRF2007-NH. Projekt wykonany dla GUGiK przez OPGK Lublin przy współpracy z Centrum Badań Kosmicznych PAN w Warszawie. Listopad 2013 r. [Engl. *Adjustment of the basic 1st and 2nd class tertiary network in the area of Poland, in the PL-EVRF2007-NH European reference system. Project made for GUGiK by OPGK Lublin in cooperation with the Space Research Center PAN in Warsaw. November 2013*], www.opgk.lublin.pl.

[24] www.wikipedia.org/wiki/Historia_wysokościowej_osnowy_geodezyjnej_w_Polsce.

[25] Archiwum Map Wojskowego Instytutu Geograficznego 1919–1939: Niekomercyjny projekt udostępnienia skanów map i materiałów geograficznych wydanych przez Wojskowy Instytut Geograficzny (WIG) w latach 1919–1939 [Engl.: *Map of the Military Institute of Geography 1919-1939: Non-commercial project to provide scans of maps and geographical materials issued by the Military Geographical Institute (WIG) in the years 1919-1939*] http://maps.mapywig.org/m/WIG_maps/various/ /Small_scale_maps/SIEC_NIWELACYJNA_POLSKI_WIG_1939.jpg.

Przesłano do redakcji: 22.08.2018 r.
Przyjęto do druku: 28.09.2018 r.

CZASOPISMO INŻYNIERII LĄDOWEJ, ŚRODOWISKA I ARCHITEKTURY
JOURNAL OF CIVIL ENGINEERING, ENVIRONMENT AND ARCHITECTURE
JCEEA, t. XXXV, z. 65 (3/18), lipiec-wrzesień 2018, s. 25-34, DOI:10.7862/rb.2018.39

Tetiana KROPYVNYTSKA[1]
Myroslav SANYTSKY[2]
Iryna GEVIUK[3]

PROPERTIES OF PORTLAND-COMPOSITE CEMENTS WITH ZEOLITE TUFF

Growing requirements for protection of the environment every year gradually increase production of cements with a high content of mineral additives and clinker cements should be considered as cements for special purposes. The strong development of a quaternary Portland cement composite system containing blast-furnace slag, zeolite tuff and limestone powder is presented. The composition and particle size distribution of the constituents are optimized by the incremental coefficient of the surface activity of the zeolite-containing Portland composite cements. Zeolite tuff and limestone powder of high specific surface area lead to the increase of the surface activity of the entire system and a corresponding improvement in the performance of the cement. It was shown that low-energy Portland-composite cements "green cements" obtained by separate grinding are characterized by higher early compressive strength. The optimization of Portland-composite cements was carried out and the relationship between the phase composition, microstructure and strength of the cement matrix were investigated. The main role of zeolite is to improve the properties of cement stone by reducing the quantity and size of hydrate calcium hydroxide with increasing of low alkali calcium hydrosilicates. It is shown that a synergistic combination of mineral additives of different groups with substantial reduction of high energy-consumption clinker component in the Portland-composite cements allows to improve rheological properties and provides of strength increase of binder.

Keywords: Portland-composite cement, zeolite tuff, particle size distribution, compressive strength, properties

1. Introduction

The basic principles of the sustainable development strategy in the cement industry, providing optimum using of non-renewable natural raw materials, application of energy saving technologies, utilization of industrial wastes as well

[1] Corresponding author: Tetiana Kropyvnytska, Lviv Polytechnic National University, 12 S. Bandera str., 79013 Lviv, Ukraine, e-mail: tkropyvnytska@ukr.net

[2] Myroslav Sanytsky, Lviv Polytechnic National University, 12 S. Bandera str., 79013 Lviv, Ukraine, e-mail: msanytsky@ukr.net

[3] Iryna Geviuk, JSC "Ivano-Frankivsk Cement", e-mail: irynageviuk@ukr.net

as comprehensive environmental protection and reduction of CO_2 emissions. Large-scale production of efficient composite eco cements ensures the implementation of the cement industry of progressive models of rational use of natural raw materials, fuel, electricity with minimal greenhouse gas emissions, but also allows to implement cleaner production practices [1, 2].

The main problem for process engineering of composite cements is to prepare and mix suitable combinations of clinker and interground additives so that the performance lies in the same range as comparable Portland cements. Most cement plants use granulated blast furnace slag and fly ash as a mineral additives and limestone as microfiller. These various blended cements, especially the ternary and quaternary, were optimized with a synergistic effect, allowing component ingredients to compensate for any mutual shortcomings [3]. At the same time an excellent supplementary cementitious material is a type of natural pozzolanic material – zeolite tuff. They have unique characteristics such as high specific surface area and cation exchange capacity. Like other pozzolanic materials, the replacement of cement by natural zeolite tuff can improve the mechanical properties of cement and concrete composites. The exploitation of natural zeolite tuff, when used as a partial replacement for cement, can lead to a considerable economic benefit and durability [4, 5]. Principles governing the properties of such multi-component quaternary composite cements are examined and some results are discussed in this article.

The purpose of work is to investigate the impact of ultrafine mineral additives of various types on the physical and mechanical properties of Portland cement composition, phase composition and microstructure of cement paste.

2. Materials and methods

Ordinary Portland cement CEM I 42,5R JSC "Ivano-Frankivsk Cement" composed of C_3S: 62.42, C_2S: 13.62, C_3A: 7.06, C_4AF: 12.32, mass. %, was used in the investigation. Limestone powder with 95 mass. % $CaCO_3$ was used as micro-filler. Grain granulated blast furnace slag (GGBFS) consisting of 92-96 mass. % $CaO + SiO_2 + Al_2O_3 + Fe_2O_3$ and zeolitic tuff with 70-73 mass.% SiO_2 provided from Sokyrnytsky quarry were utilized as mineral additives. Portland-composite cements were obtained by mixing of CEM I 42,5R, GGBFS, zeolite tuff and limestone powder. The chemical analysis of materials are presented in Figure 1.

Grain size of particles was measured by laser granulometr Mastersizer 3000. The coefficient of incremental surface activity K_{isa}, which shows the influence of particle content in total volume was calculated by the product of surface activity coefficient and incremental volume of each fraction [6].

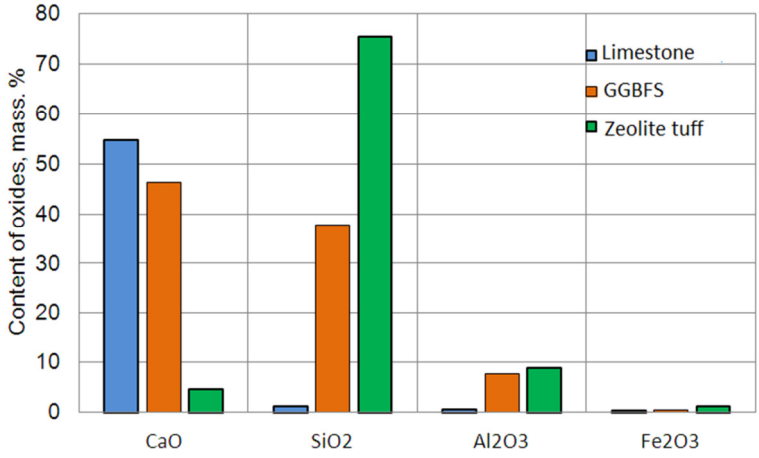

Fig. 1. Chemical analysis of additives

The phase composition of the resulting products was determined by X-ray powder diffraction: patterns were recorded at room temperature with Co Kα radiation on a PANalytical X'pert Pro diffractometer equipped with the X'celerator detector in the 2θ range from 5° to 70° (step 0.033°, time/step 50s). Scanning electron microscope was used for studying the crystals and morphology of the cement stone surface. The evaluation of the properties of Portland-composite cement was carried out through a flowing and compressive strength tests.

The compressive strength data of the multi-component cements was determined on 40×40×160 mm mortar prisms with water/cement ratio of 0.50 according to EN 196-1. Determination the workability of fresh cement mortars (consistence by flow table) was carried according to EN 1015-3. The mortars with weight ratio of cement to sand 1:3 were manufactured with constant W/C = 0.5 for sulphate and magnesia resistance tests. Mortar specimens of size 40×40×160 mm were cured 24 hours in a climate air. After remoulding the specimens were kept 27 days in water, and then either in water (reference) or sodiums sulphate solution (10.0 mg SO_4^{2-} per litre) and magnesium chloride (10.0 mg Mg^{2+} per litre) for 365 days, respectively.

3. Results and discussion

Particle size distribution of cementitious materials used to produce composite cements was studied. The Blaine specific surface areas of CEM I 42,5R, GGBFS, zeolitic tuff and limestone powder were 3,960; 4,600, 12,000 and 10,060 cm²/g. The particle size distribution of CEM I, the grain granulated blast furnace slag, the zeolitic tuff and of the limestone powder are presented in Figure 2.

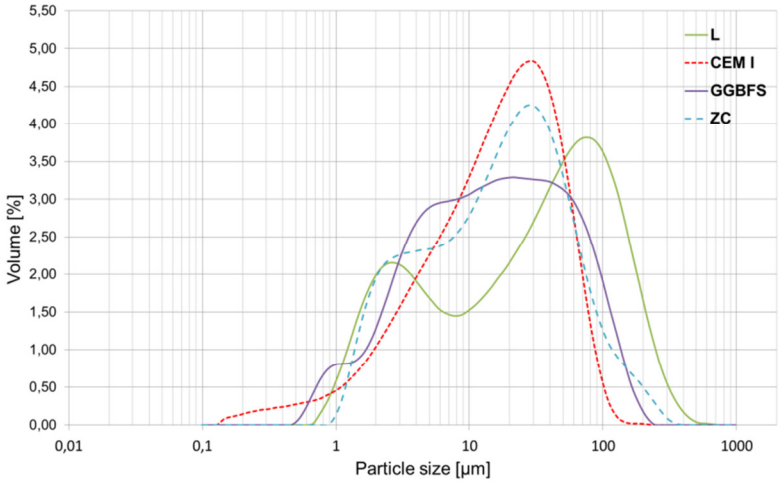

Fig. 2. Particle size distribution of the main constituents

On the differential curve of the particle distribution, the maximum for CEM I is 6.84 µm, and for GGBFS, zeolite tuff and limestone powder – 3.35, 4.38 and 3.96 µm accordingly. The volume mean diameter D [4;3] for CEM I corresponds to 17.7 µm, and for the mineral additives in the range of 28.6 to 71.9 µm. Furthermore the surface area mean diameter D[3;2] for CEM I shows a value of 3.79 µm, those of the mineral additives lay in the range of 4.62 to 6.66 µm. The maximum value for CEM I shown on the differential curve of the particle distribution, is 6.84 µm; GGBFS, zeolitic tuff and limestone powder show maxima at 3.35, 4.38 and 3.96 µm respectively (Figure 3). This indicates that the fine fraction determines the surface area of particles of the cementitious systems.

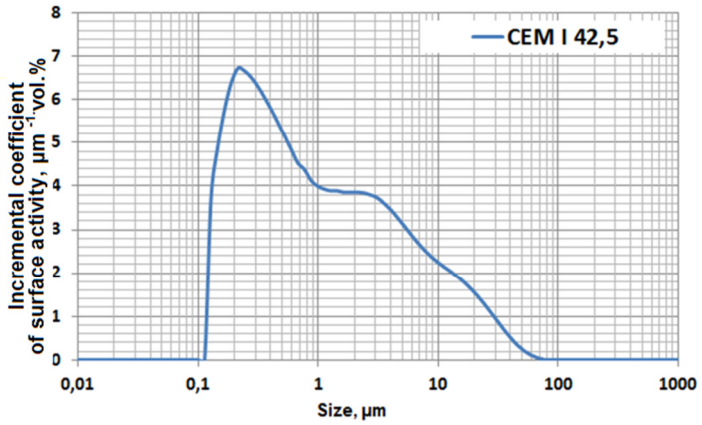

a)

Fig. 3. The surface distribution of CEM I 42,5 (a), GGBFS (b), zeolite tuff (c) and limestone powder (d)

a

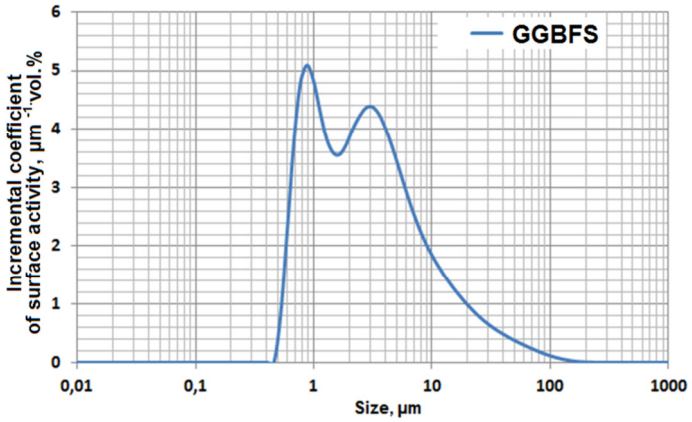

b)

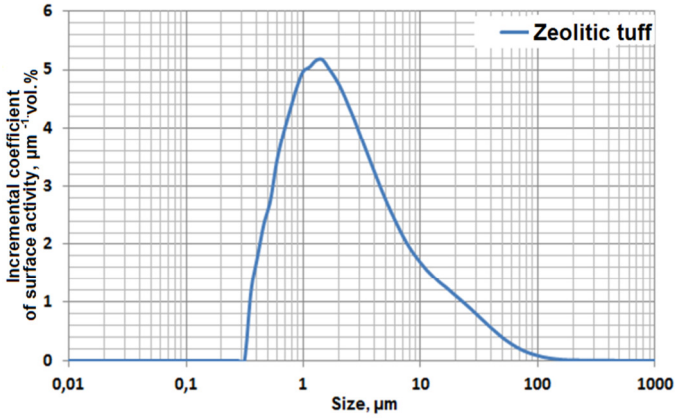

c)

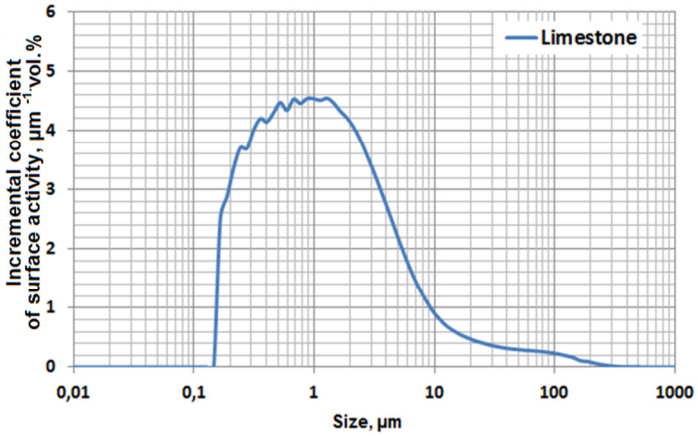

d)

Fig. 3 (cont.). The surface distribution of CEM I 42,5 (a), GGBFS (b), zeolite tuff (c) and limestone powder (d)

Portland-composite cements obtained by mixing of Portland cement CEM I 42,5R, zeolite tuff and limestone powder in different proportions. According to the particle size distribution of Portland-composite cement (SSA=4,250 cm^2/g) fraction Ø1, Ø5, Ø10, Ø20 and Ø60 µm are respectively 4.75, 18.58, 31.62 and 85.56%, and the grain size D_{10}, D_{50} and D_{90} corresponds to 2.13, 20.5 and 69.7 µm (Figure 4a). The maximum value of K_{isa} (6.45 m^{-1}·vol.%) of CEM II/B-M(S-P-L) 32,5R achieved for a fraction 0.354 µm, and for a fraction of 5 µm this coefficient decreases 2.3 times and with further particle size increasing is significantly reduced (Figure 4b).

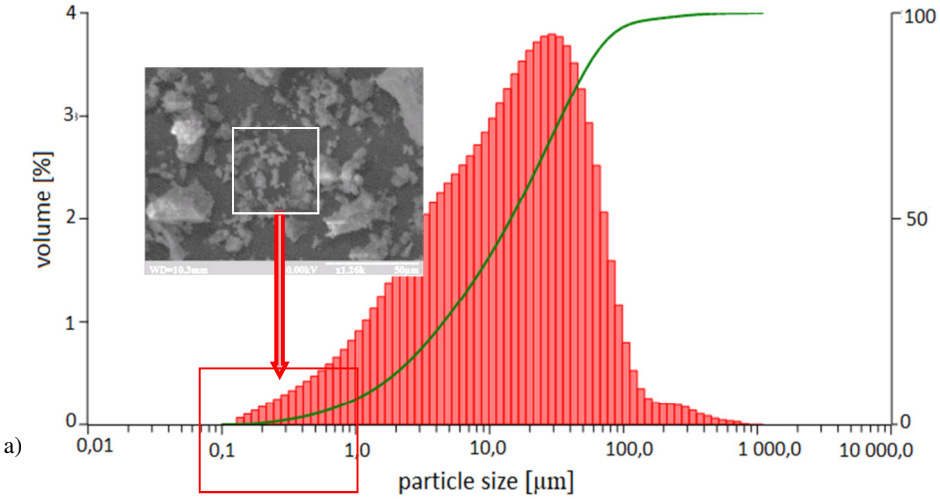

a)

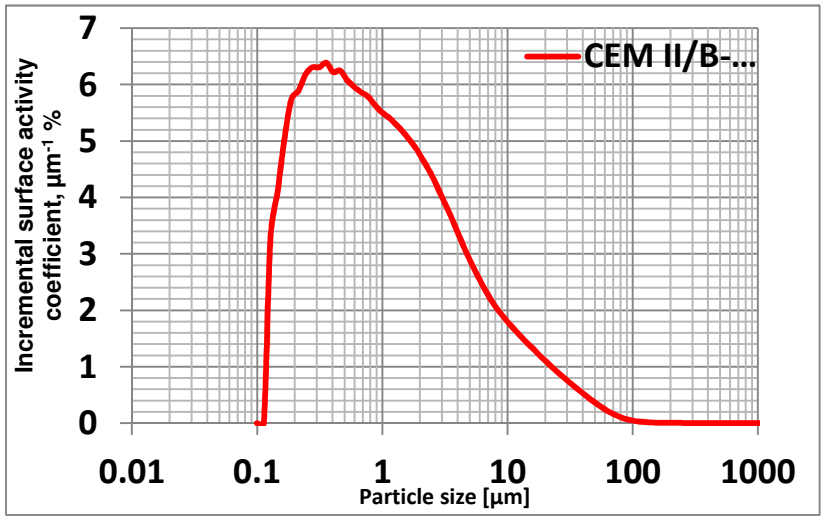

b)

Fig. 4. Particle size distribution (a) and coefficient of incremental surface activity Kisa (b) of Portland-composite cement CEM II/B-M(S-P-L) 32,5R

Isoparameter lines of influence of zeolite tuff and limestone powder concentration after 28-days and 90-days mortars strength in quaternary Portland-composite cements is shown in Figure 5. From these diagrams, the optimal balance between non-clinker constituents that realize the workability more than 190 mm flow and 28-days compressive strength greater than 38.2 MPa is 17.5 mass.% GGBFS, 10.0 mass.% zeolite tuff and 7.5 mass.% limestone powder.

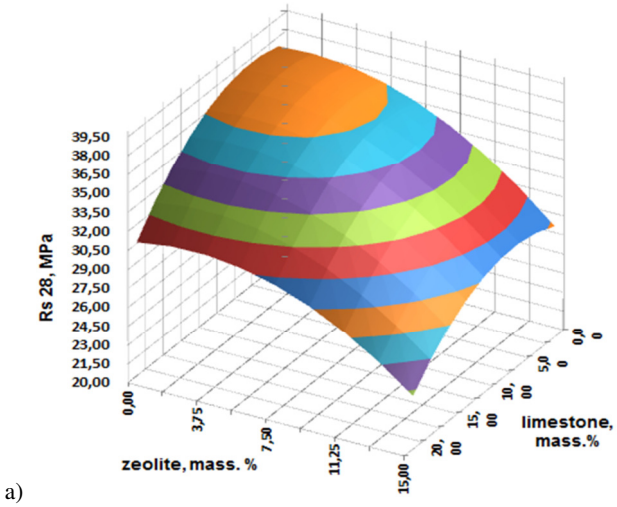

a)

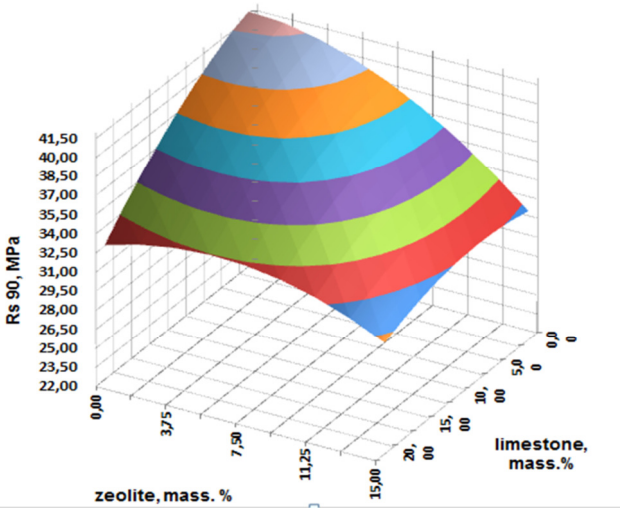

b)

Fig. 5. The isoparametric lines of 28-days (a) and 90-days (b) compressive strength of Portland-composite cement CEM II/B-M

For purpose of comparison, the X-ray diffraction lines of calcite at d/n=0.303, 0.249 nm, of the calcium hydroxide at d/n=0.490, 0.263 nm and of ettringite at d/n=0.973, 0.561 nm were chosen to follow up the variation in their intensities in the paste of the quaternary components mixed with a water/cement ratio of 0.4 and cured for 28 days (Figure 6). It was found that the intensity of the d-value lines of the calcium hydroxide is lower than those of the reference paste made of CEM I by around two folds. This is explained by the pozzolanic reactivity of the clinoptilolite present in the zeolite tuff used which promotes the binding of calcium hydroxide and form calcium silicate hydrates. Active forms of SiO_2 and Al_2O_3 in the composition of aluminum-containing pozzolana promote better binding of calcium hydroxide into low-basic calcium hydrosilicates, which indicates that the acceleration of puzzolanic reaction. This in turn affects the ultimate compressive strength, the permeability and chemical durability of quaternary zeolite-containing Portland-composite cements significantly.

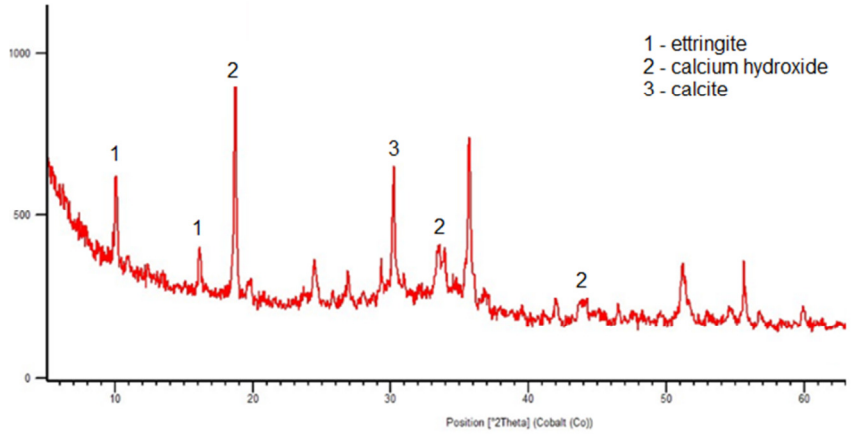

Fig. 6. X-ray diffraction lines of Portland-composite cement CEM II/B-M(S-P-L) 32,5R after 28 days of hardening

The dense structure of the hydrated solid phase is provided by AF_m- i AF_t-phases into gel-like C-S-H phase (Figure 7a). The use natural zeolite material containing clinoptilolite with high pozzolanic activity promotes fuller binding of calcium hydroxide in calcium hydrosilicates and significantly affects the ultimate compressive strength, permeability and chemical durability of quaternary zeolite-containing Portland-composite cements. According to EDX (Figure 7, b), the relative content of elements in interpore space in the sample of cement paste meets ettringite crystals. Fine particles of carbonate due to the effect of "fine powder" and chemical interaction with the products of hydration of alumo-containing phases with the formation of structurally active hexagonal AF_m-phases promote the synthesis of cement paste strength.

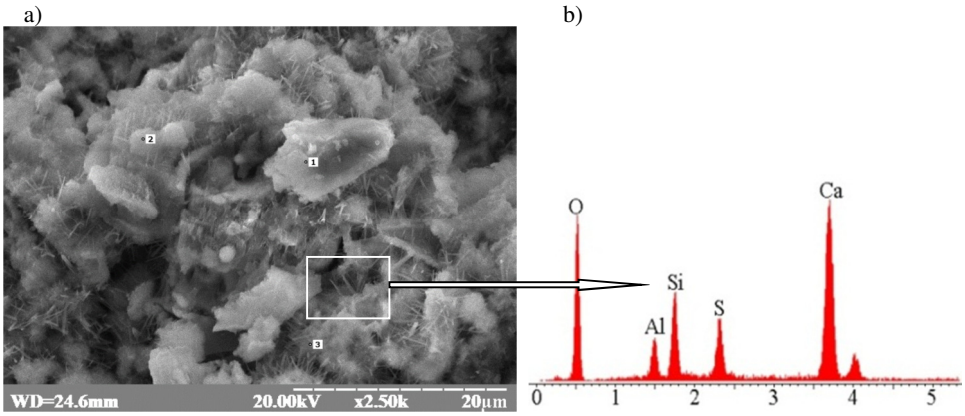

Fig. 7. SEM images (a) and EDX spectrum (b) of paste based on Portland-composite cement CEM II/B-M(S-P-L) 32,5R after 28 days of hardening

The research results of construction and technical properties of Portland-composite cement with zeolite tuff CEM II/B-M(S-P-L) 32,5R in Table 1. The optimum particle size distribution of the finely ground zeolite tuff and limestone powder provided high early strength of the quaternary Portland-composite cement CEM II/B-M(S-P-L) 32,5R. This cement was characterized by a high-water retention capacity of 98.9%, a homogeneity and a stability of the mix without sedimentation; the bleeding of Portland-composite cement paste is 15.2%. Furthermore, the GGBFS and zeolite tuff, as well the reduced CaO content suggested the improved chemical resistance to aggressive natural waters and soils. Non-clinker constituents GGBFS and zeolite tuff after 365 days provide higher resistance into aggressive sulfate $R_{sulphate}/R_{water}$=1.04 and magnesia $R_{magnesia}/R_{water}=1.01$ environments. The lowering clinker factor ratio in CEM II/B-M (S-P-L) 32,5R reduces the CO_2 discharge in the cement production process 1.46 times/ 1 ton cement.

Table 1. Properties of Portland-composite cement CEM II/B-M(S-P-L) 32,5R

Property	Results
Loss on ignition, %	1.17
Sulfate content (as SO_3), %	2.55
Water demand, %	29.0
High-water retention capacity, %	98.9
Bleeding, %	15.2
Segregation, %	3.9
Heat of hydration after 168 h, J/g	285
Sulphate resistance after 365 days	1.04
Magnesia resistance after 365 days	1.01

4. Conclusion

The rheological properties of the strength development of Portland-composite cement CEM II/B-M improve and its density increase due to the following factors: 1) the optimization of the particle size distribution of the constituents using the values of incremental coefficient of surface activity, 2) the effect of the hydraulic properties of the GGBFS combined with the pozzolanic action of the zeolite tuff, 3) the filling effect of the finely dispersed limestone powder, 4) the reduction in the clinker factor. Based on the results obtained, high quality quaternary zeolite-containing Portland-composite cements can be produced which advantage is to lower the energy consumption and CO_2 emission and the indication of a better sustainability.

References

[1] Schneider M., Romer M., Tschudin M., Bolio H. Sustainable cement production present and future. Cement and Concrete Research, Vol. 41, 7, p. 642–650, 2011.

[2] Sanytsky M., Kruts T., Kropyvnytska T., Rusyn B. Sustainable Green Engineered Composites Containing Ultrafine Supplementary Cementitious Materials. 14th International Congress on the Chemistry of Cement (ICCC 2015), Beijing, China, 1, p. 265.

[3] Muller M., Ludvig H-M., Ben Haha M., Zajac M. Optimization of multi-component cements containing cement clinker, slag, V-fly ash, limestone. 19th Internationale Baustofftagung, 2015, Weimar, Germany, 1, p. 449–456.

[4] Smrčková E., Bačuvčík M., Janotka I. Basic Characteristics of Green Cements of CEM V/A and V/B Kind. Advanced Materials Research, Vol. 897, p. 196–199, 2014.

[5] Snellings R., Mertens G., Elsen J. Evaluation of the Pozzolanic Activity of Natural Zeolite Tuffs. 14th International Congress on the Chemistry of Cement (ICCC 2015), Beijing, China.

[6] Kryvenko P., Sanytsky M., Kropyvnytska T., Kotiv R. Decorative multi-component alkali activated cements for restoration and finishing works. Advanced Materials Research, Vol. 897, p. 45–48, 2014.

Przesłano do redakcji: 24.11.2017 r.
Przyjęto do druku: 25.09.2018 r.

CZASOPISMO INŻYNIERII LĄDOWEJ, ŚRODOWISKA I ARCHITEKTURY
JOURNAL OF CIVIL ENGINEERING, ENVIRONMENT AND ARCHITECTURE
JCEEA, t. XXXV, z. 65 (3/18), lipiec-wrzesień 2018, s. 35-42, DOI:10.7862/rb.2018.40

Jarosław TATARCZAK[1]
Jarosław SIKORA[2]

THE USE OF THERMIONIC EMISSION PHENOMENON AS SUPPORT FOR RENEWABLE ENERGY SOURCES

Energy converters using the phenomenon of thermionic emission to generate electricity and their applications related to renewable energy sources (RES) have been presented. Taking into account new technical solutions, hybrid systems combining thermionic energy converters (TEC) with other energy generators, e.g. with PV cells, the Stirling engine, improving the efficiency of the entire electric energy generating system, have been described. Leading technologies related to thermionic energy conversion and TEC hybrid systems powered by solar radiation have been shown in the tables. The dynamic development of TEC technology in recent years, in our opinion, will contribute to the wider interest of research communities to use the thermionic emission phenomenon to generate electricity.

Keywords: thermionic emission, renewable energy sources, thermionic energy converters, hybrid systems, electric energy

1. Introduction

Renewable energy sources already were used by humans thousands of years ago for example to mill grain, allow traveling across the sea using to the strength of the wind. Over time, the importance of machinery increased, that were powered by the energy of water and wind movement [1]. In the industrial era many new technical solutions were created. In 1747, the French astronomer Jacques Cassini developed a solar furnaces, which was able to get the temperature above 1,000ºC. Then, in 1773 another French scientist Antoine Lavoisier obtained a temperature allowing melting of iron (above 1,500ºC). Currently, solar furnaces are able to heat, using a focused beam of sunlight, a given material up to a temperature of 3,000ºC [1, 2].

[1] Corresponding author: Jarosław Tatarczak, Politechnika Lubelska, Katedra Automatyki i Metrologii, ul. Nadbystrzycka 38A, 20-618 Lublin; jaroslaw.tatarczak@gmail.com
[2] Jarosław Sikora Politechnika Lubelska, Katedra Automatyki i Metrologii, ul. Nadbystrzycka 38A, 20-618 Lublin; tel. 81 538 43 04; jaroslaw.sikora@pollub.pl

During the intensive development of the industry (at the turn of the 17th and 18th centuries), the demand for fossil fuels (coal or oil) increased which were used by steam engines and then by combustion engines. At that time, an innovative technical solution emerged that was associated with the conversion of thermal energy directly into mechanical energy. It was a thermal engine created by Robert Stirling, patented in 1816 (Patent No. 4081). Currently, this engine can be powered by burning fossil fuels, using waste heat or by solar energy.

The photovoltaic phenomenon was first observed in 1839 by Alexandre Edmond Becquerel (the father of the future Nobel laureate in physics - Henri). He noted rise in electrical current as a result of a chemical reaction induced by sunlight [3]. This technology did not find a wider application until 1954 when the first photovoltaic (PV) module was developed in the Bell Laboratory for the space programs.

Due to the lack of oxygen in the orbital space, fuel combustion is not possible (or very complicated). Space programs have caused intensive development of converting thermal energy into electricity using thermionic emission powered by radioactive decays energy [6].

The phenomenon of thermionic emission has been studied since the late nineteenth century. In 1873, British scientist Frederick Guthrie observed that the red-hot iron ball in air could retain a negative charge [5]. Then in 1885, American inventor Thomas Edison observed the flow of electric current between hot and cold electrodes placed in a vacuum. Owen Richardson determined the relationship between the thermionic electron current density and the work function and the temperature of the cathode [5]:

$$J = A \cdot T_C^2 e^{-\varphi_C / kT_C} \tag{1}$$

where: A is the Richardson's constant, T_C is the cathode temperature, ϕ_C is the cathode work function, k is the Boltzmann's constant.

A device implementing energy conversion method using thermionic emission was called the thermionic energy converter (TEC) and was one of the first that directly converted thermal energy into electricity.

2. Analysis of TEC technology

TEC technology is divided into: vacuum (VTEC) and vapour (e.g. caesium) converter. An example of output current-voltage characteristic of VTEC, determined for $T_c = 1{,}200\,\mathrm{K}$, $T_a = 300\,\mathrm{K}$, $\varphi_c = 1{,}8\,\mathrm{eV}$, $\varphi_a = 1{,}2\,\mathrm{eV}$, $d = 10\,\mu\mathrm{m}$, is presented in Fig. 1.

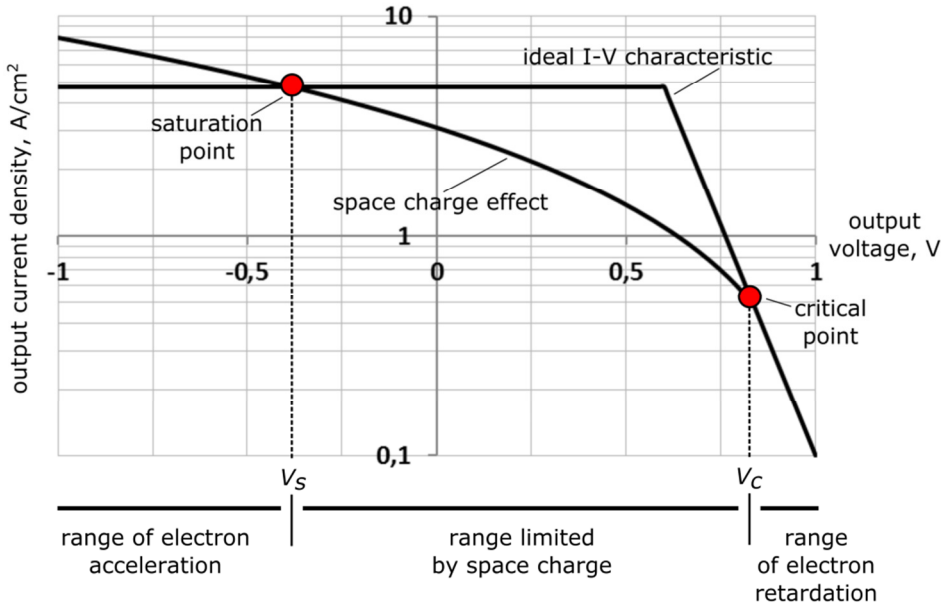

Fig. 1. An example of output current-voltage characteristic of TEC. V_s is saturation voltage, V_c is critical voltage

It is seen from this figure that the space charge decreases the output current density in respect to the ideal I-V characteristic. The main task of caesium vapour is to lower the work function of the cathode and reduce the effect of space charge [7]. The efficiency of the tested TEC converter was within the range of (0.5 ÷ 15.1)%, with maximum power densities: (0.2 ÷ 6) W/cm^2 [12].

Many technical solutions have been created, which were often combinations of TEC and an additional structural element. A list of leading technologies is given in the table below.

Table 1. Leading technologies related to thermionic energy conversion

Short name	Full name	First written references	Compatibility with RES
VTEC	vacuum thermionic energy converter	1959 [10]	✓
-	vapor thermionic energy converter	1962 [7]	✓
MTC	microminiature thermionic converter	2000 [9]	✓
PETE	photon-enhanced thermionic emission	2010 [10]	✓
NETEC	near-field enhanced thermionic energy conversion	2017 [11]	✓

The global trend towards miniaturization, also affect the development of technology TEC. In 2001, a microminiature thermionic converter (MTC) was patented. Reducing the distance between the electrodes limits the distance that electrons must overcome. This has a positive effect on the efficiency of TEC. The temperature of the proposed solution should be between 530 and 1,030ºC. Despite the promising model efficiency of 15÷25%, these values have not been achieved [8].

In 2010, a new phenomenon of photon-enhanced thermionic emission (PETE) was described [10]. PETE converter powered by sunlight gives the theoretical efficiency at: 11.2÷48.6%. However, assuming that an additional work cycle (e.g. Stirling engine) is connected to the PETE converter, the overall efficiency could be as high as 70.4% [12].

In 2017, for generating electric energy a near-field enhanced thermionic energy conversion was proposed [11].

3. Renewable energy sources and thermionic emission

Renewable energy sources are often related to a multi-stage energy conversion. For example, the difference in pressure in the atmosphere causes the air movement which powers the blades of the turbine, changing| the wind kinetic energy into the mechanical energy. This energy is then converted by electric generator for electricity. A similar situation occurs in the case of hydroelectric power plants which use potential and kinetic energy of water to power generation. Water that falls on the water turbine blades rotates the electric generator's rotor, thus generating electrical energy.

The use of biomass also requires the conversion of energy in many stages. In order to release the chemical energy accumulated in plants, they should be burned or gasified. The further stages of converting thermal energy is analogous to solutions in fossil fuel power plant. In such power plants, fuel (e.g. coal) is burned in the furnace and heats the water. Further, water is converted to steam. Then as a result of the pressure difference (compression and later condensation), it moves and rotates the steam turbine blades. Steam turbine drives a generator to produce electricity. This water cycle in a closed system is called the Rankine cycle. For gases, the Brayton-Joule cycle is the same process.

The above examples prove that the processes of energy conversion from RES are often multi-stage. Each stage has a certain efficiency of converting energy into another form. A solar radiation conversion into electricity has two important features. The first feature is the possibility of direct conversion of solar radiation into electricity (using, for example, photovoltaic cells). Consequently, the second feature is the lack of necessity to use moving parts.

Hybrid solutions combine several devices with different properties to improve the efficiency of the entire system. At each energy generation stage electricity would be obtained. For example, heat is supplied to the thermionic

energy converter (by solar radiation or biomass burning), resulting in electricity generation. Then wasted heat (from TEC) powers the next energy conversion stage, for example, Rankin cycle or Stirling engine.

4. TEC-RES hybrid systems

Thermionic energy converters are powered by heat. Heat sources (>1,000ºC) associated with RES require some technical solutions to concentrate energy. They can be divided into solutions: related to the combustion of biomass and the concentration of solar radiation. The last solution can be divided into five main categories of solar concentrators: heliostat field reflectors, parabolic dish reflectors, parabolic trough reflectors, linear Fresnel reflectors and Fresnel lenses [12].

Systems powered by solar energy are the most ecological solutions because they do not produce any greenhouse gases. The table below presents hybrid solutions of TEC devices powered by solar radiation.

Table 2. TEC hybrid systems powered by solar radiation

Short name		**PETE**	**TIPV**	**NETEC**
Full name		photon-enhanced thermionic emission	thermionic-photovoltaic converter	near-field enhanced thermionic energy conversion
An additional phenomenon		photoemission	photovoltaics	near field thermal radiation
The possibility of an additional cycle		Stirling engine, Rankin cycle	no data in the literature	no data in the literature
Max. efficiency	1,000ºC	41% [a)]	55%	39%
	1,200ºC	45% [b)]	52%	40%
Max. power density	1,000ºC	no data in the literature	1 W/cm^2	0.5 W/cm^2
	1,200ºC	no data in the literature	1.3 W/cm^2	1.05 W/cm^2
Literature (year)		[13] (2016)	[14] (2016)	[11] (2017)

Concentration of sunlight: [a)] x225 [b)] x1000

The technologies presented above have a diverse structure. The PETE converter, presented in Fig. 2a, uses at least two electrodes for converting solar radiation into electricity. Advanced solutions use a multi-junction system with different cathodes increasing the efficiency of the entire system, due to the more efficient conversion of selected wavelengths of solar radiation [13].

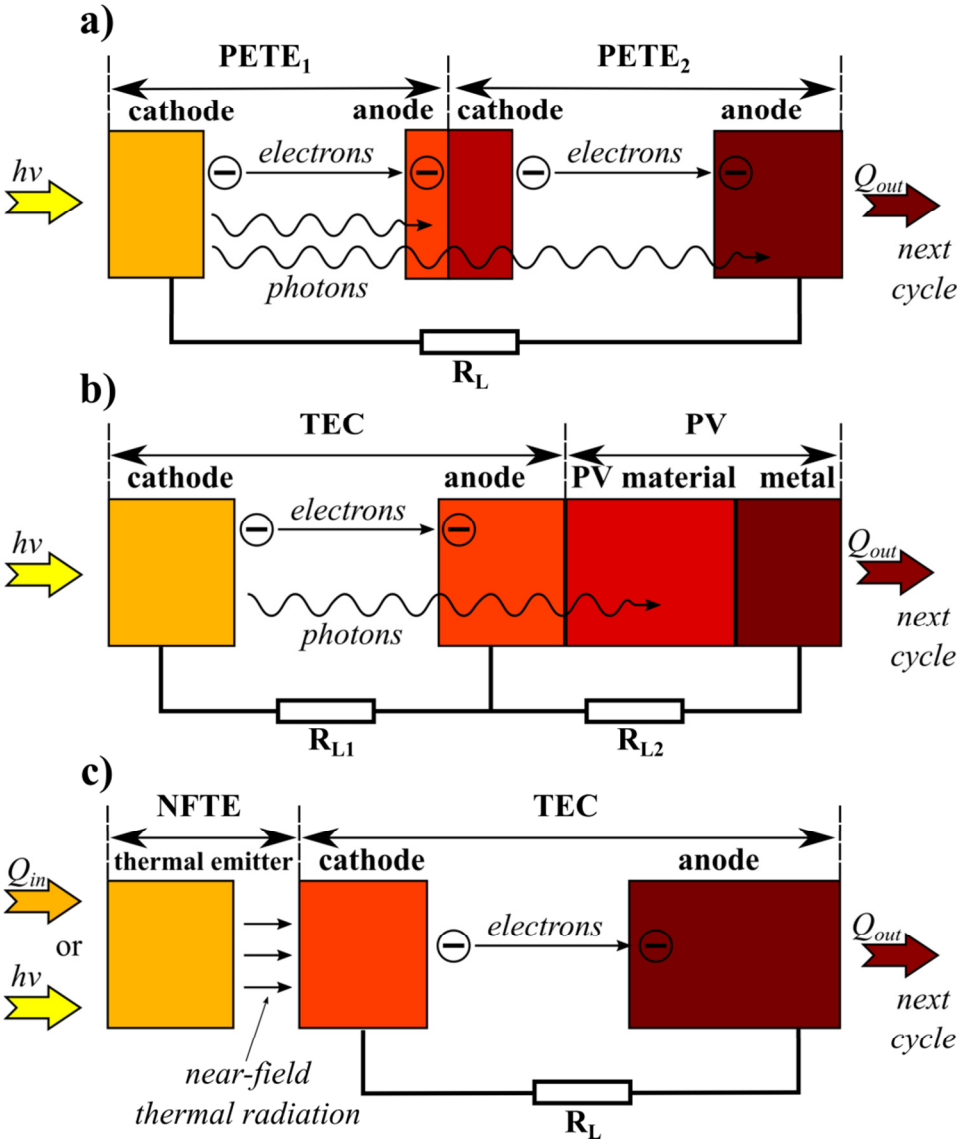

Fig. 2. Simplified diagrams of hybrid TEC technologies: a) PETE converter with a two-junction system [13], b) Thermionic-photovoltaic converter [14], c) TEC powered by a near field thermal radiation (NETEC [11]). R_L, R_{L1}, R_{L2}, are load resistor, Q_{in} is the input heat, Q_{out} is the output (wasted) heat, hv is the energy of light quantum

Thermionic-photovoltaic converter (Fig. 2b), used features of the thermionic emission and photovoltaic phenomenon, was proposed in 2016. A transparent anode (with low work function) of the TEC is connected to the PV converter. The PV material is GaSb or InGaAs. In the back of the TIPV, a metal reflector

reflects the high energy photons back to the PV layer. The anode and PV layer are maintained at a temperature of about 300K [14].

The next hybrid converter uses phenomenon occurring at the nano scale, so-called a near-field thermal radiation. A simplified diagram of the near-field enhanced thermionic energy converter (NETEC) is presented in Fig. 2c. It contains a thermal emitter which is separated from the cathode by a distance smaller than the radiation wavelength (less than 100 nm) which allows to generate ten times more electricity at a given temperature with respect to TEC type converters [11].

5. Conclusion

In relation to electricity generation, the phenomenon of thermionic emission over a long period of time was studied only by a small group of researchers, in compared to the photovoltaic phenomenon. The recent development of technology, including the emergence of new materials and technologies at the micro scale (MEMS), has contributed to the wider interest of research communities to use the thermionic emission phenomenon to generate electricity.

Currently, an important goal is, among others, to combine thermionic energy converters with other energy generators, e.g. with PV cells, the Stirling engine because hybrid solutions can significantly improve the efficiency of the entire electricity generating system powered by renewable energy sources.

References

[1] B. Sørensen, A history of renewable energy technology, Energy Policy, vol. 1, pp. 8–12, 1991.

[2] J. B. Gálvez, S. M. Rodríguez, E. Delyannis, V. G. Belessiotis, S. C. Bhattacharya and S. Kumar, Solar Energy Conversion And Photoenergy Systems: Thermal Systems and Desalination Plants-Volume I, EOLSS Publications, pp. 366–370, 2010.

[3] L. E. Chaar, L. A. Lamont and N. E. Zei, Review of photovoltaic technologies, Renewable and Sustainable Energy Reviews, vol. 5, pp. 2165–2175, 2011.

[4] D. B. Go, J. R. Haase, J. George, J. Mannhart and R. Wanke, Thermionic energy Conversion in the Twenty-first Century: Advances and Opportunities for Space and Terrestrial Applications, Frontiers in Mechanical Engineering, pp. 1–17, 2017.

[5] O. W. Richardson, Thermionic phenomena and the laws which govern them, Nobel Lecture, 1929.

[6] B. Kania, Termoemisyjne generatory energii elektrycznej – problemy, rozwiązania, zastosowania, Trendy i rozwiązania technologiczne – odpowiedź na potrzeby współczesnego społeczeństwa, tom 2, Lublin, Wydawnictwo Naukowe TYGIEL, 2017.

[7] N. Rasor, The cesium vapor thermionic converter. I. Limitations imposed by emission processes, Advan. Energy Conversion, 1962.

[8] D. B. King, L. P. Sadwick and B. R. Wernsman, Microminiature Thermionic Converters. USA Patent US 6,294,858 B1, 2001.

[9] D. B. King, K. R. Zavadil and J. A. Ruffner, Results from the microminiature thermionic converter demonstration testing program, Collection of Technical Papers. 35th Intersociety Energy Conversion Engineering Conference and Exhibit (IECEC), pp. 272–282, 2000.

[10] J. W. Schwede, I. Bargatin, D. C. Riley, B. E. Hardin, S. J. Rosenthal, Y.Sun, F. Schmitt, P. Pianetta, R. T. Howe, Z. Shen and N. A. Melosh, Photon-enhanced thermionic emission for solar concentrator systems, Nature Materials, p. 762–767, 1 August 2010.

[11] M. Ghashami, S. K. Cho and K. Park, Near-field enhanced thermionic energy conversion for renewable energy recycling, Journal of Quantitative Spectroscopy and Radiative Transfer, vol. 198, pp. 59–67, 2017.

[12] G. Xiao, G. Zheng, M. Qiu, Q. Li, D. Li and M. Ni, Thermionic energy conversion for concentrating solar power, Applied Energy, pp. 1318–1342, 2017.

[13] G. Segev, Y. Rosenwaks and A. Kribus, Limit of efficiency for photon-enhanced thermionic emission vs. photovoltaic and thermal conversion, Solar Energy Materials & Solar Cells, vol. 140, p. 464–476, 1 May 2015.

[14] A. Datas, Hybrid thermionic-photovoltaic converter, Appl. Phys. Lett., pp. 1040–1055, 2016.

Przesłano do redakcji: 26.04.2018 r.
Przyjęto do druku: 25.09.2019 r.

CZASOPISMO INŻYNIERII LĄDOWEJ, ŚRODOWISKA I ARCHITEKTURY
JOURNAL OF CIVIL ENGINEERING, ENVIRONMENT AND ARCHITECTURE
JCEEA, t. XXXV, z. 65 (3/18), lipiec-wrzesień 2018, s. 43-53, DOI:10.7862/rb.2018.41

Olena MITRYASOVA[1]
Nataliya BOGATEL[2]
Piotr KOSZELNIK[3]
Renata GRUCA-ROKOSZ[4]

WASTEWATER CONTROL SYSTEM AS AN ASPECT OF ENVIRONMENTAL ASSESSMENT OF INDUSTRIAL ENTERPRISE'S ACTIVITY

In order to reduce the influence of wastewater from enterprises on the environment extreme relevance is gained by improvement of the monitoring system at each stage of technological process. A new tool is calculation of the polluting substances concentration is suggested to be entered into the monitoring system on the basis of determination of material balance of technological process of production that will allow prediction of qualitative and quantitative composition of sewage for the selected period. The system can be used in any enterprise, but the example with all calculations is given for the Mykolaiv Branch of "SUN InBev Ukraine" which became the object of research. The scope of the study covered the process of wastewater formation of the enterprise. Realization of tasks demanded the use of general scientific methods: analysis, synthesis, systematization and generalization in the course of studying of the corresponding literature on the research subject; modelling, formalization, comparison – at drawing up the calculation scheme of concentration of the polluting substances in sewage; supervision - during studying the technological scheme of production; and also methods of mathematical data processing in MS Excel.

Keywords: wastewater, pollutants, material balance, environmental management

1. Introduction

Sewage from industrial enterprise is the main source of pollution of superficial water objects. The issue of environmental security enterprises of food industry, namely the aspects of qualitative composition of effluents, is presented

[1] Corresponding author: Olena Mitryasova, Petro Mohyla Black Sea National University, Mykolaiv, Ukraine, lesya.solis28@gmail.com, https://orcid.org/0000-0002-9107-4448
[2] Nataliya Bogatel, Petro Mohyla Black Sea National University, Mykolaiv, Ukraine
[3] Piotr Koszelnik, Faculty of Civil and Environmental Engineering and Architecture, Rzeszow University of Technology, Rzeszow, Poland, pkoszel@prz.edu.pl, https://orcid.org/0000-0001-6866-7432
[4] Renata Gruca-Rokosz, Faculty of Civil and Environmental Engineering and Architecture, Rzeszow University of Technology, Rzeszow, Poland, renatagr@prz.edu.pl, https://orcid.org/0000-0001-8222-2480

in publications (2–5). Control of sewage from plants now has only the statistical character. Therefore extreme relevance is gained by improvement of the monitoring system behind sewage at each stage of the technological process taking into the rules of acceptance of wastewater and surface water objects according standards (6; 7; 8−11). The system consists of drawing up a material balance of the technological process, definition of the main polluting substances on the basis of calculation of masses and concentration of the substances in sewage made for a certain period. A similar system allows seeing a full picture of impact of the enterprise on the environment, in particular on the water resources, to know, what impact each process has on the enterprise in the general sewage pollution. The system helps to determine the concentration of those substances in wastewater which is not defined with the use of laboratory measures. Though, complete to replacement of the laboratory control over sewage is not the purpose of the offered system, it can add its results, because single tests on wastewater are not always indicative.

The objective of the research is the modernization of the wastewater control system on the basis of calculation of substances' mass balance. In order to meet the objective there is a need to solve the following problems:

- the analysis of the technological process of the enterprise, drawing up scheme of sewage formation;
- the calculation of concentration of the polluting substances in sewage of the plant for a certain period;
- the development of recommendations on optimization of the wastewater control system.

The offered system can be used at any industry enterprise, but the example with all calculations is provided for the Mykolaiv Branch of "SUN InBev Ukraine" which became the object of the research. The formation process of wastewater of the enterprise has been selected as the scope of research.

General scientific methods are applied in order to execute the tasks such as analysis, synthesis, systematization and generalization; modelling, formalization, comparison drawing up the scheme of calculation of the polluting substances concentration in sewage; supervision during studying the technological scheme of production and also methods of mathematical data processing in MS Excel.

2. Methods and experimental procedures

The modern wastewater control system in Ukraine consists in periodic sampling, carrying out the laboratory analysis of their structure and informing the enterprise on the conducted research (Fig. 1). However, the prospect of achieving sustainable development is possible when not only a simple measurement of sewage composition is taken, and when their structure is controlled at each production phase. Such system allows the presentation of a positive impact of the plant on the environment, to estimate the contribution of

each division to the general influence, to control the sewage formation process and to operate production in order to reduce the impact on the environment. There is a possibility of forecasting the qualitative and quantitative composition of sewage for any period in all divisions of the enterprise, which is an essential addition to the laboratory methods of analysis, which are not always indicative, demand time, not all elements of a substance can be defined.

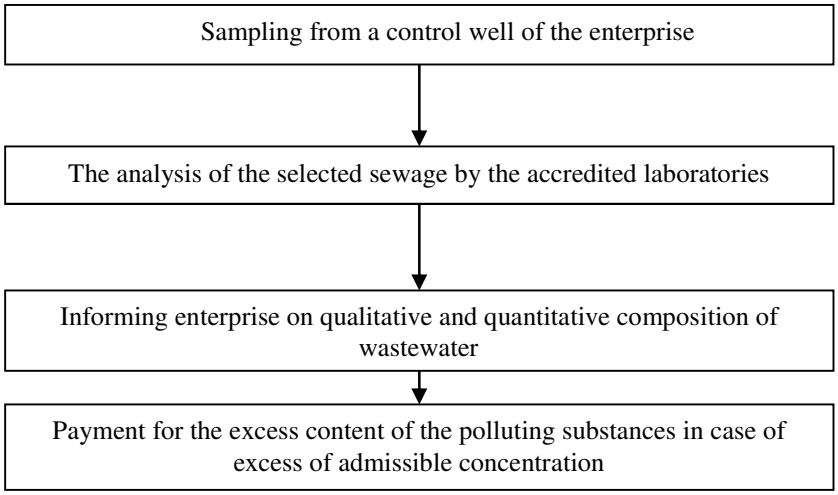

Fig. 1. The present wastewater control system

For modernization of the wastewater control system there was a need of studying of the technological scheme of production. The analysis of the process (the production of beer as an example of enterprise "SUN InBev Ukraine") showed the main points of wastewater formation:

1) Reception of barley and malt (there is no use of chemicals and dumping of industrial sewage).
2) Barley crushing (there is no use of chemicals and dumping of industrial sewage either).
3) Preparation of water for beer production: chemicals for reduction of water in the corresponding quality are used.
4) Preparation of beer wort consists of the following stages:
   - grout – extraction of malt's soluble substances and transformation under the influence of enzymes of insoluble substances;
   - filtration – separation of beer mash from a pellet. Mash and insoluble substances in water - a pellet is received [5];
   - mash boiling with hop. Mash comes to the machine where hopes are added and boiled. Mash is sterilized during cooking; enzymes are inactivated; bitter substances of hop are dissolved in mash, proteins coagulate [2];

- separation from hop and cooling [5]. The sewage containing organic pollution, particles of diatomaceous earth, a pellet and the dissolved components of detergents are respectively formed.

5) Mash is fermented. Special types of cultural yeast are used in brewing which ferment mash with formation of alcohol and carbon dioxide [3]. Fermentation takes place in two stages:
   - main fermentation. It is characterized by intensity of the process and fermentation of the most part of sugars (maltose, glucose, fructose and others);
   - young beer is cooled for the best sedimentation of yeast and transferred for the subsequent main fermentation.

   The waste, containing organic pollution, shares of yeast, pellets, beer and dissolved components of detergents are respectively formed.
6) Ready beer is filtered on the kizelgur filters. For beer which is poured in barrels, using separations. At this stage water and detergents are used, the sewage containing components of the used means and organic pollution is formed [3].
7) Preparation of a container and beer barrelling: water for washing a container with the use of the aggressive washing substances. The sewage is sated with various aggressive substances from the remains of labels gets to the sewage, flew down and so forth.
8) Department of quality control of beer: a number of chemicals which are necessary for determination of quality indicators of the ready-made product, mash, malt, water and so on are used. Insignificant pollution of very low concentration gets to sewage.
9) Department of logistics: low-quality beer merges in the sewerage that means high organic pollution.
10) Auxiliary production: water is also used for economic domestic needs.

The carried-out analysis allows determination of the main divisions polluting sewage such as department of brewing, including filtration, packing and logistics. Therefore it is necessary to study the means that are used in these divisions, and what polluting substances compose the sewage. The brewing department uses a number of chemicals and means. At the brewing stage: solution of nitric acid HNO_3; solution of phosphoric acid H_3PO_4; solution of sodium hydroxide NaOH; P3-stabicip OXI; P3-topactive 200; at the stage of fermentation and filtration of beer: solution of nitric acid HNO_3; solution of sodium hydroxide NaOH; P3-oxonia active 150; P3-topax 66; P3-oxonia; P3-trimeta DUO; Hlorantoin; P3-ansep CIP. The mentioned substances get to the sewage together with organic pollution: shares of the yeast; extract losses; beer losses; diatomaceous earth shares; share pellet.

The packaging department of uses the following materials: solution of phosphoric acid H_3PO_4; solution of nitric acid HNO_3; solution of sodium

hydroxide NaOH; P3-oxonia active; P3-topax686; P3-topax 56; P3-stabilon WT; P3-oxonia; P3-stabilon plus; P3-topactive 200; P3-topactive DES; DryExx; P3-polix XT; P3-lubodrive; P3-oxonia active 150; P3-ansep CIP.

The Logistics department conducts regular showers substandard products.

The chemical compositions of means which are used by enterprise were studied. For example, detergent P3-topax56 is characterized by the following composition: H_3PO_4 – 25÷30%; 2-(2-butoksyetoksy) ethanol – 2.5%; surfactant (alkylaminoxides) – 2.5%; P – 9.6 %, N – 0.18%, COD – 170 mg O_2/g. Similar results obtained for all means, but we choose to calculate the average amount of each substance content.

The technological scheme of production with the image of the main stages is made for modernization of wastewater control system. We will represent all necessary resources, chemicals and means which are used in the enterprise and which as a result can get to the composition of sewage in Fig. 2. Thus technological operation is "a black box" for us. We are interested in only those substances which are on the entrance and at the exit at the technological process.

At the exit, wastewater will be full of those substances that are used in the company at a particular time. Besides, from the brewing department the remains of beer, yeast, diatomaceous earth, a pellet and extract get to the sewage. Their structure may be different, however, for calculation we use their average data given to contents of nitrogen, phosphorus and COD.

Analyzing the composition of the means used at the enterprise, the structure of organic pollution, and the Rules of Admission of Sewage in the Municipal Sewerage of the City to control composition of sewage, we choose the following indicators:

- COD − this indicator is given for all used means, and also for organic pollution. It is an integrated and informative indicator of water pollution [4];
- phosphates are a part of some means;
- surfactants are part of some means;
- nitrogen content calculated by the nitrate form, as part of some assets is nitric acid. Nitrogen in the ammonium and nitrite form, regulated by the Rules, is not contained in the compounds, but it is a part of organic matter, and then can go into the ammonia, nitrite and nitrate form. Based on this we also take into account the total content of nitrogen.

As daily calculation is made generally to know the load of local treatment facilities, it is necessary to consider also the general content of phosphorus. Therefore this indicator will also enter the calculations.

The analysis of structure of the used substances shows that the numerous amounts of chemicals are their part. All these substances will be presented in the form of certain indicators: COD, phosphates, surfactants, nitrates, general nitrogen.

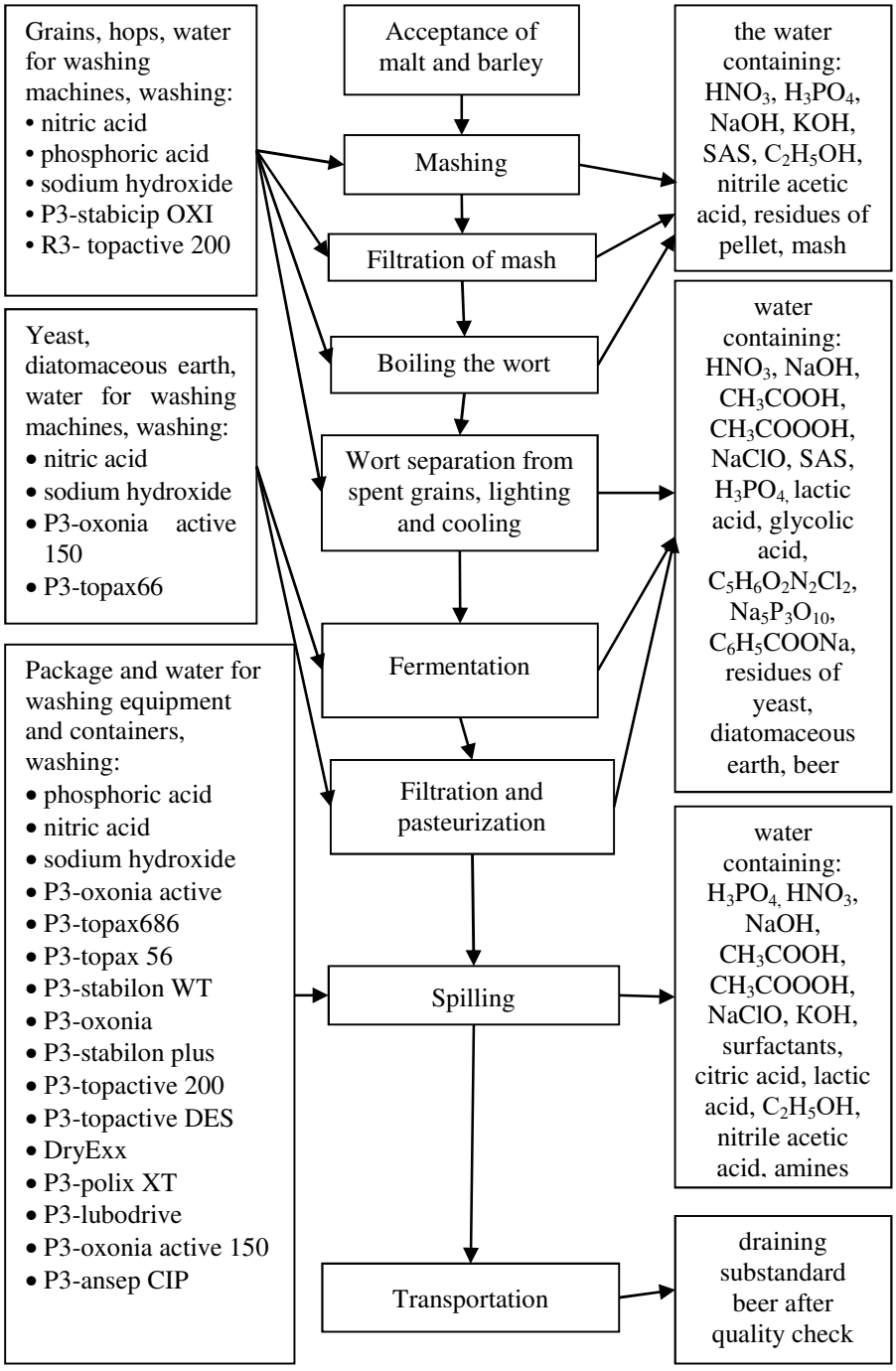

Fig. 2. Scheme of wastewater formation

The calculation procedure is presented by the list of actions. The example is given for one month:

1. To determine the mass of a pollutant using the formula (1):

$$m(pollutant) = w(pollutant\ in\ mean) \cdot m(men) = \frac{M(pollutant\ in\ substance)}{M(substance)} \cdot w(substnce\ in\ mean) \cdot m(mean), g \quad (1)$$

where: *M (pollutant in substance)* − the molar mass of the pollutant in the substance, g/mol,
M (substance) − the molar mass of the substance, g/mol,
w (substance in mean) − mass fraction of substance containing pollutants in means,
m (mean) − the mass of the used means, g.

The calculation was performed for each of the selected pollutants, determining the mass of phosphate, nitrate, total nitrogen, surfactants, COD and for each mean used in departments: brewing, packaging and logistics. For example, to find the mass of phosphates, we determine their weight in substance which contains phosphates. In the brewing department of phosphates contain only in P3-trimeta DUO in the form of phosphoric acid. For example we find the mass of phosphates using the formula 1 if we know the mass of means and a share of phosphoric acid:

$$m(PO_4^{3-} in\ P3 - trimeta\ DUO) = \frac{95\frac{kg}{kmol}}{98\frac{kg}{kmol}} \cdot 0.4 \cdot 525kg = 203.57\ kg$$

COD indicator for each means is given in mg O_2/g, and the mass of means is considered in kg. Therefore COD for various means is determined by a formula (2):

$$COD_{tot.mean} = COD_{mens} \cdot m_{mean} \cdot 1000, mg\ O_2 \quad (2)$$

For organic pollution we use the accepted data, considering the formula (3):

$$COD_{tot.substance} = COD_{substance} \cdot m_{substance} \cdot 1000, mg\ O_2 \quad (3)$$

To calculate the COD for the brewing department one should consider the following substances: P3-topax66, P3-trimeta DUO, P3-ansep CIP, and the remains of diatomaceous earth, yeast extract and beer pellet that enter the wastewater.

2. Determine the total mass of a particular pollutant in the department and across the entire enterprise according formula (4).

$$\Sigma m(pollutant) = \Sigma m\left(pollutant_{d.brewing.}\right) + \Sigma m\left(pollutant_{d.packaging.}\right) + \Sigma m\left(pollutant_{d.logistics.}\right) \quad (4)$$

where: $\Sigma m\ (pollutant_{d.brewing.})$, $\Sigma m(pollutant_{d.packaging.})$, $\Sigma m(pollutant_{d.logistics.})$ - the total weight of a particular pollutant for a specific branch, consisting of a mass of pollutant in each mean.

3. To determine the concentration of pollutants using the formula (5):

$$c(pollutant) = \frac{\Sigma m(pollutant) \cdot 1000}{V(wastewater}, g \cdot m^{-3} \quad (5)$$

where: $\Sigma m\ (pollutant)$ - the total mass of pollutants in all substances, kg,
$V\ (wastewater)$ - the amount of wastewater for a certain period, m^3.

Example of calculation of concentration of phosphates (volume of wastewater is 14,779 m^3):

$$c(PO_4^{3-}) = \frac{482.97kg \cdot 1000}{14779m^3} = 32.67\ \frac{g}{m^3}$$

4. To predict the level of pollution and to make the relevant decisions, for each substance we determine the planned volume of its usage, and also we can compare the planned norm of use with a real volume. Such tool allows fast identification of the main sources of pollution, those departments which exceed the norms of use and to taking measures for rapid response to reduction of impact on the environment. For this purpose in calculation we will define not only the actual volume of use of means, but also the planned one. For determination of the planned mass of use of a certain means we use a formula (6):

$$m_{planned} = norma \cdot V_{panned.bear} \quad (6)$$

here: *norma* – the rate of use of a specific product, $kg \cdot hl^{-1}$,
$V_{planned.besr}$ – the amount of beer that planned release, hl.

Here is an example of calculation for the brewing department of nitric acid, $V_{planned.bear} = 78930$ hl:

$$m_{planned}(HNO_3) = 0.07\frac{kg}{hl} \cdot 78930ch = 5525.1kg$$

To calculate the actual number of specific product per a production unit, use the formula (7):

$$costs = \frac{m_{actual}}{V_{actual.beer}} \tag{7}$$

where: m_{actual} – the actual mass of the used means, kg

$V_{actual.beer}$ – the volume of beer actually released, hl.

5. The result is the generalized data where the mass of the polluting substances on departments, their total mass and concentration are specified.

To show viability and effectiveness of a similar calculation we show the obtained data in the form of the schedule. Fig. 3 shows the calculated COD for the selected period indicating the volume of beer produced.

Such calculation is necessary to exercise control of compliance to admissible concentration not to be relied by single analyses which often happen inexact, for decision-making and modification of the technological processes, for adaptation of the technological process of production to new requirements, for the best representation of an overall picture of activity of the enterprise.

Thus, the proposed system of calculation of concentration of the pollutants is the additional effective instrument of the wastewater control system of the plant, allows identification of the processes that causes the most pollution. This system allows making decisions on reduction of influence on environment by change or improvement of production process, replacing some means so on (Fig. 4).

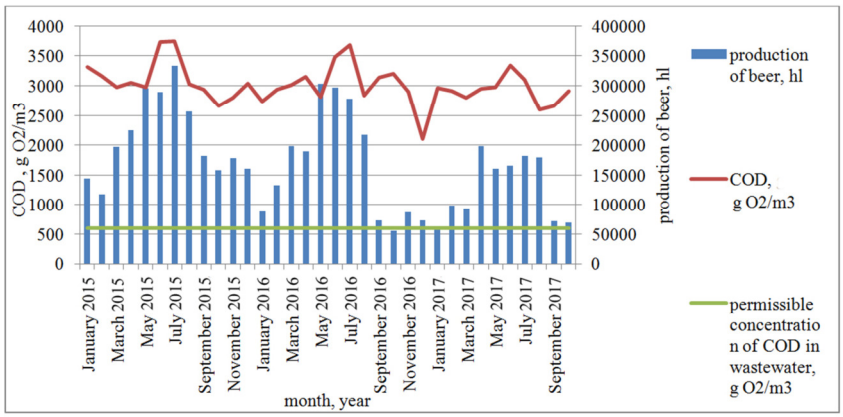

Fig. 3. The dynamics of the COD indicator changes calculated COD of wastewater

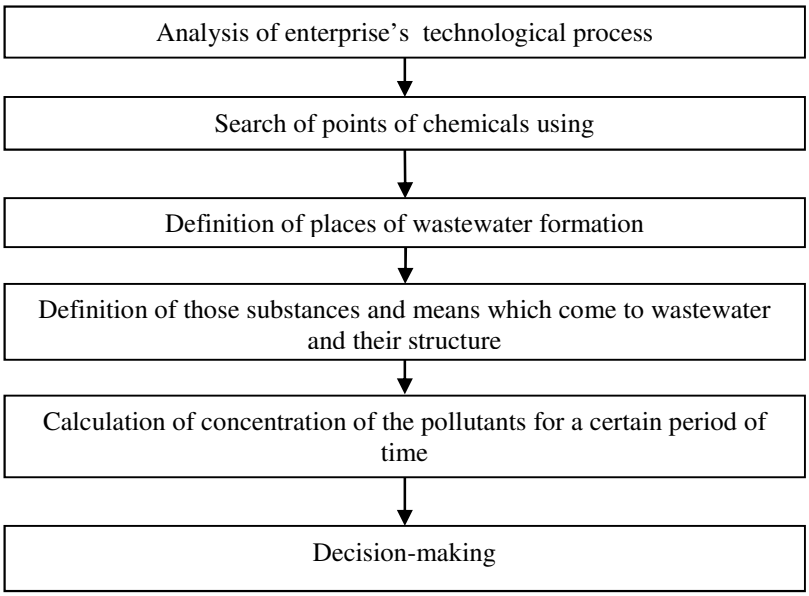

Fig. 4. The modernization wastewater control system

3. Conclusions

The proposed wastewater control system is one of the main aspects of environmental assessment of industrial enterprise's activity. The main problem of the plants of the brewing industry is the use of a great amount of water and the formation of the wastewater polluted by various substances. The pollutants consist of a pellet, diatomaceous earth, yeast, beer remains, etc., and also components of those means which are used in the plant in the certain period of time. The wastewater control system has the stating character: single tests at the exit from the enterprise one time a week are investigated, and then it is determined if the company complies with the standards, but this approach is not quite correct. Therefore, there is a need to carry out a continuous wastewater control by the introduction of the new tool on the basis of calculation of the pollutants concentration.

This system has a number of functions: illustrative, as it shows all production processes and gives a better picture of the overall impact on the environment; controlling, as calculation shows the stage on which of the process the most waste water is generated, which unit is the biggest polluter; the result is valid, not single concentration of pollutants; predicting: by data of the use norms of means and of the planned quantity of production, we can expect the qualitative and quantitative composition of wastewater at the exit from each department and from the enterprise in general; management, after all, on the basis of the analysis of the obtained data on processes which make the greatest

pollution, it is possible to make operational decisions on reduction of impact on environment; informative: provided data on the concentrations of substances, including those that are not controlled by laboratory methods.

The recommended system is not intended to replace the laboratory analysis. It is the additional effective wastewater control instrument. It may be adapted for any other production.

References

[1] Mitryasova, O., Bogatel, N.: Modernization of the Wastewater Control System in the Food Industry. Agricultural Engineering, 4(156): 79–89, 2015.
[2] Kolotylo, D.M., Sokolovsky A.T., Garbuz S.V. et al.: Technological Processes of Industries. Kyiv, KNEU, ISBN 966-574-494-1, 2003.
[3] Kunze, B.: Technology of Malt and Beer. Translated from the German. St. Petersburg, Profissiya, ISBN: 5-93913-006-2, 2001.
[4] Muravyov, A.G.: Guidelines for the Determination of Water-quality by Field Methods. St. Petersburg, Christmas +, ISBN 5-89495-113-5, 2004.
[5] Kovalevskaya, L.P.: General Technology of Food Manufactures. Moscow, Kolos, ISBN 5-94343-104-7, 1993.
[6] The Guide to Environmental, Health and Work Protection for Brewing Production, 2007. http://www.ifc.org/wps/wcm/connect/a388c000488554ccb42cf66a6515bb18/Breweries%2B-%2BRussian%2B-%2BFinal_.pdf?MOD=AJPERES.
[7] ISO 14040. Environmental management − Life cycle assessment − Principles and framework, 2006. http://www.iso.org/iso/ru/catalogue_detail?csnumber=37456.
[8] Rules of Admission of sewage of the enterprises in municipal and departmental systems of the sewerage of settlements of Ukraine. 19.02.2002 No. 37.
[9] Rules of Admission of sewage in the municipal sewerage Mykolaiv. – Mykolaiv: Mykolaiv city council. Executive committee, 2003.
[10] Rules of protection of a surface water from pollution by sewage. 25.03.1999 No. 465.
[11] Water Code of Ukraine from 06.06.1995 № 213 / 95-BP. http://www.transport-ukraine.eu/en/docs/water-code-ukraine.

Przesłano do redakcji: 29.08.2018 r.
Przyjęto do druku: 28.09.2018 r.

CZASOPISMO INŻYNIERII LĄDOWEJ, ŚRODOWISKA I ARCHITEKTURY
JOURNAL OF CIVIL ENGINEERING, ENVIRONMENT AND ARCHITECTURE
JCEEA, t. XXXV, z. 65 (3/18), lipiec-wrzesień 2018, s. 55-63, DOI:10.7862/rb.2018.42

Viola HOSPODAROVA[1]
Nadezda STEVULOVA[2]
Vojtech VACLAVIK[3]
Tomas DVORSKY[4]

PROPERTIES OF COMPOSITES INCORPORATING CELLULOSIC FIBERS

Nowadays, with the understanding of the importance of the green building concept, there is a constantly increasing demand for ecological construction materials. The application of raw materials from renewable sources such as wood, plants and waste to building materials preparing has gained a significant interest in this research area. With the consideration of environmental consciousness, natural fibers are biodegradable so as they can alleviate the problem of massive solid waste produced and relief the pressure of landfills, they are used for replacing other non-degradable materials for product development.
In this experimental work, wood pulp and recycled waste paper fibers in addition 0.2%, 0.3% and 0.5% were used. The fiber cement composites were subjected to a characterization of their composition including the assessment of a complex set of basic physical and mechanical properties after 7 and 28 days of hardening. Experimental results show that application of small amount of cellulosic fibers lead to a reduction of density up to 6% when compared with the reference composite. However, cement composites based on wood pulp showed better mechanical properties such as compressive and flexural strength in comparison with cement composites with recycled waste paper fibers.

Keywords: cellulosic fibers, building material, fiber cement composite, density, mechanical properties

[1] Corresponding author: Viola Hospodarova, Technical University of Kosice, Faculty of Civil Engineering, Institute of Environmental Engineering, Vysokoskolska 4, 04200, Kosice, Slovakia, +421556024278, viola.hospodarova@tuke.sk

[2] Nadezda Stevulova, Technical University of Kosice, Faculty of Civil Engineering, Institute of Environmental Engineering, Vysokoskolska 4, 04200, Kosice, Slovakia, +421556024126, nadezda.stevulova@tuke.sk

[3] Vojtech Vaclavik, VŠB - Technical University of Ostrava, Faculty of Mining and Geology, Institute of Environmental Engineering, 17. listopadu 15/2172, 70833, Ostrava-Poruba, Czech Republic, +420597323377, vojtech.vaclavik@vsb.cz

[4] Tomas Dvorsky, VŠB - Technical University of Ostrava, Faculty of Mining and Geology, Institute of Environmental Engineering, 17. listopadu 15/2172, 70833, Ostrava-Poruba, Czech Republic, +420597323546, tomas.dvorsky@vsb.cz

1. Introduction

It is widely known that the rising carbon dioxide emissions level in the atmosphere is causing an increase of the global temperature of the earth that demands an urgent global response. In this sense, the atmospheric concentration of CO_2 has increased from a pre-industrial concentration of about 280 ppm to around 390 ppm at present. Approximately 50% of these emissions are produced by the building sector, during both the construction and the operational phase of buildings. The building sector is responsible for about 40% of the European Union total final energy consumption and 36% of its total CO_2 emissions. Innovations to improve the energy efficiency of buildings are thus of practical importance [1]. The field of environmental engineering has emerged to investigate ways of enhancing the ecological value of concrete structures in an effort to maximize their potential and reduce carbon footprint. The environmental footprint of concrete can be reduced by both ways. One is a partial replacement of traditional binder – Portland cement by alternative pozzolanic by-products [2] and waste materials [3], the second opportunity is to use natural fibers/aggregates as filler replacement. With respect of these ideas, the use of more environmentally friendly materials obtained from renewable sources with sustainable processes could be an interesting solution for the reduction of CO_2 emissions [4].

Renewable ligno/cellulosic raw materials are one of the most promising biodegradable polymers owning good mechanical properties and process ability. Natural fibers exhibit advantages such as low density, low cost, good thermal and acoustic insulation properties, easy processing, excellent strength and high specific modulus [5, 6]. Therefore, this fibrous material is widely used for processing so-called "green" or "eco" concretes [7].

Natural fibers such as sisal, jute, cotton, flax, hemp, kenaf, wood, agricultural waste and waste from papermaking process (waste paper) and so on, have already been considered as potential alternatives to traditional fibers (steel fiber, polymer fibers, glass fiber), given their environmental friendliness and ready availability in fibrous form and by the fact that they can be extracted from plant leaves at low cost [8, 9]. Natural fiber reinforced composites also offer other advantages such as reduced dependence on non-renewable energy/material sources, lower pollutant emissions, lower greenhouse gas emissions, enhanced energy recovery, and biodegradability. Composites with natural fiber reinforcements are currently considered amongst the most promising structural materials in sustainable engineering technologies [10].

Many studies describing the use of cellulose-based fibers as a reinforcement for cement-based composites have been published [11–13]. Also recycled cellulosic fibers obtained from waste paper packaging [14], waste packaging boxes and papers [12, 15] were used in cement based composites.

The aim of the present research was to investigate the use of cellulosic fibers coming from two sources (wood pulp and recycled waste paper) in cement

composites. Their physical (density) and mechanical properties (compressive and flexural strength) were tested after 7 and 28 days of hardening. Two types of cementitious composites were produced with various cellulosic fiber contents (0.2%, 0.3% and 0.5%) with the same w/c ratio of 0.55. For comparison there was prepared reference sample (without fibers).

2. Materials and methods

2.1. Materials

Ordinary Portland cement type I 42.5 N obtained from Cement Factory Ltd. (Povazska cementaren Ladce, Slovakia) was used in the preparation of all the cement-based samples. Standard silica sand as filler was acquired from company Filtracni pisky Ltd (Chlum, Czech Republic) in accordance with European standard STN EN 196-1 [16]. Two types of cellulosic fibers Greencel used in this experiment were supplied from company Greencel Ltd (Hencovce, Slovakia). The cellulosic fibers (Fig. 1) originating from different sources: bleached wood pulp and unbleached waste paper are different in the nature, morphology and dimensional characteristics. The physical and chemical properties of white wood pulp (GW-500) and grey waste paper fibers (G-500T) are presented in Table 1.

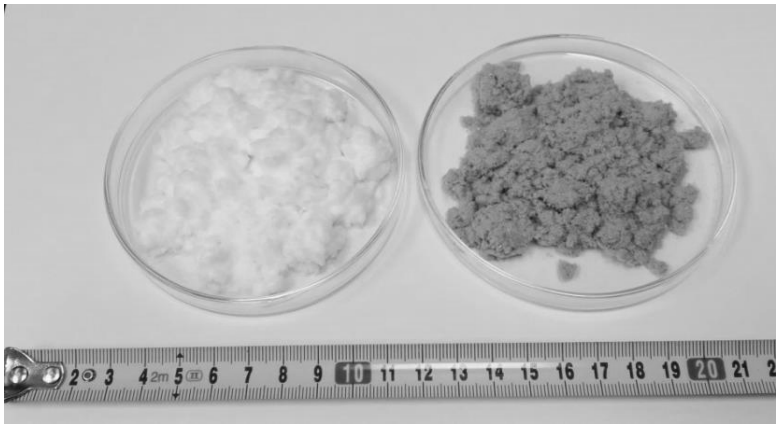

Fig. 1. Greencel cellulosic fibers from wood pulp (white GW500) and recycled waste paper (grey G-500T)

Table 1. Physical, chemical and thermal properties of Greencel cellulosic fibers

Cellulosic fiber	Cellulose content [%]	Bulk density [kg/m^3]	Max. length [μm]	Dry matter [%]	Ash [%]	Thermal conductivity [W/m.K]
GW-500	99.5	60–80	500	93	0.5	0.0674
G-500T	80	50–100	400	93	20	0.0634

2.2. Specimen preparation

Prepared cement mixtures contained 25% cement and 75% sand (cement/sand ratio of 3) at w/c ratio of 0.55. Tap water was used in preparation of mixtures in accordance with European standard STN EN 1008 [17]. The control sample was manufactured without addition of cellulosic fibers. The preparation of fiber-cement composite specimens was realized in two stages. At first, a given amount of cellulosic fibers (0.2; 0.3 and 0.5 wt.%) in the water (approximately 50 wt.% of water) was manually stirred to fiber soaking, followed with the addition of remaining water to suspension and next dispersing. Subsequently, cement and sand were added and continuous mixing by mixer to uniform fiber dispersion in the mixture proceeded. The prepared mixtures were then cast into standard prismatic steel molds (dimensions 40×40×160 mm), consolidating by a jolting apparatus and cured one day under laboratory conditions (+20°C). All samples were demolded after 24 hours and placed into water bath for up to 7/28 days. Each set of composite samples consisted of 3 prismatic bodies. Demolded fiber-cement composite samples were subjected to measurements of density and mechanical properties.

Densities of 7 and 28 days hardened fiber-cement composites were calculated in accordance with European standard STN EN 1015-10 [18]. Compressive strength and flexural strength of prepared cement samples reinforced with cellulosic fibers were measured by using a combined compression/three point bending test machines (FORM+TEST Seidner & Co. GmbH, Riedlingen, Germany) in accordance with the specifications of STN EN 1015-11 [19].

3. Results and discussion

3.1. Density of fiber cement composites

As shown in Fig. 2, changes in densities of 7 and 28 days hardened cement composites reinforced with varying amount (0.2; 0.3 and 0.5 wt.%) of cellulosic fibers obtained from wood pulp and waste paper fibers are observed. Densities of tested composites with cellulosic fibers in the matrix after 7 and 28 days hardening ranged from 2229 to 2105 kg/m^3. The increasing amount of cellulosic fibers in the hardened composites led to their lower densities about 6% when compared to reference composites. This is caused by incorporation of lightweight cellulosic fibers into the cement matrix and due to this fact density of fiber cement composite decreases in accordance with the results in paper [20]. The density values of composites based on cellulosic fibers from bleached wood pulp (GW-500) are slightly higher than values of composites with fibers from recycled paper (G-500T).

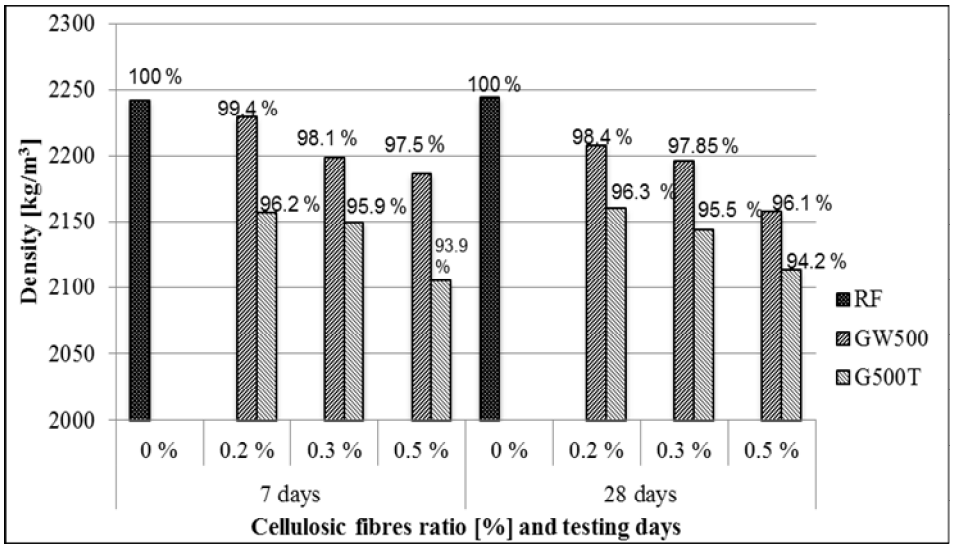

Fig. 2. Density of 7 and 28 days hardened fiber-cement composites with cellulosic fibers adding compared to reference composite RF (data in percentages above the columns indicate the ratio of the densities of fiber composites and reference composite)

3.2. Mechanical properties of fiber cement composites

The mechanical properties of cement composites reinforced with cellulosic fibers were analyzed by testing the compressive and flexural strength with three-point bending. As it can be seen in Figs. 3, 4, the cellulosic fibers addition to the matrix leads to gradual decrease in compressive and flexural strength values of 7 and 28 days cured cement composites with increasing fiber amount. However, strength values of all fibers cement based composites are lower when compared with strength parameters attributed to the reference samples. As concluded in [21, 22], adding cellulosic fibers to concrete resulted in similar behavior of fiber reinforced cement composites. This decrease in compressive and flexural strength of cellulosic fiber reinforced cement composite is probably caused by formed air voids due to the incorporation of fibers in cement matrix resulting in a reduction of bond strength between fibers and of the matrix particles, leading overall reduction in strength [23]. Composites containing cellulosic fibers from wood pulp reached higher strength values by 6–10% in comparison to cement composites reinforced with waste paper fibers. Compressive strength value of 28 days hardened concrete sample with 0.5% wood pulp (GW-500) addition was reduced by 15%, whereas the decrease in strength parameter of composite reinforced with fibers from recycled paper was even lower 26%.

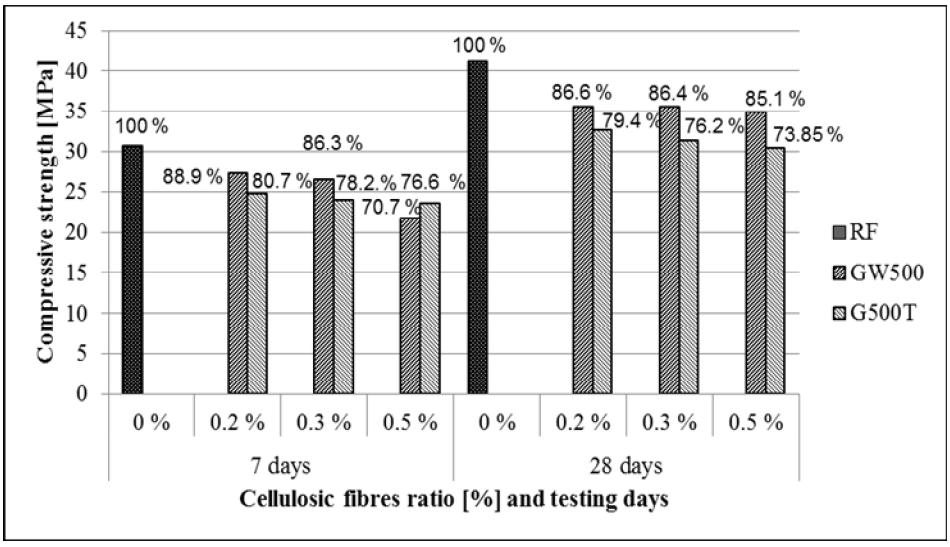

Fig. 3. Effect of Greencel cellulosic fibers adding on compressive strength of 7 and 28 days hardened fiber cement composites in comparison to reference composite RF (data in percentages above the columns indicate the ratio of the compressive strengths of fiber composites and reference composite)

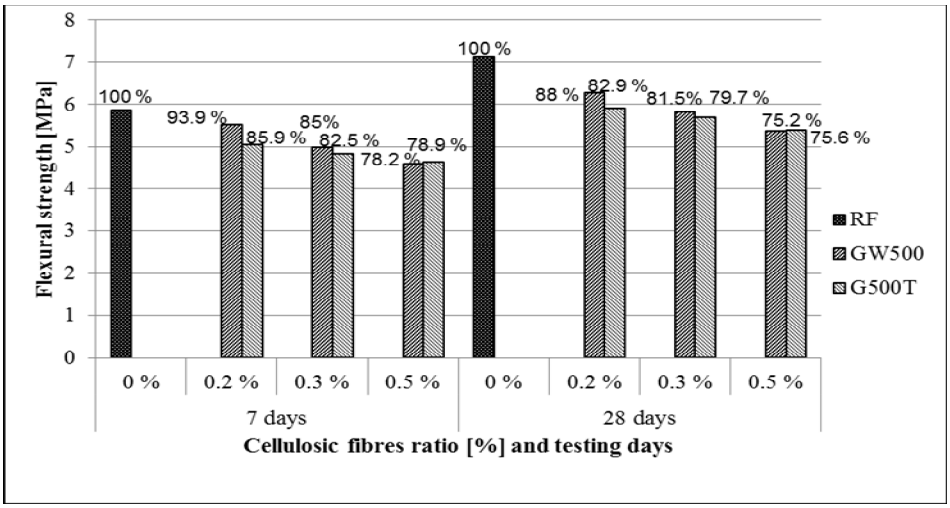

Fig. 4. Effect of Greencel cellulosic fibers adding on flexural strength of 7 and 28 days hardened fiber cement composites in comparison to reference sample (RF) (data in percentages above the columns indicate the ratio of the flexural strengths of fiber composites and reference composite)

As shown in Fig. 5, linear relationship between compressive strength and density of fiber cement composites after 28 days of hardening is observed.

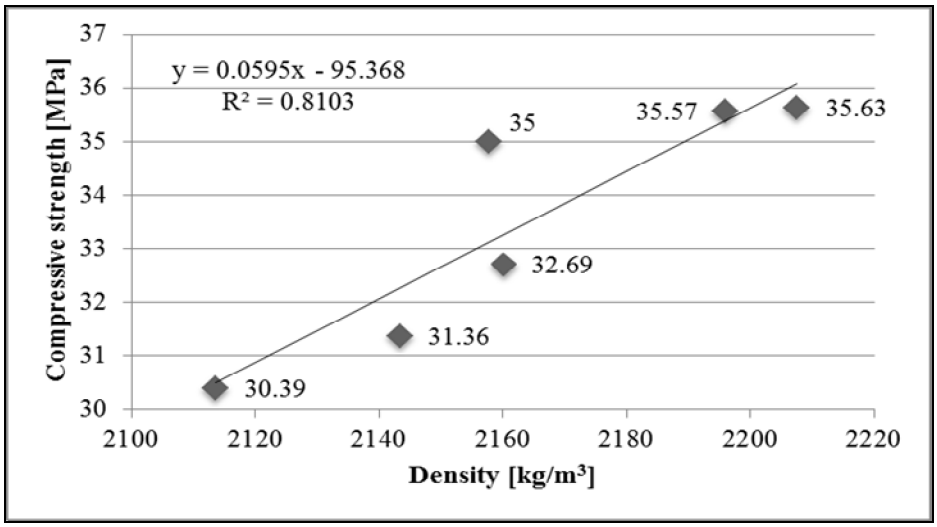

Fig. 5. Dependence of the compressive strength on density of fiber cement specimens after 28 days of curing

4. Conclusion

Changes in the density and compressive and flexural strength of 7 and 28 days hardened cement composites based on cellulosic fibers coming from wood pulp and recycled waste paper in dependence on their increasing portion (0.2%; 0.3% and 0.5%) were demonstrated. The results of comparing study of these parameters of the hardened fibers cement composites with reference sample indicated decrease in their values with increasing percentage of cellulosic fibers. However, cement composites with wood pulp showed better mechanical properties in comparison to composites with waste paper fibers. These changes can be connected with higher porosity, type of cellulosic fibers and their physico-chemical properties. Dependence of compressive strength on density of fiber cement composites is indicated.

Acknowledgement: *The authors are grateful to the Slovak Scientific Grant Agency for financial support of the project VEGA 1/0277/15 and Project Institute of Clean Technologies for Mining and Utilization of Raw Materials for Energy Use. Reg. No. LO1406.*

References

[1] Claramunt J., Fernández-Carrasco L.J., Ventura H., Ardanuy M. Natural fiber nonwoven reinforced cement composites as sustainable materials for building envelopes. Construction and Building Materials. Vol. 115, pp. 230–239, 2016.

[2] Malhotra V.M., Mehta P.K. Pozzolanic and cementitious materials. Advances in concrete Technology. Vol. 1. Gordon and Breach Publishers, Amsterdam. 1996.

[3] Cuadrado H., Sebaibi N., Boutouil M., Boudart B. Properties of concretes incorporating crushed queen scallops for artificial reefs. Proceedings of the RECIF Conference on Artificial Reefs: From Materials to Ecosystems, pp. 9–18, 2015.

[4] Giesekam J., Barrett J., Taylor P., Owen A. The greenhouse gas emissions and mitigation options for materials used in UK construction. Energy and Buildings. Vol. 78, pp. 202–214, 2014.

[5] Hwang C.L., Tran V.A., Hong J.W., Hsieh, Y.C. Effects of short coconut fiber on the mechanical properties, plastic cracking behavior, and impact resistance of cementitious composites. Construction and Building Materials. Vol. 127, pp. 984–992, 2016.

[6] Nurzyński J. Acoustic performance of composite panels and their possible use in a building. Zeszyty naukowe politechniki rzeszowskiej Nr. 283 Budownictwo i Inżynieria Środowiska. Vol. 59, No. 3, pp. 139–146, 2012.

[7] Meyer, C. The greening of the concrete industry. Cement and Concrete composites. Vol. 31, pp. 601–605, 2009.

[8] de Andrade Silva F., Chawla N., de Toledo Filho, R.D. Tensile behavior of high performance natural (sisal) fibers. Composites Science and Technology. Vol. 68, No. 15, pp. 3438–3443, 2008.

[9] Čigášová J., Števulová N., Sičáková A. New biocomposites based on hemp hurds. Czasopismo Inżynierii Lądowej, Środowiska i Architektury – Journal of Civil Engineering, Environment and Architecture, JCEEA. Vol. 32, No. 62, pp. 75–81, 2015, DOI: 10.7862/rb.2015.141.

[10] Wei J., Meyer C. Degradation of natural fiber in ternary blended cement composites containing metakaolin and montmorillonite. Corrosion Science. Vol. 120, pp. 42–60, 2017.

[11] Tonoli G.H.D., Savastano H., Fuente E., Negro C., Blanco A., Lahr F.R. Eucalyptus pulp fibres as alternative reinforcement to engineered cement-based composites. Industrial crops and products. Vol. 31, No. 2, pp. 225–232, 2010.

[12] Claramunt J., Ardanuy M., Parés F., Ventura H. Mechanical performance of cement mortar composites reinforced with cellulose fibres. In: 9th international conference on Composite Science and Technology, Italy, Sorrento, Naples. Pp. 477–484, 2013.

[13] Mohr B.J., Nanko H., Kurtis K.E. Aligned kraft pulp fiber sheets for reinforcing mortar. Cement and Concrete Composites. Vol. 28, No. 2, pp. 161–172, 2006.

[14] Bentchikou M., Guidoum A., Scrivener K., Silhadi K., Hanini S. Effect of recycled cellulose fibres on the properties of lightweight cement composite matrix. Construction and Building Materials. Vol. 34, pp. 451–456, 2012.

[15] Bentchikou M., Guidoum A., Scrivener K., Silhadi K., Hanini S. Effect of cellulose fibre on the thermal and mechanical properties of cement paste. In: Conference on the use of recycled materials in building and structures. Barcelona. Pp. 9–11, 2004.

[16] STN EN 196-1: 2016 Methods of testing cement. Part 1 Determination of strength.
[17] STN EN 1008: 2003 Mixing water concrete. Specification for sampling, testing and assessing the suitability of water, including water recovered from processes in the concrete industry, as mixing water for concrete.
[18] STN EN 1015-10: 2007 Methods of test for mortar for masonry. Part 10 Determination of dry bulk density of hardened mortar.
[19] STN EN 1015-11: 2007 Methods of test for mortar for masonry. Part 11 Determination of flexural and compressive strength of hardened mortar.
[20] Abdel-Kader A.H., Darweesh H.H. Setting and hardening of agro/cement composites. BioResources. Vol. 5, No. 1, pp. 43–54, 2009.
[21] Odera R.S., Onukwuli O.D., Osoka E.C. Tensile and compressive strength characteristics of Raffia Palm fibre-cement composites. Journal of Emerging Trends in Engineering and Applied Sciences. Vol. 2, No. 2, pp. 231–234, 2011.
[22] Hoyos C.G., Cristia E., Vázquez A. Effect of cellulose microcrystalline particles on properties of cement based composites. Materials & Design. Vol. 51, pp. 810–818, 2013.
[23] Raut A.N., Gomez C.P. Thermal and mechanical performance of oil palm fiber reinforced mortar utilizing palm oil fly ash as a complementary binder. Construction and Building Materials. Vol. 126, pp. 476–483, 2016.

Przesłano do redakcji: 24.03.2017 r.
Przyjęto do druku: 25.09.2018 r.

CZASOPISMO INŻYNIERII LĄDOWEJ, ŚRODOWISKA I ARCHITEKTURY
JOURNAL OF CIVIL ENGINEERING, ENVIRONMENT AND ARCHITECTURE
JCEEA, t. XXXV, z. 65 (3/18), lipiec-wrzesień 2018, s. 65-72, DOI:10.7862/rb.2018.43

Kamil RÓŻYCKI[1]

THE INFLUENCE OF HEAT SOURCE LOCATION ON SURFACE TEMPERATURE DISTRIBUTION OF THE INDOOR SIDE OF EXTERNAL WALLS IN AN UNINSULATED APARTMENT IN WARSAW DURING THE HEATING SEASON

This article presents the influence of the heat source location to surface temperature distribution of the indoor side of external walls in an uninsulated apartment in Warsaw during the heating period. The apartment is located in a multi-family residential building. This building has never been thermomodernized and therefore it is highly energy-consuming. In 2016, an air-to-air heat pump was installed in the apartment and replaced the existing heat source, a dual-function gas boiler. The device is used both for heating the apartment during the heating period and cooling it during the summer. Such system works particularly well in non-insulated objects, in which the partition's internal surface temperature changes dynamically as the outside temperature changes. This article describes the results of the thermovision test of the walls of this flat. The surface internal temperature distribution on the selected three walls was examined under different atmospheric conditions while maintaining similar internal conditions.

Keywords: air-to-air heat pump, uninsulated building, thermovision, alternative heating system, walls

1. Introduction

The Central Statistical Office in Poland (Polish name: GUS) indicated in 2014 [1], that as much as 31% of final energy was consumed by households which ranks it highest among other groups of users in Poland. It turns out that as much as 68,8% of the energy used was needed for heating. In Poland, where around 80% of buildings are at least 30 years old [2], this situation is increasingly being corrected. The main way to improve the energy efficiency of buildings is to thermomodernize them. Thermomodernization measures include first of all improvement of thermal insulation of the building's external partitions, including external walls, roof, floor (if technical conditions allow it), replacement of

[1] Kamil Różycki, Politechnika Warszawska, Zakład Chłodnictwa i Energetyki Budynku, ul. Nowowiejska 21/25 00-665 Warszawa; tel. 500752994; krozycki@itc.pw.edu.pl

windows and doors, modernization of the heating system and system of hot water preparation.

Due to the large scale of the problem, it is not possible to thermomodernize all buildings at once. While in the case of single-family buildings the possibility of making upgrades improving their condition depends on one, sometimes several people, in the case of multi-family housing the situation is more complicated, depends on many people and the costs are much higher. In an apartment in a multi-family building, if applying additional insulation is not possible, the heating source can be replaced.

In this work, installation of an air-to-air heat pump was analyzed. This infrequently utilized solution can successfully operate as an alternative heat source in apartments. Thermal comfort is a very important factor from the point of view of the user. Buildings that are not thermally insulated are much more exposed to changes in external conditions. During winter, when the outside temperatures are low, the indoor temperature drops quickly. A similar situation occurs in the summer, high external temperature affects the increase of internal temperature. This article analyzes the influence of outside temperature in the winter on the wall's internal temperature and its distribution. In order to investigate the temperature distribution of internal walls in the analyzed apartment, measurements were carried out using infrared thermography using a thermal imaging camera.

2. Technical data of the analyzed building

This analysis examines a real flat of 100 m^2, located on the last floor of a multi-family residential building in Warsaw in III climate zone. The building is characterized by a low energy standard of the external partitions. The external walls are made of a slag hollow brick (40 cm) and the wooden roof was insulated with mineral wool (10 cm) about 20 years ago. The apartment has two alternative heating systems. The first of these is a dual-function gas boiler (used for heating and hot water preparation). The second one is a split type air conditioning system which was installed at the beginning of 2016. The intention of the apartment owner was to cool the flat in the summer. In the 2016–2017 heating season as an experiment he decided to use the air-to-air pump system as an alternative heating system. The wall unit of the heat pump is located in one of the corners of the living room and provides heat to the whole apartment.

3. Thermovision of external walls of the examined apartment

The author of this article carried out experimental studies in the heating season 2017–2018, which showed that the use of an air-to-air heat pump (Figure 1), even in a flat with a low energy standard can be economically more advantageous than central gas heating [3]. The conducted analysis indicated that

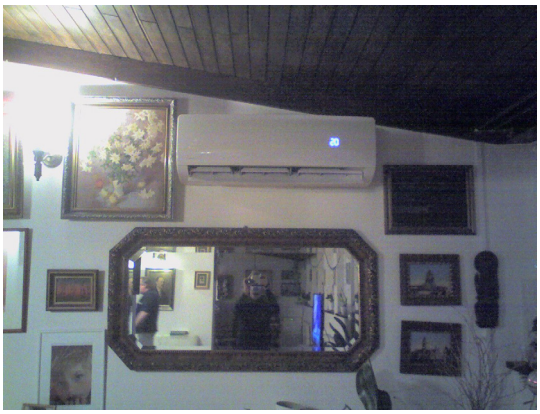

Fig. 1. Air-to-air heat pump

when the heat pump works in one room, temperature in rooms located further from the heat source can be lower. However, this phenomenon did not have a negative impact on the comfort of using the whole flat. In order to check the temperature distribution of walls from the inside infrared thermography, commonly called thermovision, was used. The tests were carried out at various outside temperatures, in several rooms of the flat. The heating device was set up in such a way as to heat the flat to 22°C.

3.1. Thermovision examination

Infrared thermography is a technique for measuring, displaying and recording the surface temperature of the tested objects, based on measurement of incoming infrared radiation [4]. The radiation that reaches the thermal imaging camera originates from the object being studied, as well as from the ground, clouds, sky and surrounding objects [5]. The result is so-called a thermogram, which is a picture illustrating the temperature distribution. This technique allows contactless measurement of the temperature distribution over a large area and from a considerable distance [6]. As a result tests can be carried out in both small and multi-story buildings [4].

According to the PN-EN 13187 standard [7], the increased heat transfer through building partitions is needed to use thermography. This means that tests can be carried out during the heating season. An additional condition that should be met is the corresponding difference in external and internal temperature of the building. The mentioned Polish norm [7] recommends the temperature difference of at least 5°C. Most auditors indicate that in Polish climate conditions, the minimum difference should be 15°C [4]. Thermovision tests are performed most often in the evening or at night, so the results are not affected by solar radiation. The smallest temperature amplitudes during the day and night during the heating season are observed between November and February, which

makes them the best months to perform such tests [4]. When executing the thermovision test, it is necessary to specify and enter into the measuring device several parameters. These include: the distance of the camera from the tested object, ambient temperature, temperature of the sky, relative humidity and the emissivity coefficient of the tested surface.

3.2. Thermographic measurements

The measurements described in this article was carried out using a FLIR B400 thermal imaging camera with an infrared image resolution of 320×240 pixels. The tests were carried out on three different days, each around 6 pm. These days were characterized by good weather conditions, i.e. during the day there were no significant amplitudes in the outside temperature, nor was there any precipitation. In addition, a constant temperature in the flat was maintained throughout the day. The apartment was heated by air-to-air heat pump, both in the testing day and the day before. The measurements assumed the emissivity of the examined surfaces at the level of 0.85. The most important information on the measurement data is presented in Table 1.

Table 1. Measurement data

Measurement number	Date of measurement	External temperature °C
1	27.01.2017	-2,1
2	2.01.2018	1,1
3	8.01.2018	-5,6

During the tests, the surface temperature distribution of the indoor side on three selected walls of the flat was measured. Each wall separates the flat from the external environment and each one is facing a different cardinal direction. The first one (hereinafter referred to as wall 1, Figures 2, 3) is the wall on which the heat pump is located. The second wall (wall 2, Figures 4, 5) is also located in the living room. The heating device is located about 6 m from the measuring point. The third wall (wall 3, Figures 6, 7) is located in the room furthest from the heat pump. Examples of thermograms and corresponding photos of three walls on 8th January 2018 are shown in Figures 2–7. The red frames on Figures 2, 4 and 6 show the thermograms area (Figures 2, 4 and 6).

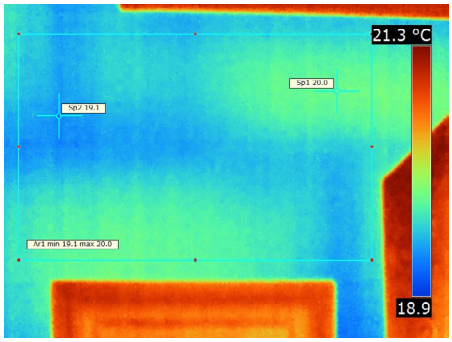

Fig. 2. Thermogram of the wall No. 1 – 8/01/2018

Fig. 3. Photo of the wall No. 1 – 8/01/2018

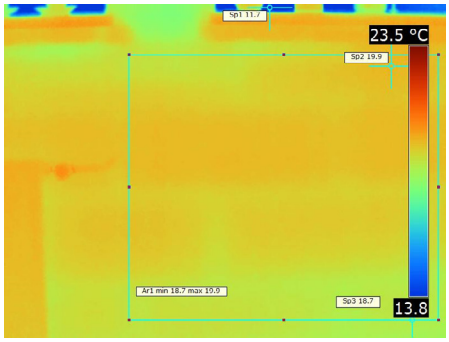

Fig. 4. Thermogram and photo of the wall No. 2 – 27/01/2017

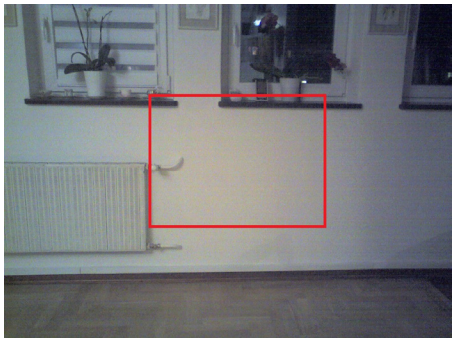

Fig. 5. Photo of the wall No. 2 – 8/01/2018

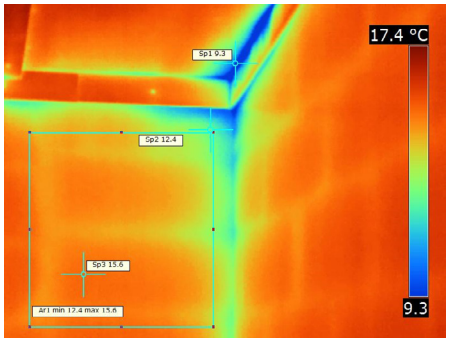

Fig. 6. Thermogram and photo of the wall No. 1 – 27/01/2017

Fig. 7. Photo of the wall No. 3 – 8/01/2018

4. Analysis of the results

In Chapter 4, Figures 8–10, the temperature distribution on the internal surface of the walls number 1–3 are shown, depending on the outside and inside temperatures of the given apartment. The temperatures were read from the thermal camera.

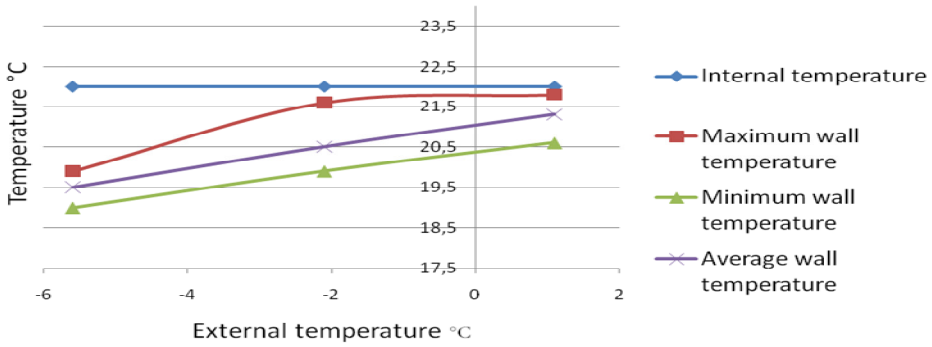

Fig. 8. Surface temperature distribution of the wall depending on the outside temperature – wall 1

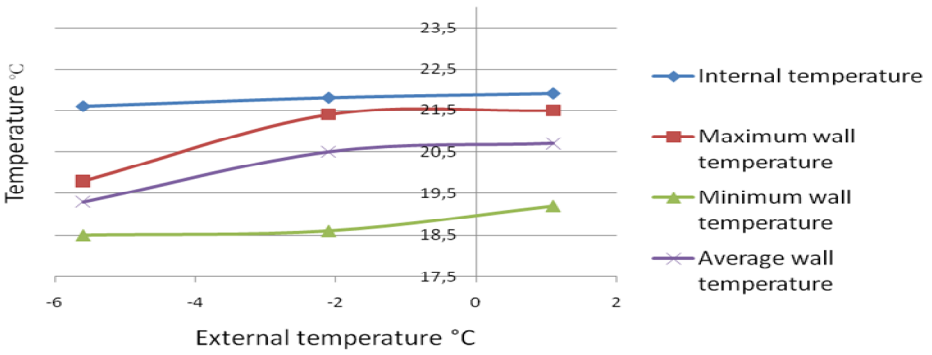

Fig. 9. Surface temperature distribution of the wall depending on the outside temperature – wall 2

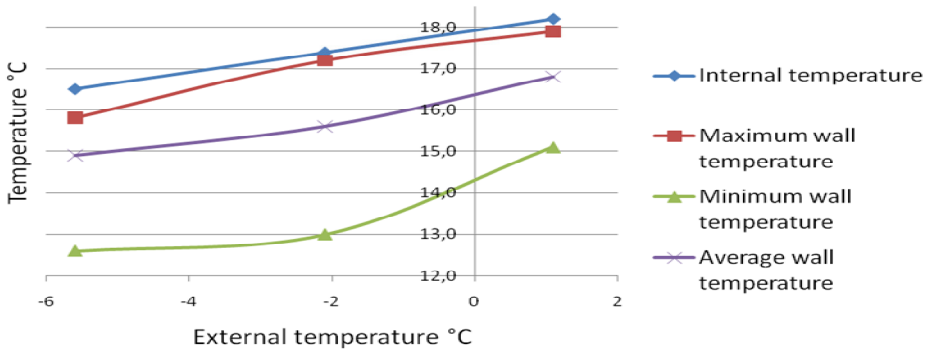

Fig. 10. Surface temperature distribution of the wall depending on the outside temperature – wall 3

Analyzing the results presented in Figures 8–10 allowed for some interesting conclusions. However, it should be noted that the analyzed surface temperature distribution of the indoor side of external walls were limited by portions of the walls and the actual surface temperature distribution over a larger area could differ from presented measurements. As previously indicated, wall 1 is the wall on which the heating device is located. Wall 2 is in the same room, however the examined part of the field is located about 6 m from the heat pump. Wall 3 is located in the room farthest away from the heat pump. The first conclusion may be drawn from the graphs on the indoor temperature prevailing in the rooms and the dynamics of its changes. The internal walls' surface temperature is lower when the outside temperature is lower and the measuring point is further away from the heating device. Surface temperature is also less stable and more distant from the assumed temperature of 22°C. However, residents of the examined apartment have a bedroom in the coldest room and are satisfied that the room has a lower temperature than the rest.

As expected, all the maximum, minimum and average temperatures of the indoor side of external partitions decrease together with the external temperature, which is caused by the increase of the heat exchange intensity with the external environment.

It is noted that the difference between the maximum and minimum temperature on the surface of wall 3, relative to walls 1 and 2 is observed. This is the result of a selected surface sample which contains a corner fragment in which a thermal bridge occurs. On the chosen wall, it was not possible to choose another representative fragment of the surface (large window area, wall covered with furniture). In another case, the difference between the indicated temperatures would be at a similar level as on walls 1 and 2.

On walls 1 and 2, the difference between the maximum surface temperature on the indoor side of wall and the internal temperature in a given apartment is much higher than on wall 3. This dependence is particularly noticeable at the lowest outdoor temperatures. This phenomenon results from the fact that in a room with wall 3 there is much lower internal temperature than in a room where there are walls 1 and 2, which causes higher intensity of heat exchange with the external environment of walls 1 and 2 and higher heat losses.

5. Conclusions

Heating an apartment with an air-to-air heat pump can be an interesting alternative to traditional heating systems, especially in non-insulated buildings that require thorough thermomodernization. Regarding people for whom the cost of modernization is too high or technical conditions do not allow for insulation of walls (a historic building or owned by a larger group of people) the use of an air-to-air heat pump can reduce bills while maintaining sufficient thermal comfort. Apart from the fact that this solution is considered to be more

ecological than conventional solutions, the additional advantage is a small difference in the final thermal comfort during the heating period. This article, in which a thermovision was used, has shown that regardless of the prevailing external conditions the apartment has satisfactory thermal conditions. An additional advantage not described in this article is the possibility of cooling the apartment during the summer and in non-insulated buildings, especially in the summer, in which there is strong overheating. The use of a heating device placed in the corner of the apartment, as in the tested flat, seems not to be optimal. If the device would be placed in the central part of the apartment, it would improve the overall comfort of living. It seems that in the coming years, the air-to-air heat pump will be increasingly used as a heat source.

References

[1] Główny Urząd Statystyczny: Efektywność wykorzystania energii w latach 2004–2014, Warszawa 2016.

[2] Główny Urząd Statystyczny: Zamieszkane budynki, Narodowy Spis Powszechny Ludności i Mieszkań 2011, Warszawa 2013.

[3] Różycki R., Duda L.: Analiza porównawcza pracy kotła gazowego i powietrznej pompy ciepła w rzeczywistym mieszkaniu w zależności od warunków zewnętrznych, Rynek Energii (to be published).

[4] Wiśniewski T.S.: Ocena izolacyjności przegród budowlanych za pomocą termografii w podczerwieni, Polska Energetyka Słoneczna, nr 3–4, 2007, s. 16–29.

[5] Więcek B., Pacholski K., Olbrycht R., Strąkowski R., Kałuża M., Borecki M., Wittchen W.: Termografia i spektrometria w podczerwieni. Zastosowania przemysłowe, Wydawnictwa Naukowe PWN, Warszawa 2017.

[6] Jaworski J.: Sprawność cieplna budynków określana metodą radiometryczną, Polska Energetyka Słoneczna, nr 3–4, 2005, s. 13–18.

[7] PN-EN 13187:2001 Thermal performance of buildings – Qualitative detection of thermal irregularities in building envelopes – Infrared method.

Przesłano do redakcji: 18.04.2018 r.
Przyjęto do druku: 28.09.2018 r.

CZASOPISMO INŻYNIERII LĄDOWEJ, ŚRODOWISKA I ARCHITEKTURY
JOURNAL OF CIVIL ENGINEERING, ENVIRONMENT AND ARCHITECTURE
JCEEA, t. XXXV, z. 65 (3/18), lipiec-wrzesień 2018, s. 73-82, DOI:10.7862/rb.2018.44

Justyna ORWAT[1]

COMPARISON ANALYSIS OF THE THEORETICAL AND FORECASTED VALUES OF MINING TERRAIN CURVATURES WITH REFERENCE TO THEIR VALUES CAUSED BY MULTI-DEPOSIT EXPLOITATION CONDUCTED AT THE GREAT DEPTH

In this article were presented the results of comparison analysis of mining terrain curvatures values, which were caused by a multiple exploitation of hard coal in several coal beds numbered 338/2, 341 and 358/1. The curvatures values (observed on the measuring line) were compared with their theoretical values calculated on the base of subsidence forecasted by the use of the Białek's formula (with the values of its parameters determined from the survey results) and with the curvatures values modeled with this formula directly. On the base of this comparison, there was made an evaluation of effectiveness of made forecasts and conducted theoretical calculations. Taking into account the values of correlation coefficients and standard deviations between the 'measured' and theoretical, and forecasted graphs of curvatures, it was defined which graphs fit better to the real results of geodesic measurements. It should be marked that an exploitation of three coal beds was conducted by the longwall system with the roof rocks falling into the post-exploitation emptiness, at a great depth amounts from 600 m (the 338/2 coal bed) to 1,000 m (the 358/1 coal bed). The influences coming from the exploitation of these coal beds were observed within 10 years on 53 points of measuring line, which was located above the middle of the B – 2 longwall in the 338/2 coal bed and parallel to the runs of excavations in this coal bed. The surveys of the points heights and distances between the measuring points were done in the three– and four–monthly cycles. Based on these measurements, the values of mining terrain curvatures were designated.

Keywords: multi-seams extraction; exploitation at the large depth; observed, theoretical and forecasted curvatures of mining terrain; J. Białek's formula

1. Introduction

The observed values of mining terrain curvatures caused by underground mining exploitation of hard coal deposits are compared with the curvatures values obtained from numerical modeling.

[1] Justyna Orwat, Politechnika Śląska, Katedra Eksploatacji Złóż, ul. Akademicka 2, 44-100 Gliwice; justyna.orwat@polsl.pl

Curvatures are designated from subsidence of three neighboring points of measuring line [1] stabilized in the ground above an exploitation field. Thus the curvature value occurs along of two neighboring segments of measuring line. It's difficult to say in which place of these segments occurs a curvature value determined from the survey results [2]. Therefore it's assumed that this value occurs in the middle point of these segments. Only when the segments have the same lengths, the curvature value occurs exactly in measuring point.

Forecasts of deformation indicators values of mining terrain (inter alia of curvatures) are getting done for the measuring points.

To make an evaluation of effectiveness of made forecasts, it's necessary to compare the forecasted values of curvatures with the empirical values or their average values [3, 4]. But the question is how to compare the curvatures values 'measured' along the segments and forecasted in the points? Can be compared the forecasted values, mainly calculated by use of the formulas of the geometric-integral theories of exploitation impacts with the 'measured' values, calculated only as the difference of subsidence measured in the points and divides by an average length of the neighboring segments?

Therefore in the article have been presented the comparison results of 'measured' values of curvatures conventionally assigned the mid–points of two neighboring segments with the curvatures values forecasted in the points by use of Białek's formula [5–8] (with the values of its parameters determined from the results of geodesic measurements) and with the theoretical values of curvatures (see more in the point 2.4) calculated using the same formula as when calculating of 'measured' values of curvatures (using only the subsidence forecasted in the points and the measured lengths of segments). On the base of values of standard deviations and correlation coefficients between the 'measured', forecasted and theoretical values of curvatures, it was possible to indicate which graph (forecasted or theoretical) describes better the observed values of curvatures.

2. Research methods

In this point have been presented a real case of hard coal exploitation carried out in several coal seams occur at great depths and the obtaining methods of the observed, forecasted and theoretical values of mining terrain curvatures.

2.1. Exploitation case

Some hard coal mine located in the southern part of Poland has been carried out in the years 2001–2011 an exploitation of hard coal in seams named 338/2, 341 and 358/1 (figure 1). Coal excavation was conducted by the use of longwall system with the roof rocks falling into the post-exploitation emptiness.

The 338/2 coal bed was exploited in the years 2001–2006 at the depth of 600 m. The height of longwalls numbered from B-1 to B-4 and C-1 was amounted from 2.5 m to 3.0 m.

Hard coal was excavated from the 341 seam in the years 2007–2011 by the use of longwalls numbered from B-1 to B-4. This coal seam was occurred at the depth of 635 m and its thickness was amounted from 2.3 m to 3.0 m.

The 358/1 coal seam was exploited at the depth of 1000 m and the height of longwalls numbered from B-1 to B-7 was amounted from 2.0 m to 2.9 m. Exploitation of this coal bed took place in the years 2002–2006.

Inclination of these coal beds was amounted from 4° to 6° in the south-eastern direction.

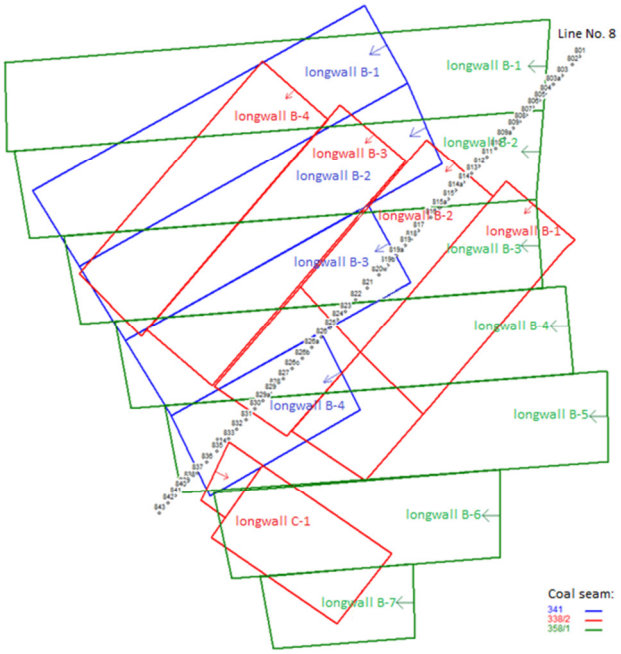

Fig. 1. Longwalls in the 338/2, 341, 358/1 coal seams and the measuring line No 8 (source: own elaboration)

2.2. Observed curvatures

Mining exploitation impacts on terrain surface have been observed at the measuring line No 8 which was established above the middle of longwall B-2 in the 338/2 coal seam, parallel to the runs of mining excavations located in this coal bed. Line was consisted of 53 measuring points and an average distance between subsequent points was amounted 35 m.

There have been carried out the geodesic survey before the beginning and after the ending of exploitation of the 338/2, 341 and 358/1 coal seams. There were measured the absolute heights of points in reference to the 'Kronsztadt' level and the lengths of measuring line segments.

On the base of difference of the points heights measured before and after the exploitation, there were designated the subsidence of measuring points (S_i) caused by exploitation of three coal beds. On the base of subsidence of three neighboring points S_{i-1}, S_i, S_{i+1} and the average length of two neighboring segments $L_{i-1,i}$; $L_{i,i+1}$, there were calculated the 'measured' values of curvatures in points connecting the subsequent segments C_i from the following formula [9–10]:

$$C_i^{meas} = 2\frac{S_{i-1}^{meas} - 2S_i^{meas} + S_{i+1}^{meas}}{L_{i-1,i}^{meas} + L_{i,i+1}^{meas}} \tag{1}$$

where: C_i^{meas} – curvature 'measured' in the i point connecting two neighboring segments [$10^{-6} \cdot 1/m$];
$L_{i-1,i}^{meas}$ – measured length of the i-$1,i$ segment [m];
S_{i-1}^{meas} – measured subsidence of the i-1 point [mm];
i – measuring point.

2.3. Forecasted curvatures

The forecasted values of curvatures have been calculated in the measuring points by the use of the *EDBJ1a* computer program and using the second derivative of the Białek's formula for calculation of subsidence [6–7]:

$$S_f = (1 - a_s)s(r_1) + a_s s(r_2) - A_1\left(2 + \frac{A_3}{2}\right)\frac{s(r_1)[r_1\gamma(r_1)]^2}{A_3\left[\frac{s(r_1)}{2} + \frac{s(r_2)}{2}\right]^2 + [r_1\gamma(r_1)]^2} \tag{2}$$

where: β – range angle of main influences [°];
γ – simplified octahedral strain [mm/m];
A_1 – dimensionless multiplier which takes into account an asymmetry of subsidence trough profile;
$A_3 = 6.667$;
S_f – final subsidence [mm];
a_s – coefficient constant for each subsidence trough, it defines what part of final subsidence was calculated by the use of the r_i radius ($a_s = 0.4 \div 1.25A_1$);
h – exploitation depth [m];
r_i – radius of influences dispersion for each subsidence trough [m];
$r_1 = \frac{h}{tg\beta}F_r(A_1)$;
$r_2 = 2r_1$;
$s(r_1)$, $s(r_2)$ – subsidence calculated using the Knothe's formula with the use of two different radiuses of influences dispersion r_1, r_2 [mm].

For calculation of curvatures values forecasted after the termination of exploitation in three coal seams, there were used the parameters values of the Białek's formula determined from the results of geodesic measurements conducted after an extraction end in all longwalls and all hard coal beds. These values have been calculated by the use of the *TGB* computer program, namely: $a = 0.889$; $\mathrm{tg}\beta = 2.520$; $A_1 = 0.138$.

There were taken into account the immediate impacts in done predictions of the subsidence and curvatures values.

2.4. Theoretical curvatures

The theoretical values of curvatures have been calculated from the same formula as when calculating of 'measured' curvatures. The subsidence values measured in the points have been replaced by the subsidence values forecasted by the use of the Białek's formula with the values of its parameters determined from the survey results:

$$C_i^{theor} = 2\frac{S_{i-1}^{fore} - 2S_i^{fore} + S_{i+1}^{fore}}{L_{i-1,i}^{meas} + L_{i,i+1}^{meas}} \tag{3}$$

where: C_i^{theor} – theoretical value of curvature in the i point connecting two neighboring segments [$10^{-6} \cdot 1/m$];
$L_{i-1,i}^{meas}$ – measured length of the *i-1,i* segment [m];
S_{i-1}^{fore} – subsidence forecasted by the use of the Białek's formula in the *i-1* point [mm];
i – measuring point.

There have been adopted the measured lengths of line sections in the formula number 3, because these lengths are real and most appropriate after the exploitation completion in three coal seams.

To differentiate the curvatures values obtained on the way of direct forecasting by the use of the Białek's formula from the curvatures values calculated by the use of the formula (3), the second one have been named as the theoretical curvatures because they have been obtained from the subsidence values predicted by the use of a chosen theory of mining exploitation influences.

3. Research results

At the figure 2 have been presented the 'measured', forecasted by the use of the Białek's formula and theoretical graphs of curvatures along the measuring line No 8, calculated on the base of formulas (1)–(3) and after the ending of exploitation in the 338/2, 341 and 358/1 coal seams. A red continuous line means the 'measured' graph of curvatures, a green continuous line presents the forecasted graph of curvatures and a blue continuous line represents the theoretical graph of curvatures.

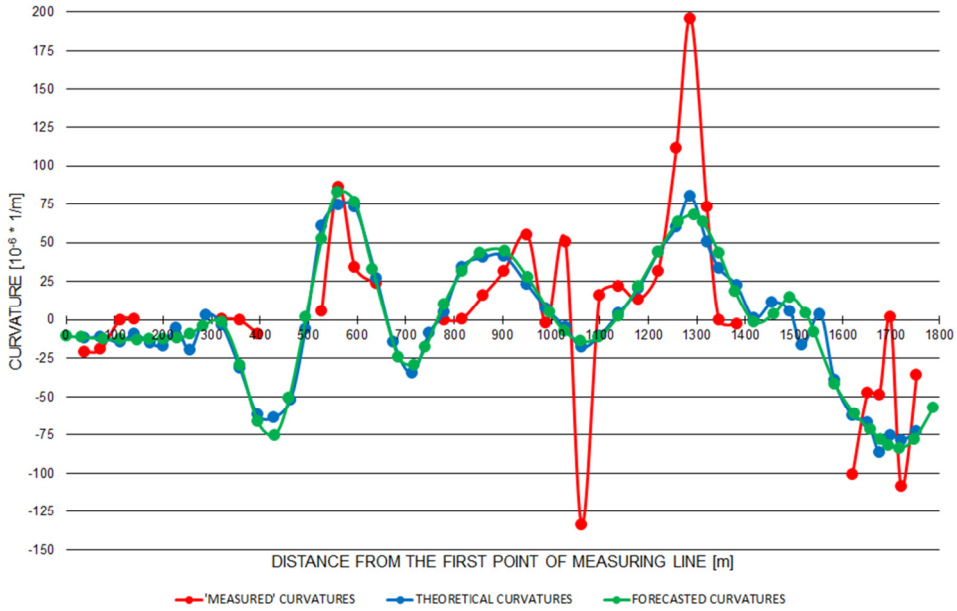

Fig. 2. 'Measured', forecasted and theoretical graphs of curvatures along the measuring line No 8 (source: own elaboration)

In order of comparison of curvatures 'measured' graph with their forecasted and theoretical graphs, there have been calculated the values of: the R correlation coefficient between these graphs, the P percentages of extreme 'measured' curvatures which correspond the extreme forecasted and the extreme theoretical curvatures, and the standard deviation marked as σ obtained from the formula (4):

$$\sigma_{Cmeas}^{Cfore/theor} = \sqrt{\frac{\sum_{i=1}^{n}(C_{imeas} - C_{ifore/theor})^2}{n-1}} \tag{4}$$

where: $\sigma_{Cmeas}^{Cfore/theor}$ – standard deviation between the 'measured' curvatures and the forecasted / theoretical curvatures [$10^{-6}\cdot$1/m];
C_{imeas} – 'measured' value of curvature in the i point [$10^{-6}\cdot$1/m];
$C_{ifore/theor}$ – forecasted / theoretical value of curvature in the i point [$10^{-6}\cdot$1/m];
i – measuring point;
n – number of points.

The results of done calculations have been shown in the table 1.

Table 1. Comparison of curvatures 'measured' values with their forecasted and theoretical values (source: own elaboration)

'Measured' curvatures	
C_{meas}^{max} [10^{-6}·1/m]	195.83
C_{meas}^{min} [10^{-6}·1/m]	-133.54
Forecasted curvatures	
C_{fore}^{max} [10^{-6}·1/m]	82.60
$Pmax_{Cmeas}^{Cfore}$ [%]	42.18
C_{fore}^{min} [10^{-6}·1/m]	-83.60
$Pmin_{Cmeas}^{Cfore}$ [%]	62.60
R_{Cmeas}^{Cfore}	0.6488
σ_{Cmeas}^{Cfore} [10^{-6}·1/m]	∓46.36
Theoretical curvatures	
C_{theor}^{max} [10^{-6}·1/m]	80.25
$Pmax_{Cmeas}^{Ctheor}$ [%]	40.98
C_{theor}^{min} [10^{-6}·1/m]	-86.36
$Pmin_{Cmeas}^{Ctheor}$ [%]	64.67
R_{Cmeas}^{Ctheor}	0.7178
σ_{Cmeas}^{Ctheor} [10^{-6}·1/m]	∓42.35

4. Results discussion

From the curvatures graphs shown at the figure 2 and the data presented in the table 1 results that the minimal 'measured' curvature reached the value of -133.54·10^{-6} 1/m and it occurred about 1,050 m from the beginning of measuring line. The maximal 'measured' curvature reached the value of 195.83·10^{-6} 1/m and it occurred about 1,300 m from the first point of measuring line.

The minimal forecasted curvature reached the value of -83.60·10^{-6} 1/m and it occurred about 1,720 m from the first point of measuring line. The maximal forecasted curvature reached the value of 82.60·10^{-6} 1/m and it occurred in 560-th meter of measuring line.

The minimal theoretical curvature reached the value of -86.36·10^{-6} 1/m and it occurred about 1,680 m from the beginning of measuring line. The maximal theoretical curvature reached the value of 80.25·10^{-6} 1/m and it occurred about 1,300 m from the 801 point.

The percentages values of extreme 'measured' curvatures which correspond the extreme forecasted and the extreme theoretical curvatures indicate that the extreme values of forecasted and theoretical curvatures reached the values more than half smaller than the extreme values of 'measured' curvatures. It can be seen that the percentages values of minimal 'measured' curvatures ($Pmin_{Cmeas}^{Cfore}$ = = 62.60% and $Pmin_{Cmeas}^{Ctheor}$ = 64.67%) are bigger than the values of percentages of maximal 'measured' curvatures ($Pmax_{Cmeas}^{Cfore}$ = 42.18% and $Pmax_{Cmeas}^{Ctheor}$ = = 40.98%).

The extreme forecasted and theoretical curvatures occurred generally in the other places than the extreme 'measured' curvatures but the minimal forecasted and the minimal theoretical curvatures occurred in principle in the same places.

As can be seen at the figure 2, the forecasted curvatures (green line) and the theoretical curvatures (blue line) have similar graphs. However, to the 'measured' graph of curvatures fits better the theoretical graph of curvatures than the curvatures forecasted graph. It's evidenced by the values of: the *R* correlation coefficient (R_{Cmeas}^{Ctheor} = 0.7178) which is higher than for the forecasted curvatures (R_{Cmeas}^{Cfore} = 0.6488) and the σ standard deviation (σ_{Cmeas}^{Ctheor} = $\mp$42.35·10^{-6} 1/m) which is smaller than for the forecasted values of curvatures (σ_{Cmeas}^{Cfore} = $\mp$46.36· 10^{-6} 1/m).

5. Summary and conclusions

In this article was shown an example of hard coal exploitation conducted at the large depth amounted 745 m in three coal seams numbered 338/2, 341 and 358/1. For observation of mining exploitation influences on terrain surface, it was established a measuring line No 8 which was consisted of 53 measuring points. This line was located above the middle of exploitation field and parallel to the run of longwall B-2 in the 338/2 coal bed. At measuring line were carried out the geodesic surveys of points altitudes and distances between neighboring points. On the base of surveys results, there were calculated the measured values of points subsidence and, based on them, the 'measured' values of segments curvatures. The value of 'measured' curvature was adopted in the joint point connecting two neighboring sections. It was also done the prognosis of curvatures values in measuring points. Forecast was done using the *EDBJ1a* computer program and by the use of the Białek's formula with the values of its parameters determined from the results of geodesic measurements. Additionally there were calculated the theoretical values of curvatures from the analogical formula as when calculating of 'measured' values of curvatures but instead the measured subsidence there were used the forecasted subsidence.

This method allows to solve the problem of comparison ambiguity of the curvatures 'measured' along the line segments and forecasted in the measuring points. As indicate made calculations, a theoretical graph of curvatures fits to the

empirical data better than a forecasted graph of curvatures. But also this method isn't free from defects. However, it occurs a problem: what lengths of measuring line segments should be used, since the prognosis is made before an exploitation start. Then aren't known the segments lengths after the termination of exploitation. It can be assumed the designed lengths of sections known before stabilization of measuring line points in the ground or the segments lengths measured in the first measuring cycle which takes place before an exploitation beginning.

Acknowledgements: *This article has been arised thanks to the funds of the 06/050/BKM_17/0046 project realized at the Faculty of Mining and Geology of Silesian University of Technology in Gliwice.*

References

[1] Mielimąka R.: Wpływ kolejności i kierunku eksploatacji prowadzonej frontami ścianowymi na deformacje terenu górniczego [Impact of sequence and direction of mining exploitation conducted by the use of longwalls excavations on mining terrain deformations], Wydawnictwo Politechniki Śląskiej, Gliwice 2009, s. 43.

[2] Ostrowski J.: Deformacje powierzchni terenu górniczego [Deformations of mining terrain surface], Wydawnictwo Akademii Górniczo-Hutniczej, Kraków 2015, s. 415–417.

[3] Orwat J.: Ocena skuteczności modeli zastosowanych do reprognozy krzywizn terenu górniczego w oparciu o przeciętne przebiegi ich wartości pomierzonych [Appraisal of effectiveness of the models used to a reprognosis of the values of mining area curvatures made in relation to the average courses of their measured values], Systemy Wspomagania w Inżynierii Produkcji, nr 6(3), 2017, s. 171–180.

[4] Orwat J., Mielimąka R.: Approximation of average course of measured curvatures of mining area with reference to their forecast values by Białek's formulas, AIP Conference Proceedings, vol. 1863, 2017, pp. 130003-1 – 130003-4.

[5] Białek J.: Algorytm obliczania chwilowych i czasowo ekstremalnych wskaźników deformacji przestrzennej dynamicznej niecki osiadania wraz z oprogramowaniem [Calculation algorithm of the temporary and time-extreme deformations indicators of dynamic subsidence trough with software], Politechnika Śląska, Gliwice 1980, praca doktorska niepublikowana.

[6] Białek J.: Nieliniowy matematyczny model osiadania powierzchni w czasie wskutek prowadzonej eksploatacji górniczej [Non-linear mathematical model of surface subsidence in the time as a result of conducted mining exploitation], Zeszyty Naukowe Politechniki Śląskiej, seria Górnictwo, z. 38, 1985.

[7] Białek J.: Opis nieustalonej fazy obniżeń terenu górniczego z uwzględnieniem asymetrii wpływów końcowych [Description of an unidentified phase of mining terrain subsidence with inclusion of final influences asymmetry], Zeszyty Naukowe Politechniki Śląskiej, seria Górnictwo, z. 194, 1991.

[8] Białek J.: Algorytmy i programy komputerowe do prognozowania deformacji terenu górniczego [Algorithms and computer programs to forecasting of mining terrain deformations], Wydawnictwo Politechniki Śląskiej, Gliwice 2003, s. 35.

[9] Popiołek E., Ostrowski J., Milewski M.: Próba oceny przydatności krzywizny profilu niecki obniżeniowej jako wskaźnika zagrożenia obiektu poddawanego wpływom podziemnej eksploatacji górniczej (na przykładzie złoża LGOM) [Evaluation attempt of curvature usefulness of subsidence trough profile as an indicator of object threat which is subject to influences of underground mining exploitation], Przegląd Górniczy, nr 11, 1995, s. 1–7.

[10] Popiołek E.: Ochrona terenów górniczych [Protection of mining terrains], Wydawnictwo Akademii Górniczo-Hutniczej, Kraków 2009, s. 42–45.

Przesłano do redakcji: 08.08.2018 r.
Przyjęto do druku: 28.09.2018 r.

CZASOPISMO INŻYNIERII LĄDOWEJ, ŚRODOWISKA I ARCHITEKTURY
JOURNAL OF CIVIL ENGINEERING, ENVIRONMENT AND ARCHITECTURE
JCEEA, t. XXXV, z. 65 (3/18), lipiec-wrzesień 2018, s. 83-90, DOI:10.7862/rb.2018.45

Sergiy SOLODKYY[1]
Iurii SIDUN[2]
Oleksiy VOLLIS[3]

ACIDS IN BITUMEN EMULSIONS

In the article there is proved the possibility of using ortho-phosphoric acid with special emulsifiers instead of hydrochloric acid – for the production of road cationic slow-setting bitumen emulsions. There is ascertained the difference between used for bitumen emulsions distilled binder (Nybit E85 bitumen), produced from heavy crude oil, and oxidized bitumens (grade 70/100 bitumen produced by JSC Mozyr Refinery and grade BND 60/90 bitumen of JSC UkrTatNafta), produced from light crude oil. The difference is analyzed between physical-mechanical indices of distilled and oxidized bitumens. Eight bitumen emulsion formulations were developed based on usage hydrochloric acid, three bitumens and three emulsifiers (Redicote E-11, Redicote 404 and Redicote E-4875), as well as four formulations based on usage of ortho-phosphoric acid, two bitumens and two emulsifiers (Redicote EM44 and Redicote C-320). There was investigated the influence of hydrochloric and ortho-phosphoric acids upon the physical-technical indices of road cationic slow-setting bitumen emulsions and the difference was ascertained between the indices of bitumen emulsions based on distilled and oxidized bitumens. Bitumen emulsion formulations were developed based on usage of ortho-phosphoric acid and special emulsifiers for the class of cationic slow-setting emulsions for slurry seal and microsurfacing mixtures.

Keywords: bitumen emulsion, hydrochloric and ortho-phosphoric acids, slurry seal and microsurfacing mixtures

1. Introduction

Bitumen emulsions found the broad-range usage in the road construction world-wide. The application of bitumen in a form of emulsion have a number of advantages: application of organic binding materials in a form of emulsion allows decreasing bitumen consumption for 20÷30% w/w due to formation of

[1] Corresponding author: Sergiy Solodkyy, National University «Lviv Polytechnic», Institute of Building and Environmental Engineering, 12 Bandera str., Lviv, s.solodkyy@ukr.net

[2] Iurii Sidun, National University «Lviv Polytechnic», Institute of Building and Environmental Engineering, 12 Bandera str., Lviv, siduniurii@gmail.com

[3] Oleksiy Vollis, National University «Lviv Polytechnic», Institute of Building and Environmental Engineering, 12 Bandera str., Lviv, vollisaleksey@gmail.com

thinner bitumen film around the grains of mineral materials; absence of necessity for emulsion and aggregate pre-heating allows saving fuel-power resources; extension of road season due to road works performance at the temperature not less than 5°C; possibility of wet aggregate treatment and road works performance with wet base; emulsions storage is simple and does not require warehouses with complicated heating system. It is extremely important that emulsions allow working at as unfavorable weather conditions, as making impossible (even in presence of surfactants) to reach the necessary quality of works with application of hot mixes. It is possible to use road emulsions as a binder for plenty of road technologies. In spray applications the emulsion is used for surface dressing (chip seal), fog seal, scrub seal, graded aggregate seal, tack coat, prime coat, penetration macadam and dust control. In mix applications it is used for slurry seal, microsurfacing, cape seal, open-graded cold mix, dense-graded cold mix, soil stabilization, pre-coated chips, stockpile mix and RAP [1–2]. The results of theoretical investigations and practical application of bitumen emulsions have shown that the greatest effect is reached with cationic bitumen emulsions applied.

2. Analysis of recent investigations and publications

A lot of investigations were done on application and modification of cationic bitumen emulsions, both world-wise [3–6] and in the Ukraine in particular [7–8]. Still, the review of scientist's publications, both the domestic and foreign ones, has shown that the issues of application of this or that acid in an emulsion are cleared-up insufficiently. It is known that for the production of cationic bitumen emulsion it is possible to use hydrochloric, ortho-phosphoric and acetic acids. Let us address out attention to the first two ones – as the most used in production. In Ukraine there is widely used hydrochloric acid for emulsions – due to the worked-up technology of its application. (Though in the world-scale the usage of ortho-phosphoric acid is not a problem). Let us try to compare these acids. Hydrochloric acid is rather aggressive and highly corrosive, while that may lead to destruction of technological equipment. The labor safety during the working process shall be on the raised level. Besides, in the Ukraine it is required that acid implies getting license for work with precursors. Therefore, the usage of hydrochloric acid not just leads to increase of cost of technology, but also requires a whole chain of additional technological modifications, both that of the personnel's working place itself, and of the production equipment – at installation stage and in course of its operation.

Significant contribute into investigation of the problem of acid usage for emulsions was made by A. James [9–10]. He asserts that alternative acids can provide for advantages in operation indices at the stage of final application of emulsion. Reaction of acid with aggregate, along with resulting changes of pH make significant influence upon the cationic emulsions breakage. Besides, the

choice of acid makes influence upon the process, while the products received will potentially make influence upon the adhesion and rheology of the residual [11]. A. James together with T. Ng analyzed the usage of ortho-phosphoric acid for slurry seal and microsurfacing technologies and determined the peculiarities and advantages of application of this acid for the said technologies [12–13].

The purpose of this work is determination of the efficiency of ortho-phosphoric acid application for production of slow-setting cationic bitumen emulsions (based on the accessible materials), as well as determination of its influence on the emulsion quality.

3. Main part

For the production of bitumen emulsions based on hydrochloric and ortho-phosphoric acids there were taken popular in Ukraine raw materials, namely: oil distilled-bitumen grade Nybit E85 produced by Nynas (Sweden), oil viscous oxidized road bitumen grade 70/100 produced by JSC Mozyr Refinery (Belarus Republic), oil viscous oxidized road bitumen grade BND 60/90 JSC UkrTatNafta (Ukraine), emulsifiers Redicote E-11, Redicote 404, Redicote E-4875NPF, Redicote EM44 and Redicote C-320 produced by AkzoNobel (Sweden).

Physical-mechanical properties of bitumens are presented in Table 1. Penetration (Pen) and Ductility (D) were determined at 25 ºC.

According to Table 1, the difference between the oxidized bitumens and the distilled ones consists in the fact that the first ones have the larger plasticity interval (Softening Point is higher, while Fraaß breaking point is lower). For their part, distilled bitumens have substantially lower paraffin content and perceptibly higher total acid no., while that can be explained by differences in crude-oil and its processing technology.

Table 1. Physical-mechanical indices of bitumens

No	Type of bitumen	Name and value of indices					
		Softening Point, ºC	Pen, 0,1mm	D, cm	Fraaß breaking point, ºC	Paraffin content, % mass	Total acid no., mg KOH/g
1	Nybit E85	47	80	>100	-11	0,5	3,5
2	70/100 Mozyr Refinery	48	75	100	-21	4,5	0,6
3	BND 60/90 UkrTatNafta	49	72	84	-18	5,4	0,5

Production of bitumen emulsions was done on Danish laboratory batch bitumen-emulsion plant type DenimoTech SEP-0,3R (figure 1). Bitumen

emulsion formulations were developed for getting cationic slow-setting emulsions (CSS) intended for usage in slurry seal and microsurfacing technologies. Formulations with hydrochloric acid are presented in Table 2, while with ortho-phosphoric acid – in Table 3.

Fig. 1. Lab bitumen emulsion plant SEP-0,3R of Danish company DenimoTech

Table 2. Formulations of bitumen emulsion based on hydrochloric acid

No of formulation and type of bitumen	Components of emulsions, % w/w					
	Bitumen	Emulsifier Redicote E-11	Emulsifier Redicote 404	Emulsifier Redicote E-4875NPF	Hydrochloric acid in water phase till pH	Water
1.1) Nybit E85	61,0	1,1	–	–	2,5	till 100
1.2) Nybit E85	61,0	–	1,1	–	2,5	till 100
2.1) 70/100 Mozyr Refinery	61,0	1,1	–	–	2,5	till 100
2.2) 70/100 Mozyr Refinery	61,0	–	1,1	–	2,5	till 100
2.3) 70/100 Mozyr Refinery	61,0	–	–	0,8	2,0	till 100
3.1) BND 60/90 UkrTatNafta	61,0	1,1	–	–	2,5	till 100
3.2) BND 60/90 UkrTatNafta	61,0	–	1,1	–	2,5	till 100
3.3) BND 60/90 UkrTatNafta	61,0	–	–	0,8	2,0	till 100

Table 3. Bitumen emulsion formulations based on ortho-phosphoric acid Formulations of bitumen emulsion based on hydrochloric acid

No of formulation and type of bitumen	Components of emulsions, % w/w				
	Bitumen	Emulsifier Redicote EM44	Emulsifier Redicote C-320	Ortho-phosphoric acid in water phase till pH	Water
4.1) 70/100 Mozyr Refinery	61,0	1.1	–	2,5	till 100
4.2) 70/100 Mozyr Refinery	61,0	–	1,1	2,5	till 100
5.1) BND 60/90 UkrTatNafta	61,0	1.1	–	2,5	till 100
5.2) BND 60/90 UkrTatNafta	61,0	–	1,1	2,5	till 100

According to recommendations [12-13], production of efficient emulsions for slurry seal and microsurfacing technologies is possible not only based on high-acidic bitumen (in our case Nybit E85), but also on low-acidic one – with application of special emulsifiers. As those latter ones, there were taken the recommended by AkzoNobel emulsifiers – Redicote EM44 and Redicote C-320. These two emulsifiers are intended for rapid-setting emulsions, but in combination with ortho-phosphoric acid they provide for getting high-quality slow-setting emulsions.

Physical-mechanical indices of bitumen emulsions based on hydrochloric acid are presented in Table 4, while based on ortho-phosphoric acid – in Table 5.

Table 4. Physical-technical indices of bitumen emulsions based on hydrochloric acid

Index	Requirements according to [14]	Bitumen emulsions							
	ECS-60 (CSS)	1.1	1.2	2.1	2.2	2.3	3.1	3.2	3.3
Appearance	Homogeneous dark-brown liquid	Fits the requirements							
Hydrogen ions concentration, pH	1.5-6.5	2.52	2.60	2.95	2.99	2.86	2.83	2.82	2.93
Homogeneity (sieve No.014 residue), %, at most	0.25	0.01	0.01	0.01	0.01	0.01	0.01	0.01	0.01
Content of residual binding agent	58–62	61	61	61	61	61	61	61	61
Assumed viscosity at 25 ºC. (apparatus with hole diameter of 4 mm), s	5–25	7	8	6	6	7	6	7	6

Stability during storage: sieve No.014 residue, %, at most - after 7 days - after 30 days		 0.3 0.4	 0.07 0.12	 0.06 0.14	 0.06 0.14	 0.04 0.12	 0.06 0.14	 0.05 0.15	 0.06 0.17	 0.07 0.15
Adhesion of residual binding agent to macadam, points, no less		5.0	5.0	5.0	5.0	5.0	5.0	5.0	5.0	5.0
Miscibility with mixtures of grained composition	porous	Yes	Yes	Yes	Yes	Yes	Yes	Yes	Yes	Yes
	dense	Yes	Yes	Yes	Yes	Yes	Yes	Yes	Yes	Yes
Breaking index, %		180-230	189	191	196	201	197	204	198	201

Table 5. Physical-technical indices of bitumen emulsions based on orthophosphoric acid

Index		Requirements according to [14]	Bitumen emulsions			
		ECS-60 (CSS)	4.1	4.2	5.1	5.2
Appearance		Homogeneous dark-brown liquid	Fits the requirements			
Hydrogen ions concentration, pH		1.5-6.5	3.42	3.23	3.44	3.26
Homogeneity (sieve No.014 residue), %, at most		0.25	0.01	0.01	0.01	0.01
Content of residual binding agent		58–62	61	61	61	61
Assumed viscosity at 25 ºC. (apparatus with hole diameter of 4 mm), s		5–25	7	8	6	7
Stability during storage: sieve No.014 residue, %, at most - after 7 days - after 30 days		 0.3 0.4	 0.12 0.28	 0.13 0.29	 0.14 0.28	 0.12 0.26
Adhesion of residual binding agent to macadam, points, no less		5.0	5.0	5.0	5.0	5.0
Miscibility with mixtures of grained composition	porous	Yes	Yes	Yes	Yes	Yes
	dense	Yes	Yes	Yes	Yes	Yes
Breaking index, %		180-230	228	215	226	215

All the bitumen emulsions produced correspond to [14] for the grade ECS-60 (emulsion cationic road slow-setting with bitumen content from 58 to 62%) and can be applied for slurry seal and microsurfacing technologies.

From Table 4 one can see not large difference between the values of breaking index and pH of bitumen emulsions on distilled and oxidized bitumens with hydrochloric acid. Due to higher total acid number of distilled bitumens these indices of bitumen emulsions on Nybit E85 bitumen are lower than in emulsions on oxidized bitumens.

The main difference in physical-technical indices of emulsions on hydrochloric and ortho-phosphoric acids consists in the lower values of breaking index and emulsion pH, while it means higher reactivity of this emulsion. The worse indices of stability during storage mean (in emulsions on ortho-phosphoric acid) the possibility of worse bitumen emulsification during the emulsion production, i.e.: there is possibility of rapid emulsification of bitumen droplets after milling by colloid mill, while due to this phenomenon the droplets are from the very beginning larger than in the systems on hydrochloric acid. Besides, in course of testing on miscibility with mixtures of grained composition and breaking index there was noticed the increased stickiness and darker coloring of mixes on ortho-phosphoric acid – in comparison with the systems on hydrochloric acid. In general, based on the testing done, it is possible to confirm the efficiency of using ortho-phosphoric acid for production of slow-setting cationic bitumen emulsions.

4. Conclusion

1. There was ascertained the difference of physical-mechanical indices of distilled and oxidized bitumens.
2. There were developed formulations of bitumen emulsions on distilled and oxidized bitumens based on usage of hydrochloric and ortho-phosphoric acids and special emulsifiers.
3. There was determined difference between physical-technical indices of emulsions on different acids.
4. There was proved that the usage of ortho-phosphoric acid and special emulsifiers provides for production of cationic slow-setting emulsions for slurry seal and microsurfacing mixtures.

References

[1] AkzoNobel Surface Chemistry. Technical Bulletin. Bitumen emulsion. http://sc.akzonobel.com/en/asphalt/Documents/AN_Asphalt_Emulsion_TB_eng.pdf.

[2] A basic asphalt emulsion manual, Manual series No. 19 3rd edition, AEMA, USA.

[3] Koichi Takamura. Improved fatigue resistance of Asphalt emulsion residue modified with SBR Latex //AEMA Annual Meeting in Nashville, 2003.

[4] Louw K., Spence K. and Kuun P. The use of bitumen emulsions as a cost effective solution for constructing seals during winter // 8 conference on asphalt pavements for Southern Africa, September, 2004.

[5] Schilling, P., 2002. Success with Bituminous Emulsions Requires a Well Balanced Chemistry Of Emulsions, Bitumen and Aggregate, International Slurry Surfacing Association Conference, Berlin, Germany, 2002.

[6] B. Eckmann, S. Le Bec, F. Delfosse, J.E. Urbain. Formulation Of Emulsions For Micro-Surfacing. 2012 International Symposium on Asphalt Emulsion Technology. Oct. 10–12, 2012, Arlington Virginia.

[7] Zhdaniuk V. K. Properties of cationic bitumen emulsions, modified by water-based cationic latex "Butonal NS 198" / V. K. Zhdaniuk, V. Ya. Terletska / Vestnik (Herald) of Kharkiv National Motor-Road University. 2008. Edition 40. P. 17–20.

[8] Zhdaniuk V. K., Terletska V. Ya. Investigation of properties of emulsifiers for road bitumen emulsions. Vestnik (Herald) of Kharkiv National Motor-Road University. 2006. Edition 34–35.

[9] Asphalt emulsions (Chemistry and concepts), Alan James, 2nd Asphalt Technology Conference of the Americas, Austin, Texas, October 12–16th 1998.

[10] Phosphoric Acid for Microsurfacing Emulsions, Alan James and Tony Ng, European Roads Review No. 9, Revue generale des Routes et des Aerodromes, Fall 2006, pp. 4–9.

[11] AkzoNobel Surface Chemistry. Information Bulletin of Department «Additives for road construction». Europe, Middle East, India and Africa. Asphalt concrete issues. Acids in cationic emulsions. Edition 83, 2012, p. 13.

[12] AkzoNobel Surface Chemistry. Events in the field of asphalt concrete. Information Bulletin of Department «Additives for road construction». Application of cement in Slurry pavements. Europe. Edition 80, Fall 2009, p. 9

[13] AkzoNobel Surface Chemistry. Asphalt concrete issues. Information Bulletin of Department «Additives for road construction». Redipave System for rapid-setting Slurry-Seal pavement on arbitrary bitumen. Europe, Middle East, India and Africa. Edition 84, 2013, p. 6.

[14] Ukrainian standards DSTU B V.2.7-129:2013.

Przesłano do redakcji: 24.03.2017 r.
Przyjęto do druku: 28.09.2018 r.

CZASOPISMO INŻYNIERII LĄDOWEJ, ŚRODOWISKA I ARCHITEKTURY
JOURNAL OF CIVIL ENGINEERING, ENVIRONMENT AND ARCHITECTURE
JCEEA, t. XXXV, z. 65 (3/18), lipiec-wrzesień 2018, s. 91-100, DOI:10.7862/rb.2018.46

Rafał GRZEJDA[1]

COMPARATIVE ANALYSIS OF SELECTED METHODS FOR SEATING OF MACHINES USING FOUNDATION BOLTED JOINTS

Finite element modelling of elements connected in foundation bolted joints applied in the case of seating of heavy machines or devices is presented. The study is focused on joints made with the use of three different types of chocks: a steel chock, a polymer chock and a polymer-steel chock. Stiffness characteristics of the joined elements for the adopted models of the foundation bolted joint at the assembly stage are described and compared. Conclusions of paramount importance to the engineering practice are created.

Keywords: seating of machines, foundation bolted joint, foundation chock, finite element method

1. Introduction

The dynamics of industrial buildings are influenced by machines and devices installed on their floors. To reduce the vibratory effect caused by the machines in buildings vibration insulation is commonly adopted [1, 2]. In the design of the vibration insulation the way of seating of the machine on the foundation should be taken into account.

Seating of heavy machines or devices on foundations is usually carried out by means of bolted joints. In such connections special foundation chocks are also used. There are three types of these chocks [3–6]:
– steel chocks,
– polymer chocks,
– polymer-steel chocks.

The earliest known way of machinery seating is the seating using steel chocks (rigid chocks, but less frequently also chocks made as wedge chocks or adjustable chocks [7]). This seating is associated with two disadvantages occurring during the assembly of the foundation bolted joint. The first one is the

[1] Rafał Grzejda, West Pomeranian University of Technology, Szczecin, Faculty of Mechanical Engineering and Mechatronics, 19 Piastów Ave., 70-310 Szczecin; tel. 914494969; rafal.grzejda@zut.edu.pl

need to ensure even distribution of contact pressure on all the chocks by matching their surfaces and abutment surfaces of the mounted machinery and the foundation. Such actions are difficult, tedious and laborious. Additionally, in case of seating applying the preload to foundation bolts brings on considerable contact deformations between the joined elements [8].

The second way of machinery seating is the seating on cast polymer chocks. In this case, precise machining surfaces of the joined elements is not necessary. In addition, direct casting chocks under the base of the machine ensures a close fit of these surfaces together. Inequalities resulting from the roughness of the joined surfaces are filled with polymer, whereby the pressure distribution on that surfaces is more favourable than in the case of the seating using steel chocks [9]. However, a disadvantage of seating on cast polymer chocks is their creep in the operational condition, evoking relaxation of the pretension in the foundation bolts [5, 10].

The third and newest way to perform machinery seating is the seating with polymer-steel chocks. It brings together advantages of seating according to two aforementioned methods and minimizes disadvantages occurring there. In the joints made of polymer-steel chocks the creep of the chocks is significantly reduced. At the same time, abutment surfaces of the joined elements adhere closely to each other and there is no need to matching them. Additionally, in the foundation bolted joint of this type steel chocks of the same thickness in the whole area of the connection can be applied.

Foundation bolted joints often have a significant impact on vibrations, reliability and durability of the entire mechanical systems. Therefore, to analyze the problems occurring in them, knowledge about their behaviour in the assembly and operational conditions is required. In order to know this behaviour usually the appropriate stiffness characteristics are determined.

Studies on foundation bolted joints with the steel chocks and the chocks made of polymer are described, inter alia, in [11–13]. In contrast, studies on foundation bolted joints with the polymer-steel chocks are presented for example in [5, 7]. The current paper is an extension of the research on foundation bolted joints, and its primary objective is to determine the stiffness characteristics of the elements joined in the foundation bolted joint in the case of the assembly condition for all the above-mentioned its types, taking into account the steel chock, the polymer chock, and the polymer-steel chock.

An object of research are some symmetrical segments of the foundation bolted joint in the form of two rectangular plates and a rectangular chock located between the plates. The chock can be in one of the three aforementioned types. So separated systems are modelled by the finite element method (FEM) to determine the stiffness characteristics for the joined elements in the assembly state. The EPY resin compound is used as the polymer material [12, 14]. The result of the work are conclusions of key and paramount importance to the engineering practice.

2. Basics of the analysis

One of the important issues considered in the case of calculations of foundation bolted joints is the stiffness analysis of its elements. Treating the bolts as linear elements, their elastic flexibility can be determined by the instructions given in the standard VDI 2230 [15] or by using the simplified method [16]. There is no equally easy way to set down the elastic flexibility of elements joined in foundation bolted joints [13]. Therefore, to accurately determine it the finite element method is usually applied.

To analyze the above methods of seating, calculations were executed for the following models:

– FEM-S – the model with the steel chock,
– FEM-P – the model with the polymer chock,
– FEM-PS – the model with the polymer-steel chock.

In the paper, a single bolted connection separated from the foundation bolted joint, with the geometry shown schematically in Figs. 1–3, is examined. The bolted connection is created by two steel plates (2) and (4) corresponding to fragments of the machine base and the continuous footing. The chock (3) or (6), suitable for the applied method of seating, is located between the plates. Because the objective of the paper is the stiffness analysis of the joined elements, in the connection the full bolt model is not included (for a review, see [17]). The bolt is represented by a pair of steel stamps (1) and (5), by means of which the pressure from the head of the bolt and the nut is introduced. The diameter of these stamps is equal to 46 mm and it is adjusted according to the pressure area from the M30 nut.

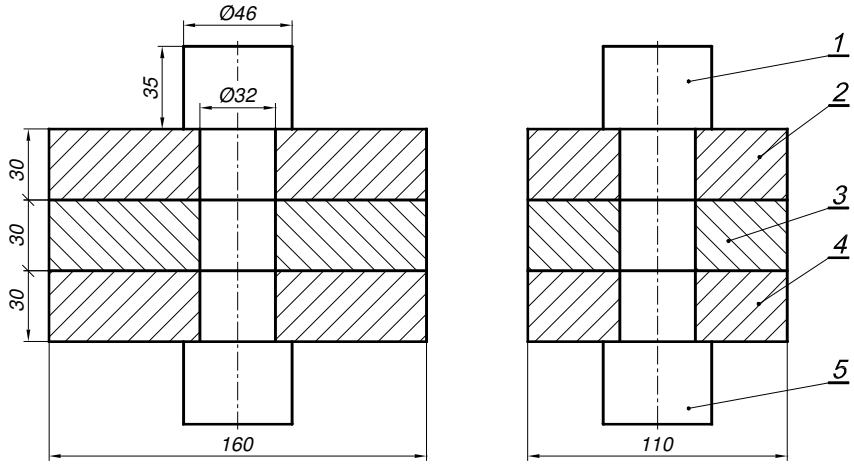

Fig. 1. Geometry of foundation bolted joint model with the steel chock: 1 – top pressure stamp, 2 – top plate, 3 – steel chock, 4 – bottom plate, 5 – bottom pressure stamp

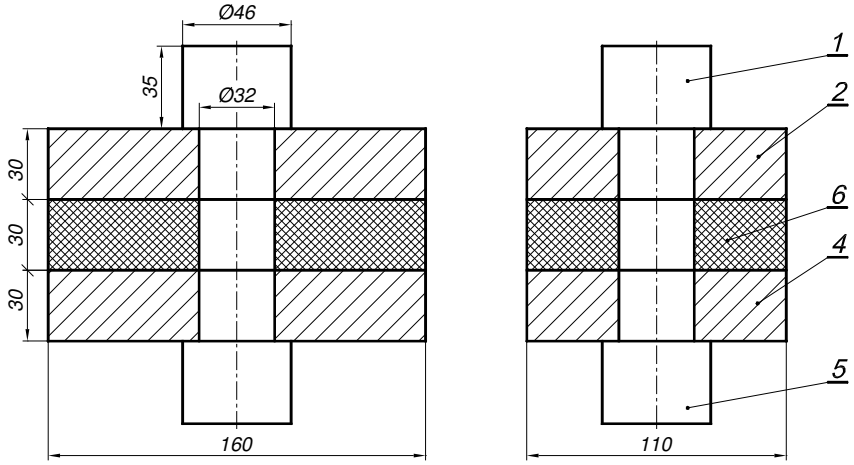

Fig. 2. Geometry of foundation bolted joint model with the polymer chock: 1 – top pressure stamp, 2 – top plate, 4 – bottom plate, 5 – bottom pressure stamp, 6 – polymer chock

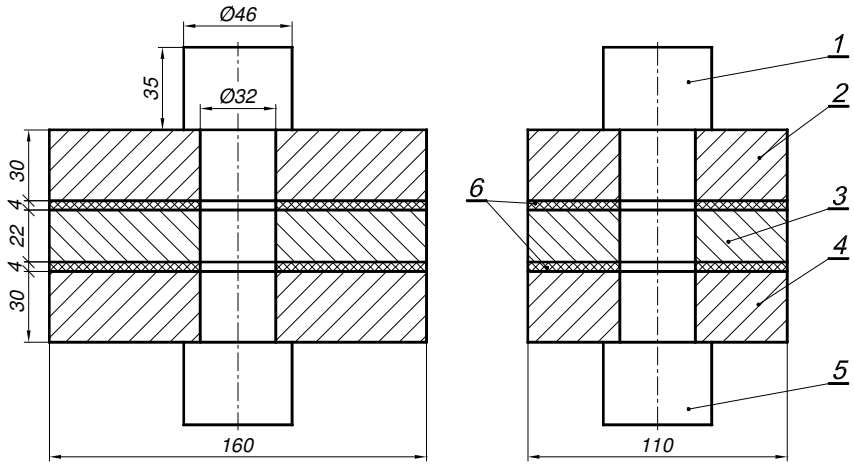

Fig. 3. Geometry of foundation bolted joint model with the polymer-steel chock: 1 – top pressure stamp, 2 – top plate, 3 – steel chock, 4 – bottom plate, 5 – bottom pressure stamp, 6 – polymer chock

3. Computational models

Calculations were performed for dimensions of the joined elements given in Figs. 1–3. On the basis of works [18, 19], it is assumed that the EPY resin compound is a linear material. Material constants for the materials used in the models are collected in Table 1.

Table 1. Characteristics of materials used for the foundation chocks

Parameter	Steel	EPY compound
Young's modulus, E [GPa]	210	7.5
Poisson's ratio, ν	0.3	0.376

In the view of two planes of symmetry occurring in the considered fragment of the foundation bolted joint, only a quarter of the connection shown in Fig. 4a, has been taken into account in the calculations.

The discrete models of the connection created in the Midas NFX 2017 R1 program is presented for all the adopted methods of seating in Figs. 4b and 5. Pursuant to results described in [13], between the steel joined elements and the steel chock the "general" model of the contact connection is applied (for a review, see [20]). Simultaneously, between the steel joined elements and the polymer layer the "welded" model of the contact connection is used. The models are fixed in the nodes on the back side of the bottom pressure stamp in the direction of the bolt axis and loaded in the nodes on the upper surface of the top pressure stamp with normal forces.

Additionally, appropriate degrees of freedom (translational and rotational) are removed in the nodes lying on the symmetry planes of the foundation bolted joint. Due to such application of boundary conditions and load, the elements joined in the foundation bolted joint models are subjected to compression, which is consistent with the actual work of these connections.

Calculations were performed using a nonlinear solver in ten steps with the incrementally increasing preload F from 0 to 200 kN.

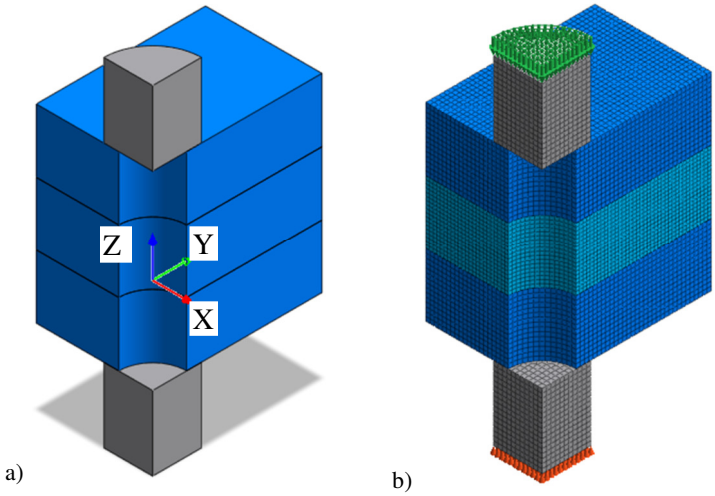

Fig. 4. Foundation bolted joint models – calculation model (a) and FEM-S model (b)

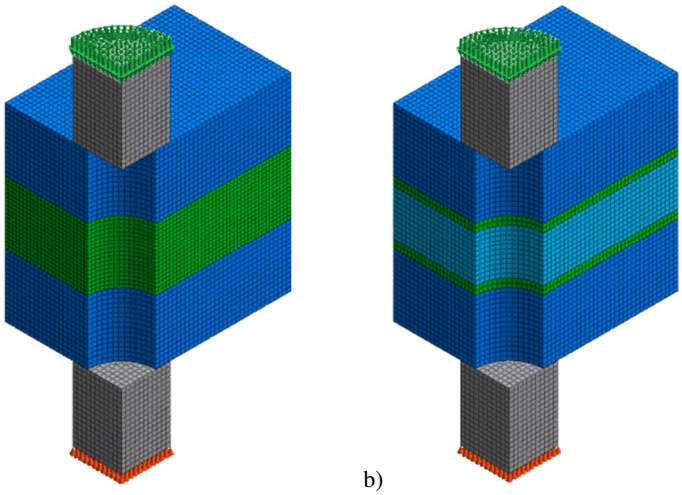

a) b)

Fig. 5. Foundation bolted joint models – FEM-P model (a) and FEM-PS model (b)

4. Results of calculations and their comparison

Examples of the calculation results for adopted FEM-models in the form of displacements in the Y0Z plane under the preload F equal to 200 kN are shown in Fig. 6.

In order to conduct comparative analysis of the calculation results respective statement of these results obtained for the tested connection and all their FEM-models is performed (Fig. 7).

In the next step, displacements of elements joined in the foundation bolted joint ΔH corresponding to the maximum value of the preload F is designated. The final parameter adopted for quantitative comparison of the computational models is the stiffness of joined elements k, calculated as [13]:

$$k = \frac{F}{\Delta H} \tag{1}$$

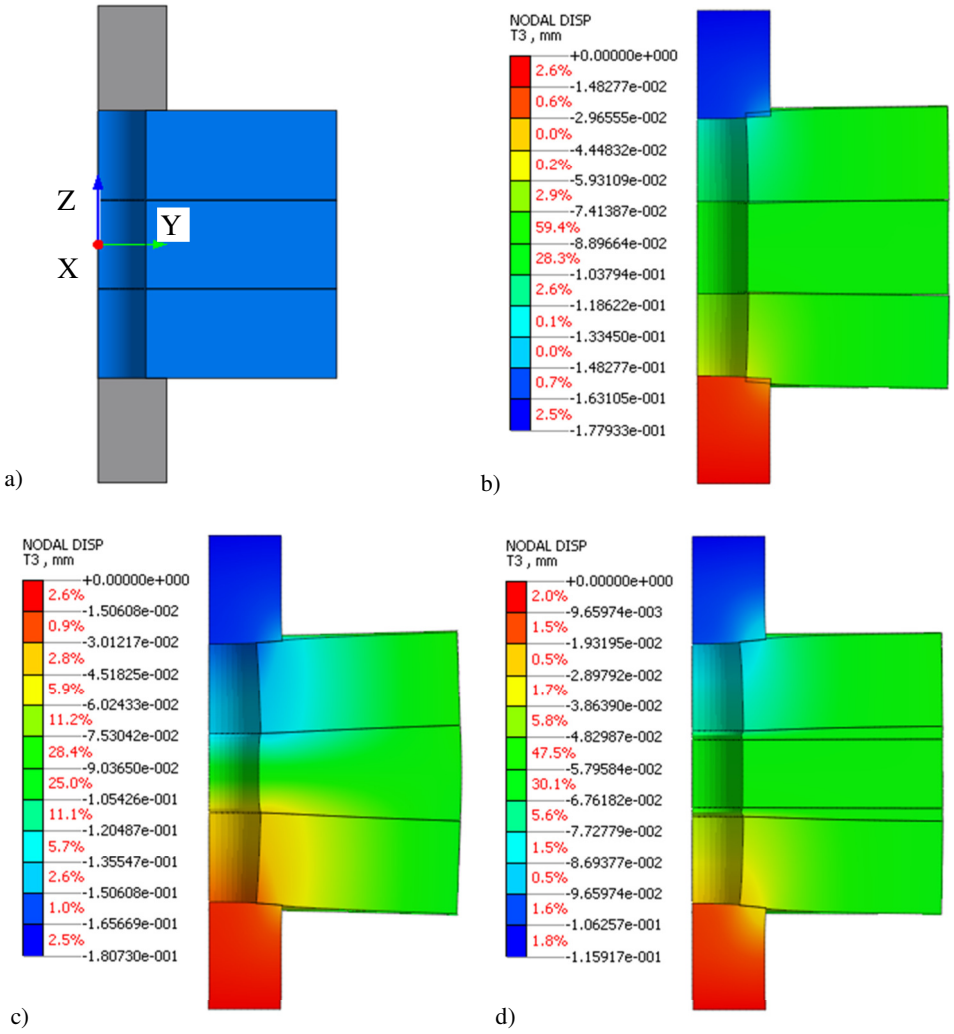

Fig. 6. Results of calculation – scheme of the model (a) and displacements in the Y0Z plane of the foundation bolted joint models loaded by the force F = 200 kN for: FEM-S model (b), FEM-P model (c), FEM-PS (d)

The stiffness values of the joined elements obtained for the adopted foundation bolted joint models are summarized in Table 2. In the case of the FEM-P and FEM-PS models as a result of the calculations linear stiffness values are given, whereas in the case of the FEM-S model stiffness value determined from the nonlinear stiffness characteristic for preload F equal to 200 kN is included.

Table 2. Stiffness values of the elements joined in the foundation bolted joint

Model	**FEM-S**	**FEM-PS**	**FEM-P**
k [kN/μm]	3.14	3.15	1.57

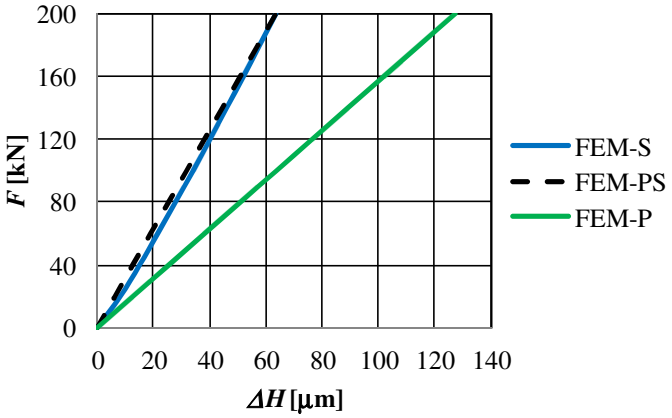

Fig. 7. Stiffness characteristics of the elements joined in the foundation bolted joint

Based on the calculation results for adopted models of the foundation bolted joint it should be stated that the use of the polymer-steel chock can lead to:
- significant improvement of foundation bolted joint stiffness in relation to the connection with the chock made of polymer,
- obtaining the foundation bolted joint with the stiffness similar to the stiffness of the connection with the steel chock.

From observation of stress maps for the FEM-P and FEM-PS models, it follows that the normal stresses for the EPY resin compound did not exceed the compressive strength values for this material [21].

5. Conclusions

In the paper foundation bolted joints made by seating in three ways is analyzed. It has been shown that the foundation bolted joint with the polymer-steel chock can have the stiffness characteristics close to the foundation bolted joint with the steel chock. At the same time, these joints are characterized by advantages appropriate for the joints with the polymer chock, among which the most important is an exact mach and strict adherence the chock to rough surfaces of the joined elements of the machinery and the foundation around the all nominal contact area.

The study should be continued in order to determine the effect of the thickness of the polymer layer in the polymer-steel chock on the stiffness characteristics of elements joined in the foundation bolted joint made with such a chock.

References

[1] Mak C.M., Yun Y.: A study of power transmissibility for the vibration isolation of coherent vibratory machines on the floor of a building, Applied Acoustics, vol. 71, no. 4, 2010, pp. 368–372.

[2] Yun Y., Mak C.M.: Assessment of the stability of isolated vibratory building services systems and the use of inertia blocks, Building and Environment, vol. 45, no. 3, 2010, pp. 758–765.

[3] General guidelines for marine chock designers, Technical Bulletin 692D, ITW Polymer Technologies, Montgomeryville 2005.

[4] Grudziński K., Grudziński P.: Tradycyjny i nowoczesny sposób posadawiania ciężkich sprężarek tłokowych na fundamentach betonowych, Przegląd Mechaniczny, nr 5, 2009, s. 15–21.

[5] Piaseczny L.: New types of washers and foundation bolts for seating marine diesel engines, Combustion Engines, vol. 48, no. 3, 2009, pp. 23–27.

[6] Guidelines for the seating of propulsion plants and auxiliary machinery, Germanischer Lloyd AG, Hamburg 2010.

[7] Piaseczny L.: Marine engine seating on polymer-metal chocking, Combustion Engines, vol. 47, no. 4, 2008, pp. 3–13.

[8] Grudziński P., Konowalski K.: Experimental investigations of normal deformation characteristics of foundation chocks used in the seating of heavy machines and devices, Part 1: Theoretical fundamentals and investigations of a steel chock, Advances in Manufacturing Science and Technology, vol. 38, no. 1, 2014, pp. 63–76.

[9] Piaseczny L.: Designing of power plant rechocking using a pourable polymer on example of ship's power plant, Eksploatacja i Niezawodnosc – Maintenance and Reliability, vol. 4, no. 2, 2002, pp. 26–38.

[10] Kawiak M., Kawiak R.: Dobór materiału na fundamentowe podkładki maszyn, Inżynieria Materiałowa – Materials Engineering, vol. 36, no. 6, 2015, s. 528–531.

[11] Piaseczny L.: Analysis of main propulsion engine seatings in ship power plants, Journal of Polish CIMAC, vol. 5, no. 1, 2010, pp. 135–142.

[12] Grudziński K., Grudziński P., Jaroszewicz W., Ratajczak J.: Assembling of bearing sleeve on ship propulsion shaft by using EPY resin compound, Polish Maritime Research, vol. 19, no. 2, 2012, pp. 49–55.

[13] Grudziński P., Grzejda R.: Wyznaczenie charakterystyk montażowych modeli fundamentowych złączy śrubowych z podkładką stalową i odlaną z tworzywa, Przegląd Mechaniczny, nr 5, 2016, s. 34–38.

[14] Urbaniak M., Ratajczak J.: Modernizacja posadowień maszyn i urządzeń okrętowych oraz przemysłowych z zastosowaniem tworzywa chemoutwardzalnego EPY, Część 1: Praktyczne zastosowania tworzywa, Inżynieria Materiałowa – Materials Engineering, vol. 36, no. 6, 2015, s. 532–536.

[15] Schaumann P., Kleineidam P., Seidel M.: Zur FE-Modellierung von zugbeanspruchten Schraubenverbindungen, Stahlbau, vol. 70, no. 2, 2001, pp. 73–84.

[16] Bouzid A.-H., Beghoul H.: The design of flanges based on flexibility and tightness, In Analysis of bolted joints, Proc. of the 2003 ASME Pressure Vessels and Piping Conference, Cleveland, Ohio, 20-24 July 2003, pp. 31–38.

[17] Grzejda R.: New method of modelling nonlinear multi-bolted systems, In Advances in Mechanics: Theoretical, Computational and Interdisciplinary Issues, Proc. of the 3rd Polish Congress of Mechanics (PCM) and 21st International Conference on Computer Methods in Mechanics (CMM), pp. 213–216, CRC Press/Balkema, Leiden 2016.

[18] Grudziński P.: Analiza odkształceń i naprężeń w fundamentowych złączach śrubowych, Część 2: Złącze śrubowe z podkładką z tworzywa, Modelowanie Inżynierskie, nr 52, 2014, s. 72–79.

[19] Grudziński K., Jaroszewicz W., Grudziński P., Ratajczak J.: 40 lat stosowania polskich tworzyw w posadawianiu maszyn i urządzeń na fundamentach, Przegląd Mechaniczny, nr 4, 2015, s. 26–35.

[20] Grzejda R.: Designation of a normal stiffness characteristic for a contact joint between elements fastened in a multi-bolted connection, Diagnostyka, vol. 15, no. 2, 2014, pp. 61–64.

[21] Urbaniak M., Grudziński K.: Wpływ szybkości odkształcania na charakterystyki mechaniczne tworzywa epoksydowego EPY® poddanego obciążeniom ściskającym, Kompozyty, nr 4, 2006, s. 24–28.

Przesłano do redakcji: 12.03.2018 r.
Przyjęto do druku: 25.09.2018 r.

CZASOPISMO INŻYNIERII LĄDOWEJ, ŚRODOWISKA I ARCHITEKTURY
JOURNAL OF CIVIL ENGINEERING, ENVIRONMENT AND ARCHITECTURE
JCEEA, t. XXXV, z. 65 (3/18), lipiec-wrzesień 2018, s. 101-110, DOI:10.7862/rb.2018.47

Paweł TWORZEWSKI[1]
Kamil BACHARZ[2]
Dorota MICHAŁOWSKA-MAZIEJUK[3]

ANCHORAGE SYSTEMS IN FRP – STRENGTHENED REINFORCED CONCRETE

The main aim of this article was to present recently evolved methods of strengthening flexural reinforced concrete beams, as well as the concrete-anchorage system bond strength problems in composites that were either surface mounted or inserted in the pre-cut grooves in the concrete cover. The focus is on the beams strengthened with the carbon FRP (CFRP – carbon fiber reinforced polymer) composites to show the basic advantages and drawbacks associated with their installation and bond performance. Domestic and foreign experiments investigating the EBR and NSMR strengthening systems were discussed to show their efficacy, common failure modes and the factors initiating the debonding process. Debonding problems and solutions to those problems were illustrated using the example of a composite material attached to the outer surface of concrete in the shear zone of reinforced concrete beams The article provides guidelines for checking the anchorage capacity for the existing longitudinal reinforcement with the simultaneous action of bending moment and shear force in the support zone of the reinforced concrete beam.

Keywords: reinforcing, strengthening, FRP, anchorage systems, failure modes

1. Introduction

External strengthening method is the most popular method used to increase the load-bearing capacity of reinforced concrete (RC) members, with the ease and speed of application being two major factors. The externally bonded systems include steel strengthening (mechanically fastened with steel dowels or adhesive

[1] Corresponding author: Paweł Tworzewski, Politechnika Świętokrzyska, Katedra Wytrzymałości Materiałów, Konstrukcji Betonowych i Mostowych, al. Tysiąclecia Państwa Polskiego 7, 25-314 Kielce; tel. 413424752; ptworzewski@tu.kielce.pl
[2] Kamil Bacharz, Politechnika Świętokrzyska, Katedra Wytrzymałości Materiałów, Konstrukcji Betonowych i Mostowych, al. Tysiąclecia Państwa Polskiego 7, 25-314 Kielce; tel. 413424752; kbacharz@tu.kielce.pl
[3] Dorota Michałowska-Maziejuk, Politechnika Świętokrzyska, Katedra Wytrzymałości Materiałów, Konstrukcji Betonowych i Mostowych, al. Tysiąclecia Państwa Polskiego 7, 25-314 Kielce; tel. 413424752;d.michalowska@tu.kielce.pl

resins) or composite strenghtening (fastened with adhesive resins and adhesive resins supplemented with anchor blocks if prestressed). The common use of FRP composites is due to their strength parameters, corrosion resistance, the possibility of using any lengths without joints, low weight, and the ease of transport and application. One of the important problems in the case of using external strengthening methods is to ensure proper anchorage, necessary for correct performance of the system and reinforcing bars in flexure and shear. Extensive studies have been devoted to developing new or improving the existing anchoring methods.

2. Methods of strengthening reinforced concrete beams using metallic and non-metallic materials attached to concrete surfaces or placed in pre-cut grooves in a concrete cover

First research in Poland on the possibility of using external steel elements for strengthening RC beams was carried out by Ciesielski in the 1970s [1]. Flat steel strips were attached to the bottom of the beam, using epoxy resin. The main problem was the concentration of tangential stresses (occurring at the primary crack location) which, by exceeding the resin strength, led to the detachment of steel plates, typically at the ends of the strengthening element due to the highest stress values in the resin. The results reported in [1] were the basis for the concept of fastening steel plates with the use of bolts inserted into RC members [2] to eliminate the bound problems. The bolts were the only joints between the plate and the strengthened member. Depending on the cross-section of the steel plates, the diameter and spacing of the bolts, an increase in load capacity (compared to the load capacity of non-reinforced elements) was in the range 50 to 166.7%. The most interesting observations included significant differences in the forces transmitted to individual bolts. This was evidently due to the presence of cracks and the randomness of their formation process, which is particularly important at high stresses in strengthened beams. The strengthening of girders of the Warsaw Central railway viaducts is an example of the use of this method [3]. The first studies on the use of carbon fibers embedded in epoxy resin for the strengthening of reinforced concrete structures were carried out in the mid-1980s at the EMPA Institute in Switzerland. It was the beginning of externally bonded fiber-reinforced polymer strengthening systems (EBR-FRP) application. One of the solutions to increase the effectiveness of the described strengthening method is to increase the area cooperating with the member/beam by embedding composite reinforcement in the grooves pre-cut in the concrete cover. Such strengthening systems are called NSMR (Near Surface Mounted Reinforcement). Enlarging the contact area of the composite material with the adhesive mortar delays the debonding from the concrete. The simulation of the efficiency of this method [4] showed that with the same surface area of

composite reinforcement applied using the EBR and NSMR methods, the load capacity increased by 43% and 137% respectively relative to the beam that was not strengthened. This was confirmed by the results presented in [5] (increase in the use of composite reinforcement strength from 30÷35% (EBR method) up to 80%. The composite reinforcement in the NSMR method needs to be inserted in the pre-cut grooves in the concrete cover, which presents a risk of cutting the existing reinforcement, which is why this method can be used only in cases, where the thickness of the reinforcement cover allows it.

In recent years, research has been carried out to eliminate premature debonding of the composite material and increase the effectiveness of strengthening method through the use of composite anchors combined with substantial reinforcement. This method allows eliminating the drawback of anchorage systems based on steel elements, i.e. susceptibility to corrosion. Reported in [6] a 30% increase in load bearing capacity was obtained with additional composite anchors.

In the 1970s, the idea of active strengthening, i.e. the use of pre-stressed fibers, was born. This solution has a number of advantages, such as lower deflections and thus reduced crack widths (greater member stiffness) and the stress reduction, especially in steel bars. Examples include the SIKA CarboDur LEOBA and STRESS-HEAD systems, Polish IBDiM system, BBR-stahlton, S & P, and NEOXE [5, 7]. The most important problem is to ensure adequate bonding, especially at the ends of the strengthening strips, where the tangential stresses are the greatest (high likelihood of debonding).Additional anchoring elements such as anchor blocks should effectively carry the stress, thereby providing protection against losses of prestressing force and, at the same time, avoid excessive compression in the composite strengthening[8]. The disadvantage of such solutions are steel elements (anchored steel plates with bolts) remaining permanently connected to the structure and exposed to corrosion. These strengthening methods are mainly used in bridge structures exposed to aggressive environments. The problem of steel corrosion can be resolved by eliminating the use of mechanical anchors, as in the EMPA systems and Tenroc Technologies (stepwise prestressing). The NSM prestressing system is being developed at the Lodz University of Technology, which, in contrast to the EBR, has been found to be much more effective.

A lot of attention has been paid in recent years to the methods of providing anchorage for shear strengthening of reinforced concrete beams. The limited possibility of obtaining a suitable anchorage in this case results from the fact that the composite strengthening cannot be fixed on the whole perimeter of the cross-section of the beam due to the presence of a floor slab. Three leading solutions can be distinguished:

- use of steel anchor plates (usually these are elements with a steel angle cross-section) fastened with steel bolts in the corner (connection of the plate with the beam). Not always, but in a majority of cases, their use is associated with the

necessity to make holes (damage to the composite fibers), which leads to undesirable concentration of stresses. If the strengthening material is carbon fiber, there is an increased risk of galvanic corrosion [9] (figure 1B),

- UA anchorage type – used mainly for flaccid composite sheets. This method consists in bending the end of the composite and fixing it in the previously prepared pre-cut grooves in a concrete cover. (This method can also be used in the case of bending reinforcements),
- use of composite anchors. The part left outside is fan-folded on the surface. Then the proper reinforcement is attached to the element prepared in this way, as shown by the SikaWrap FX Fiber Connector [10] (figure 1A).

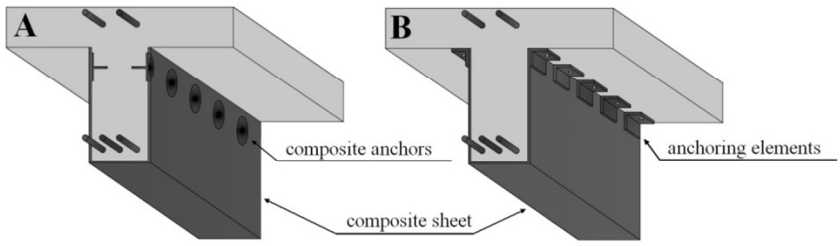

Fig 1. Anchoring the composites attached to the side surfaces of the reinforced concrete beam by means of: A-steel anchor plates, B – composite anchors

3. Cooperation with the reinforced concrete beam and proper anchorage

To use a composite strengthening material, the peel strength of the concrete substrate obtained using the pull-off method cannot be lower than 1.0 MPa. The recommendations set forth in the Fib 14 bulletin give a minimum value of 3.0 MPa [11]. These requirements have to be met to obtain the correct cooperation between the strengthening material and the strengthened element, which is not easy in old structures.

Difficulties related to ensuring proper bond and embedment of reinforcements attached to RC members result from the presence of high inter-layer shear stresses in the laminate (mainly at the end of strengthening element, e.g. CFRP laminate). This is particularly important in the case of pre-stressed composite reinforcements.

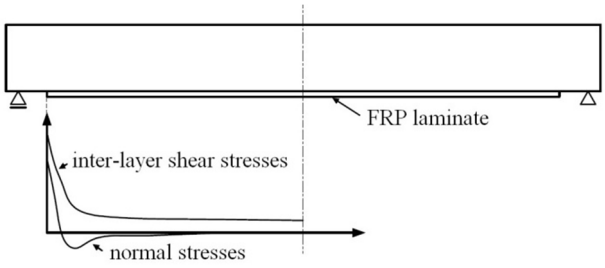

Fig. 2. Distribution of inter-layer stresses along the length of the FRP laminate

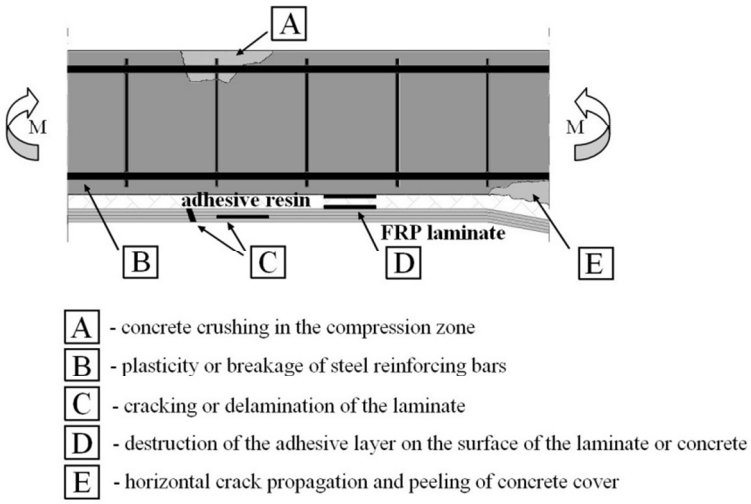

Fig. 3. Failure modes of a reinforced concrete beam strengthened with a composite laminate

Several failure modes of RC concrete beams strengthened with a composite laminate (Fig. 2, 3) can be distinguished. The three most common were reported in [12]. The first mechanism is caused by intermediate crack induced debonding (ICD). The second mechanism consists in rupturing the composite reinforcement in the middle of the element – R (rapture). The third mechanism is initiated by shear (despite working on bending) or by crushing of compressive concrete – CC, loss of anchoring at composite ends (ED – end debonding, CCS – concrete cover separation, A – anchorage failure) [11]. This mode is not typical in flexural elements and is therefore dangerous. An example of failure of the RC beam strengthened with the NSMR system is shown in figure 4. Separation of the FRP proceeded rapidly and extended over the support zone and the area of pure bending. Failure was caused by horizontal crack propagation and concrete cover peeling. The separation plane passed along the surface of the steel bars and the concrete cover remained bonded to the laminate. Research carried out at the Lodz University of Technology also showed that the pursuit of maximum use of tensile strength of composite reinforcement (especially in the absence of

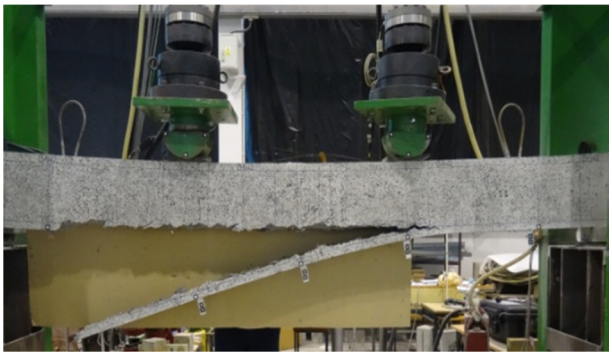

Fig. 4. Failure mode by horizontal crack propagation and peeling of concrete cover

additional anchoring) may contribute to a reduced level of structural safety due to sudden debonding, occurring with little warning (so-called brittle failure) [13].

The test results reported in [5] show that the dimensions of the element cross-section, the type of composite reinforcement, the distance of its ends from the support, the steel reinforcement scheme and the distribution of cross-section forces in the strengthened element are the parameters that affect the effectiveness of passive reinforcement. According to Barros and Sena Cruz who used the NSMR method in their study of the adhesion of composite reinforcements [14], the value of the maximum adhesive force increases with the increase in the embedment length. In [15] the aspect of composite reinforcement bond to the concrete substrate was also considered in relation to the grade of concrete. The increase in the compressive strength of concrete was found to delay the debonding of the laminate and had a beneficial effect on the adhesive stress.

In addition to the concrete strength, plasticity of steel and the related increase in crack width are important factors initiating the debonding process. The Lodz University of Technology research confirmed these factors but did not confirm the bonding reduction despite the fact that the concrete strength in the reinforced elements was very low ($f_{c,cube}$ = 20 MPa). Another factor that contributes to the composite-concrete debonding is the vertical "fault" that appears beside the inclined shear crack mainly in the elements with a low degree of transverse reinforcement [13].

Another important aspect of strengthening RC beams is the anchoring of the existing steel reinforcement, especially on external supports. The need to strengthen the structure is often associated with the design errors or use change. In both cases, some elements will have insufficient load bearing capacity, compensated by means of strengthening the additional steel reinforcement or, increasingly used, composite reinforcements. An equally important issue as determining the basic number of reinforcing elements and their anchoring is also the load bearing capacity of the existing (basic) reinforcement and appropriate anchor length [16, 17]. This is due to the fact that strengthening elements are often anchored but not put into their supports.

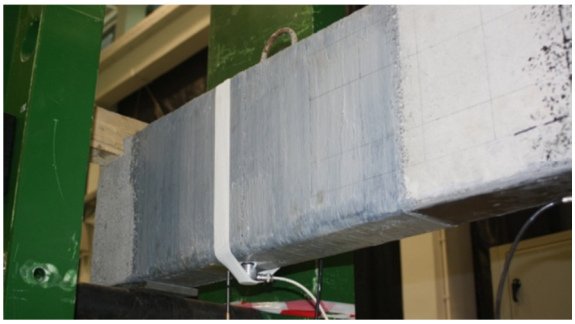

Fig. 5. Passive reinforcement of reinforced concrete beams using CFRP tapes anchored with a mat CFRP

As a result, due to the increased cross-sectional forces, basic reinforcement bars anchored in these supports are subjected to considerable stresses. Improper anchorage will lead to the pulling out the rods and in consequence to the failure of the element. Bacharz and Goszczyńska in [18] show a 30% decrease in the load capacity of the element with insufficient anchoring of the main tensile reinforcement compared to the elements with full anchorage, as a result of which the beam failed due to the main reinforcement bars breaking off in the support zone (Fig. 6). In the case described in [18], the point support in the form of a steel cylinder was used(type of support similar to those found on actual bridge structures).

Fig 6. Failure of a reinforced concrete beam with insufficient bond length in the support zone of the main tensile reinforcement [18]

As a result, the longitudinal reinforcement at the anchoring point was stressed mainly due to the shear force, not the bending moment. This is important because according to currently used Mörsch truss model, it is possible to underestimate this force, represented by the following formula

$$l_{b,rqd} = \frac{\phi}{4} \frac{\frac{M}{A_{s1} \cdot z} + \frac{0{,}5 \cdot V \cdot \left(\cot\theta - \cot\alpha\right)}{A_{s1}}}{f_{bd}} \tag{1}$$

where: ϕ – diameter of the anchored bar [mm],
A_{s1} – cross-sectional area of anchored tension reinforcement [m^2],
M – bending moment [kNm],
V –shear force [kN],
f_{bd} – limit design bond stress [MPa],
σ_{sd} –stress in anchored steel [MPa],
$\cot\theta$ – cotangens of the inclination angle of the pressed concrete struts,
$\cot\alpha$ – cotangens of inclination angle of transversal reinforcement.

Underestimated force is the consequence of the possibility of accept any value of cotangens of inclination angle of the compression struts θ from the range 1.0 to 2.0. The acceptance of 1.0 is associated with the adoption of transversal reinforcement with considerable stocks and at the same time contributes to 50% reduction in the design force carried to the longitudinal reinforcement. This situation is particularly dangerous with external support, especially joint supports with shear as a predominant force. Therefore, as confirmed by the analyses reported in [18, 19, 20], the recommended value of the $\cot\theta$ is 2.0. This value gives proper estimation of the shear force carried to the longitudinal reinforcement and safe level of shear reinforcement capacity. In addition to the designing of strengthening method, it is also important to determine the anchoring capacity of the existing longitudinal reinforcement with simultaneous bending moment and shear force assuming $\cot\theta$ equal to 2.0.

4. Summary

This review of currently used methods of strengthening flexural reinforced concrete beams and the problems of the bond of strengthening elements and existing longitudinal reinforcement shows that this subject requires further analysis. The use of composite materials as external strengthening systems for reinforced concrete elements are currently the most popular, relatively easy, and quick capacity improvement methods. In the paper, special attention was paid to the beam strengthening using carbon fiber composites, CFRP, their basic advantages and fundamental problems associated with the strengthening technology, bonding and embedment of composites. The experimental studies carried out so far in Poland and abroad were the basis for the discussion of the effectiveness of the strengthening systems, EBR and NSMR, the most frequently occurring failure modes, and the factors initiating the process of composite separation. The debonding problem was considered using the examples of composites externally strengthening the concrete surface and existing reinforcement of RC beams. Solutions were provided for the problem of insufficient bonding. In old structures, ensuring adequate adhesion of metallic and non-metallic reinforcements bonded to the surface of concrete or embeded in the concrete cover is difficult due to low concrete strength or surface condition. The selection of appropriate strengthening technology is a critical

design stage. It should take into account, for example: fire protection requirements, environmental conditions, constraints imposed by the structure and requirements set by the architect and client. The following factors should be taken into account in the design of strengthening systems: the arrangement of bars, bars diameters, the strength of steel, bond/embedment length, and the strengthening capacity of existing longitudinal reinforcement with the simultaneous effect of the new bending moment and shear force.

References

[1] Ciesielski J.: Łączenie i naprawy konstrukcji betonowych za pomocą żywic epoksydowych, Arkady, Warszawa 1976.

[2] Urban T.: Wzmacnianie konstrukcji żelbetowych metodami tradycyjnymi, PWN, Warszawa 2015.

[3] Rybak M., Łagoda M.: Wzmocnienie mostów betonowych za pomocą przyklejanego zbrojenia zewnętrznego., XVIII konferencja Naukowo-techniczna Szczecin-Międzyzdroje, Awarie budowlane, 1997, Tom 1, s. 41–50.

[4] Kotynia R.: Analysis of reinforced concrete beams strengthened with near surface mounted FRP reinforcement, Archives of Civil Engineering, LII 2, 2006, s. 305–317.

[5] Kotynia R.: Przyczepnościowe metody wzmacniania konstrukcji żelbetowych przy użyciu naprężonych kompozytów polimerowych, Przegląd Budowlany 7–8/2015, s. 49–56.

[6] Scott T. Smith, Shenghua Hu, SeoJin Kim, Rudolf Seracino: FRP-strengthened RC slabs anchored with FRP anchors, Engineering Structures, Volume 33, Issue 4, April 2011, pp. 1075–1087.

[7] Siwowski T., Michałowski J., Błażewicz S.: Nowy system sprężenia taśm kompozytowych CFRP do wzmocnienia mostów, XXIV konferencja Naukowo-techniczna Szczecin-Międzyzdroje, Awarie budowlane, 26-29 maja 2009, s. 947–960.

[8] Paśko P., Piątek B., Siwowski T.: Badania zakotwień w systemie Wzmocnienia konstrukcji sprężonymi taśmami CFRP, Budownictwo i Architektura 13(3) 2014, s. 143–150.

[9] Kanakubo T., Aridome Y., Fujita N.,Matsui M.: Development of Anchorage System for CFRP Sheet in Strengthening of Reinforced Concrete Structures, 12WCEE, 2000, s. 1831–1838.

[10] Geoffrey N. McGuirk, Sergio F. Breña: Development of anchorage system for FRP strengthening applications using integrated FRP composite anchors, Report submitted to theConcrete Research Council of the ACI Foundation, October 2012.

[11] FIB 14, Externally bonded FRP reinforcement for RC structures.

[12] Kotynia R., Staśkiewicz M.: Analiza efektywności wzmocnień żelbetowych elementów zginanych za pomocą wstępnie naprężonych kompozytów CFRP. Budownictwo i Architektura 12(1) 2013, s. 131–138.

[13] Bodzak P.: Wpływ gatunku stali zbrojenia głównego na nośność na zginanie i graniczne odkształcenia kompozytu przy wzmacnianiu taśmami CFRP, Przegląd Budowlany 11/2017, s. 47–51.

[14] Sena-Crus J., Baros J.: Bond between near-surface mounted carbon-fiber-reinforced polymer laminate strips and concrete, Journal of composites for construction, Volume 8, Issue 6, December 2004, s. 519–527.

[15] Kotynia R.: Przyczepność zbrojenia kompozytowego do betonu w żelbetowych elementach wzmocnionych za pomocą materiałów kompozytowych, zeszyt nr 16, Łódź 2008.

[16] PN-EN-1992-1-1 Eurokod 2: Projektowanie konstrukcji z betonu-Część 1-2: Reguły ogólne i reguły dla budynków.

[17] Adjukiewicz A.: Eurokod 2 – Podręczny skrót dla projektantów konstrukcji żelbetowych, Stowarzyszenie Producentów Cementu, Kraków 2009.

[18] Bacharz K, Goszczyńska B., Wpływ długości zakotwienia zbrojenia głównego na nośność strefy przypodporowej belek żelbetowych, Konstrukcje betonowe i metalowe, Wydawnictwo Uczelniane Uniwersytetu Technologiczno-Przyrodniczego w Bydgoszczy, Bydgoszcz 2015.

[19] Knauff M.: Wpływ siły poprzecznej na zbrojenie podłużne belek żelbetowych – uwagi o zasadach konstruowania, Inżynieria i Budownictwo 10 (2004), s. 549–552.

[20] Kanuff M.: Obliczanie konstrukcji żelbetowych według Eurokodu 2, Wydawnictwo naukowe PWN, Warszawa 2012.

Przesłano do redakcji:28.02.2018 r.
Przyjęto do druku: 31.03.2018 r.

CZASOPISMO INŻYNIERII LĄDOWEJ, ŚRODOWISKA I ARCHITEKTURY
JOURNAL OF CIVIL ENGINEERING, ENVIRONMENT AND ARCHITECTURE
JCEEA, t. XXXV, z. 65 (3/18), lipiec-wrzesień 2018, s. 111-118, DOI:10.7862/rb.2018.48

Wojciech ECKERT[1]

MODERNIST PARTY HOUSE IN ZIELONA GÓRA. ARCHITECTURE TO BE DISCOVERED

According to the tendency that was observed at the turn of the 1940s and 1950s, each provincial town, including Zielona Góra, was to be expanded. At that time in every area of social life, including architecture, there was a fixed set of values and symbols. Urban planning and architecture were to be adapted to the propaganda needs of the new social-political formation. A decision was made to build an elegant building, the seat of the Provincial Committee of the Polish United Workers' Party. The Central Office for Architectural and Construction Projects was entrusted with the project. The team headed by Mikołaj Kokozow designed a building reflecting the tradition of interwar architecture that linked constructivism and so called quasi-classicist modernism. The building at 23 Bohaterów Westerplatte Street in Zielona Góra is an example of socialist realism, which was a dominant style in Polish architecture in the years 1949-1956. The former Party House was designed in quasi-classicist style, decorated with quasi-historical detail. The building has a permanent position in the cultural landscape of Zielona Góra, being part of post-war history and an important element of the continuity of the cultural heritage and history of the town.

Keywords: history of architecture, modernism, social realism, monument

1. Introduction

In the Lubusz Voivodship, modernist architecture is not well identified. However, there are very significant monuments from that period: churches, schools, railway stations, post-industrial buildings, hospitals, post offices, fire stations and many others.

A very interesting example of modernism in church architecture is Christ the King Church in Gorzów Wielkopolski from 1930, designed by the Berlin architect Kurt Steinberg. Founded on a central plan in the shape of a rotunda covered with a pyramid-shaped cupola, with a detached tower on a square plan, the church is an important dominant feature in the town's panorama. Modernism in architecture is also represented in the region by numerous public buildings, e.g. L. Kruczkowski Theatre in Zielona Góra with a simple and monumental

[1] Wojciech Eckert, University of Zielona Góra, Faculty of Civil Engineering, Architecture and Environmental Engineering, ul. Licealna 9, 65-417 Zielona Góra; tel. 68 328 24 16; w.eckert@ib.uz.zgora.pl

façade, built in 1931 according to the project of the Berlin architect Oskar Kaufmann. [1] The recently "discovered", abandoned and neglected hospital building in Nowa Sól is a unique example of modern architecture from that period. This is the first hospital high rise building in former Germany and the first project by the well-known architect, specializing in hospital design, Ernst Kopp, in which he implemented innovative functional and communication solutions. [2]

2. History

In June 1950, the Polish Parliament changed the administrative division of the country. The Zielona Góra Voivodship was established with its capital in Zielona Góra. [3]

According to the tendency that was observed at the turn of the 1940s and 1950s, each voivodship capital, including Zielona Góra, was to be expanded. At that time, in every area of social life, including architecture, there was a fixed set of values and symbols. Urban planning and architecture were to be adapted to the propaganda needs of the new social-political formation. A decision was made to build an elegant building, the seat of the Voivodship Committee of the Polish United Workers' Party. A characteristic feature of architecture at that time was socialist realism in all fields of art.

The central part of the town was to be rebuilt and elegant office and public buildings as well as residential districts were to be built. In Zielona Góra, the spatial development plans included the communication line on Bohaterów Westerplatte Street. In this area, by the decision of the Presidium of the Municipal National Council in Zielona Góra and the Voivodship National Council in Poznań made in the mid-1950's, a Voivodship Administration building was to be built. The building was to have 4 conference rooms, a conference room for the Voivodship National Council, 18 departments, a library, an archive, office rooms, common rooms, workshops and garages. It was assumed that about 1,300 employees would work in the building, and the total cost of its construction would amount to 610 million zlotys at that time. By the standards of the time, the building was to impress with its splendour and become a showcase of the town (the cubature of the building was to be 61,000 m^3). However, at the beginning of 1951 the idea for the purpose of the object was changed. At that time, the Central Committee of the Polish United Workers' Party passed a resolution on the expansion of the network of seats of party committees, which were to be located in elegant buildings. For this purpose, the state budget for the year 1951 was changed considerably to cover the construction costs of the Polish United Workers' Party buildings. The Central Office for Architectural and Construction Projects was entrusted with the project. The team headed by Mikołaj Kokozow (one of the outstanding Polish architects of the 1950s) designed a building reflecting the tradition of interwar

architecture that linked constructivism and so called quasi-classicist modernism. (This architect also designed the Skra stadium or Noakowskiego Street in Warsaw). To a certain extent, Mikołaj Kokozow managed to deviate from the clear style of socialist realist architecture. However, the committee evaluating the project recommended making small changes in it to bring it in line with the socialist realist style. [4] The investment was partly funded by individual people who bought donation certificates.

However, the building of the Voivodship Committee of the Polish United Workers' Party was built as much smaller than the initial idea for the seat of the Voivodship Administration. The total area of the building was 2,783.6 m^2, and its cubature amounted to 12,605 m^3. The construction of the building was completed in August 1953 and at that time it became "the party house".

From 1953 to 1989, meetings of the Voivodship Committee of the Polish United Workers' Party were held in the building. Celebrations of public holidays and other events were also held there. After the transformation of 1989 and the dissolution of the Polish United Workers' Party, the building ceased to be the seat of the party in the voivodship. On 9 November, 1990 the Sejm of the Republic of Poland passed a law that ultimately led to the takeover of the property of the former Polish United Workers' Party by the State Treasury. The real estate that belonged to the party (including the building of the Voivodship Committee of the Polish United Workers' Party in Zielona Góra) was taken over mainly by local governments. On 13 March, 1991 the Zielona Góra municipal authorities set up a municipal company called the "Business Centre" and donated the building to it. The municipal company called the "Business Centre", which manages the building, also founded in order to find business partners for local companies. At present, the building houses the headquarters of companies and banks, and it is also a place where various training courses and conferences are held.

3. Architectural analysis

The former seat of the Voivodship Committee of the Polish United Workers' Party in Zielona Góra, later the "Business Centre", is a brick building, with plastered walls, four-storeys and a basement, and it is covered with a flat roof.

The building was built on a plan similar to the letter H and it is has a compact body. The main axis of the building is oriented on the south-west-north-east, parallel to Bohaterów Westerplatte Street, the main street of the town. The front elevation faces south-west towards the square, which is now used as a car park.

The elevations were designed as identical. The basic articulation of the walls is an arrangement of pilasters and cornice strips. An important horizontal accent is a high plinth, protruding from the face of the wall and crowned with

a cornice. Between the third and fourth floors there is an extended cornice strip, whereas the crowning cornice is a single narrow strip. The pilasters are simple in form with the heads and bases marked only with a single line. The fourth floor, in the form of a superstructure, is devoid of detail and decorations. In the south-east and north-west part of the main body, it is slightly higher than the fourth floor of the side wings. In the plinth part there are small rectangular window openings arranged irregularly. On the first, second and third floors there are two-level double windows. On the fourth, top floor there are two-level windows, single windows and two-level, double windows. Most of the original windows with wooden frames have been replaced with plastic ones. Rectangular window openings have simple profiled frames, with the exception of the window openings of the top floor, which are devoid of decorations. Moreover, the windows on the first floor are decorated with horizontal pediments and under-window panels, which are also to be found under the windows on the ground floor. The main entrance is located on the south-west façade. Two runs of wide, elegant stairs made of granite slabs lead to it. The first flight of stairs leads onto a wide terrace running through the entire width of the front elevation, surrounded by a sandstone balustrade with straight single-bar balusters. On the four outer posts of the balustrade there are nine-armed steel lanterns. The square in front of the building is paved with granite blocks and it is now used as a car park.

The front elevation has thirteen horizontal axes from the first to the third floor. There are twenty-one narrow, rectangular window openings on the top floor. The outermost axes are blind. The entrances are located centrally on the façade - on the fifth, sixth, seventh, eighth and ninth axis, they have lintels with the lint marked in plaster. The doors are wooden, double and glazed in their upper part. Above the doors, on the level of the first floor, there are port-fenêtre windows with external decorative steel balustrades with short plates.

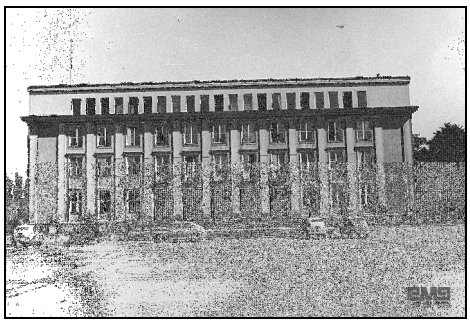

Fig. 1. The south-west front elevation, a photograph from the 1960s, the collection of the Museum of the Lubusz Region in Zielona Góra

Fig. 2. The south-west front elevation, a photograph from 2018, author: W. Eckert

The south-eastern elevation, parallel to Bohaterów Westerplatte Street, has nine-axes in the main body. The windows on the top floor are larger than the windows on the other floors. In the side wings there are two axes on the level of the first, second and third floor. On the fourth floor there are groups of three narrow rectangular window openings. The internal elevations of the side wings, perpendicular to the main body, have four axes on the level of the first, second and third floor with a blind outer axis. On the level of the fourth floor, there are five window openings. In the retracted main body of the building, in the outermost axes, there are entrance doors with low landings with several steps.

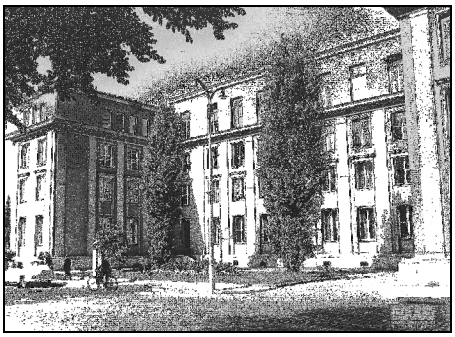

Fig. 3. A south-east view, a photograph from 1960s, the collection of the Museum of the Lubusz Region in Zielona Góra

Fig. 4. A south-east view, a photograph from 2018, author: W. Eckert

The north-eastern elevation has thirteen-axes. The outermost axes are blind. There are twenty-one narrow, rectangular window openings on the top floor. On both sides of the façade, there are entrance doors with stairs with a large platform and a steel balustrade.

The north-west elevation, which is the elevation facing the utility yard, has nine axes in the main body. The windows on the top floor are larger than the windows on the other floors. In the outermost axes of the main body there are staircase windows, which are offset vertically in relation to the other window openings. In the side wings there are two axes on the level of the first, second and third floor. On the fourth floor there are three narrow rectangular window openings. The internal elevations of the side wings, perpendicular to the main body, have four axes on the level of the first, second and third floor, with a blind outer axis. On the level of the fourth floor, the west wing has five window openings, and the east wing has three. In the eastern part, in the corner, a one-level garage with a flat roof has been added, which is adjacent to the south wall of the side wing. There is a complex of modern, one-level garages adjoined to the west wing. The square in front of the north-west elevation is paved with concrete slabs; it is used as an internal car park.

The original layout of the interior has been mostly preserved, but on the ground floor the layout has been disturbed by a modern complex of commercial stalls. On the first and the second floor, there are office rooms, which are laid out along a central corridor. The conference room, accessible from both wings, occupies the entire third floor in the main part of the building.

The floor of the hallways and corridors is paved with contemporary gres tiles, and on the fourth floor there is a parquet floor. The original door woodwork has been preserved in some parts of the building. The reinforced concrete staircase paved with terrazzo has a steel balustrade with wooden handrails. On the inside, there are still visible wall and ceiling decorations in the form of geometric shapes marked in the plaster.

Fig. 5. A donation certificate for the construction of the Party House from the 1950s, the collection of the Museum of the Lubusz Region in Zielona Góra

Fig. 6. The Conference Hall interior, a photograph from 2018, author: W. Eckert

4. Conclusions

The building at 23 Bohaterów Westerplatte Street is an example of socialist realism, which was a dominant style in Polish architecture in the years 1949–1956. The main assumption of this doctrine was that architecture should be "socialist in content and national in form". The former so-called Party House was designed in quasi-classicist style and it is decorated with quasi- historical detail. The division of the elevations is symmetrical and balanced with sparingly used, harmonious decor of quasi-classic provenance, i.e. simple pilasters, simple horizontal pediments above the windows, and recesses below the windows without ornaments, etc. The way of using and interpreting classicist solutions and architectural formulas results in a monumental, solemn form of the building. This impression is strengthened by the wide stairs within an elegant balustrade, as well as by the layout of the square in front of the building.

The building is characterized by a spacious, functional layout. Wide corridors and staircases ensure efficient communication inside the building. The interior design, which is a consistent reference to the design of the facade, is distinguished by attention to detail.

It should be emphasized that this building is one of the few objects in the town that are fully representative of the assumptions of socialist realism in architecture. At the same time, the architecture of this building is on a high artistic level.

In terms of history and urban development of the town, the building is of momentous and multidimensional significance. It is one of the first post-war buildings in the town. It is an important point of the two main communication lines of Zielona Góra - Bohaterów Westerplatte Street and the route from the Marshal's Office to the town centre.

The former is a street set out in the 1950s in the place of a former dirt road (German: Kapellenweg, 1945–1956, Topolowa Street). Planned as the main thoroughfare, it was intended to become an exquisite route with the most important public, commercial and service buildings. At present, on this street there are buildings constructed in different styles. There are also detached houses from the early twentieth century, blocks of flats from the 1950s and 1960s, commercial and service pavilions and high rise buildings from the 1970s as well as a modern shopping gallery, among which the seat of the Voivodship Committee of the former Polish United Workers' Party stands out with an elegant shape and a spacious square.

Moreover, this building is located on the axis running from the seat of the Marshal's Office through Bank Street and Bohaterów Westerplatte Street. This axis was formed after the Second World War to connect two important buildings belonging to the authorities. Plac Bohaterów and the square in front of the building of the Voivodship Committee of the former Polish United Workers' Party created a space for official state meetings, such as celebrations, demonstrations or parades. Design plans of a communication route with a similar layout can be found in urban plans from the late nineteenth century. At that time, the present Plac Bohaterów was planned to be the central part of the axis running from Sulechowska Street (German: Züllichau Strasse) to the area of today's F. Chopin Street (German Lindenberg), where a new church was to have been built. [5]

The building and the square have become a permanent feature of the cultural landscape of Zielona Góra. They are part of post-war history and an important element of the continuity of the cultural heritage and history of the town.

In the 1950s and 1960s a number of new buildings were built in Poland in towns located in the former German territories. Some of them are interesting examples of the architecture of their time. One of them is the Party House in Zielona Góra. It is worth learning about the history and architecture of these buildings. Then it will be possible to make an objective analysis of their cultural values and as a result place them under heritage protection.

References

[1] Kowalski S.: Zabytki architektury województwa lubuskiego, Zielona Góra 2010.
[2] Eckert W.: Modernistyczny budynek szpitala w Nowej Soli. Nieznane dzieło Ernsta Koppa. Przykład racjonalizacji funkcji, technologii, konstrukcji. in: Czasopismo Inżynierii Lądowej, Środowiska i Architektury – Journal of Civil Engineering, Environment and Architecture, JCEEA, volume XXXIV, issue 64, Rzeszów 2017, DOI:10.7862/rb.2017.216.
[3] Zaradny R.: Życie społeczno-polityczne w Zielonej Górze w latach 1950–1980 w: Historia Zielonej Góry. Dzieje miasta w XIX i XIX wieku. Volume II. edited by Wojciech Strzyżewski, Zielona Góra 2012.
[4] Opaska J. W.: „Soc" pod naszą ochroną. O wartościach architektury lat 50. w: Gazeta Wyborcza. Gazeta Zachodnia No. 130, of 5 June 2001.
[5] Faksymile mapy z 1871 r. „Bebauungs-Plan der Stadt Grünberg nach den vorhandenen Karten und einigenen Aufnahmen in den Jahren 1869–1871 / bearbeitet durch Königl. Kreisbaumeister" in: Gazeta Lubuska No. 210, of 7 September 2004.

Przesłano do redakcji: 04.04.2018 r.
Przyjęto do druku: 28.09.2018 r.

CZASOPISMO INŻYNIERII LĄDOWEJ, ŚRODOWISKA I ARCHITEKTURY
JOURNAL OF CIVIL ENGINEERING, ENVIRONMENT AND ARCHITECTURE
JCEEA, t. XXXV, z. 65 (3/18), lipiec-wrzesień 2018, s. 119-126, DOI:10.7862/rb.2018.49

Slávka HARABINOVÁ[1]
Eva PANULINOVÁ[2]
Eva KORMANÍKOVÁ[3]
Kamila KOTRASOVÁ[4]

ANALYSIS OF SLOPE STABILITY USING CONVENTIONAL METHODS

The paper deals with the assessment of slope stability on the road II / 595 near the village Zlatno. The assessment of slope stability was made before and after the landslide caused by floods in 2010. For proposal for a comprehensive assessment and possible remedial action is necessary to know the geological conditions and choose the appropriate method to assess slope stability. The calculation of factor of safety was made using GEO 5 software. The critical factors of safety have been determined by Petterson, Bishop and Sarma Methods. We analyzed possibilities to using these methods for assessment of slope stability. The Sarma Method is more appropriate for this calculation.

Keywords: assessment of slope stability, landslide, factor of safety, road

1. Introduction

Currently, the main cause of the extremely large landslides is primarily long-term rainfall. Continuous rain cause significant elevations in almost all water courses and floods. Slopes ground mass saturated with water are prone to landslide. Climatic factors combined with the erosion activity water courses and groundwater are major causes of slope deformations.

The overall stability of slopes including existing, affected or planned structures shall be verified in ultimate limit states (GEO and STR) [5] with

[1] Corresponding author: Slávka Harabinová, Technical University of Košice, Faculty of Civil Engineering, Institute of Structural Engineering, Vysokoškolská 4, 042 00 Košice, +421 55 602 4178, slavka.harabinova@tuke.sk

[2] Eva Panulinová, Technical University of Košice, Faculty of Civil Engineering, Institute of Structural Engineering, Vysokoškolská 4, 042 00 Košice, +421 55 602 4268, eva.panulinova@tuke.sk

[3] Eva Kormaníková, Technical University of Košice, Faculty of Civil Engineering, Institute of Structural Engineering, Vysokoškolská 4, 042 00 Košice, +421 55 602 4168, eva.kormanikova@tuke.sk

[4] Kamila Kotrasová, Technical University of Košice, Faculty of Civil Engineering, Institute of Structural Engineering, Vysokoškolská 4, 042 00 Košice, +421 55 602 4249, kamila.kotrasova@tuke.sk

design values of actions, resistances and strengths, where the partial factors defined in [5] shall be used. In analyzing the overall stability of the ground, of soil or rock, all relevant modes of failure shall be taken into account. When choosing a calculation method, the following should be considered:
- soil layering,
- occurrence and inclination of discontinuities,
- seepage and pore-water pressure distribution,
- short- and long-term stability,
- creep deformations due to shear,
- type of failure (circular or non-circular surface; toppling; flow),
- use of numerical methods.

2. Conventional methods for analysis of slope stability

There are several methods currently employed in slope stability analyses based on the equilibrium of forces, moments or the energetic equilibrium. Most frequently, it is assumed in the calculations that failure occurs along a particular slip surface. The mass of soil or rock bounded by the failure surface should normally be treated as a rigid body or as several rigid bodies moving simultaneously. Failure surfaces or interfaces between rigid bodies may have a variety of shapes including planar, circular and more complicated shapes. The shape of slip surface depends mainly on the physical and mechanical properties of soils or their arrangement in the profile. The stability analysis in question takes into account both basic principles. The first is an assumption that the slip surface developed will be circular (Petterson and Bishop Methods) and the second principle is that the slip surface will be polygonal (Sarma Method) [3].

Petterson Method is the oldest and simplest method of analysing slope stability. It is the method of slices not considering the action of neighbouring elements, i.e. the sliding mass above a circular slip surface is divided into a number of vertical slices and the forces acting on each slice are obtained, given by their self-weight and the weight of other facilities (Figure 1). If the slip surface is not known, it is necessary to determine it by the gradual optimizing calculation, i.e. by changing its parameters – locations of the centres of slip circle and the circle diameter [1].

Bishop Method is a modified and extended version of Petterson Method (Figure 2). Horizontal actions of neighbouring slices are incorporate into the calculation as well as the neutral stress on the slip surface, most commonly by means of empirically determined pore pressure coefficients [1].

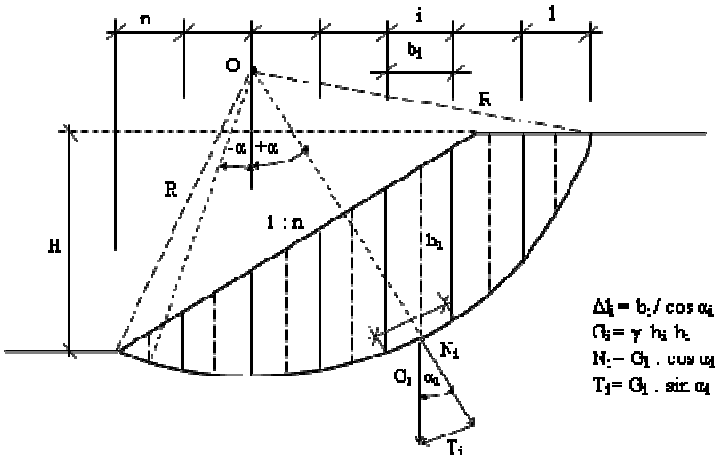

Fig. 1. Petterson Method

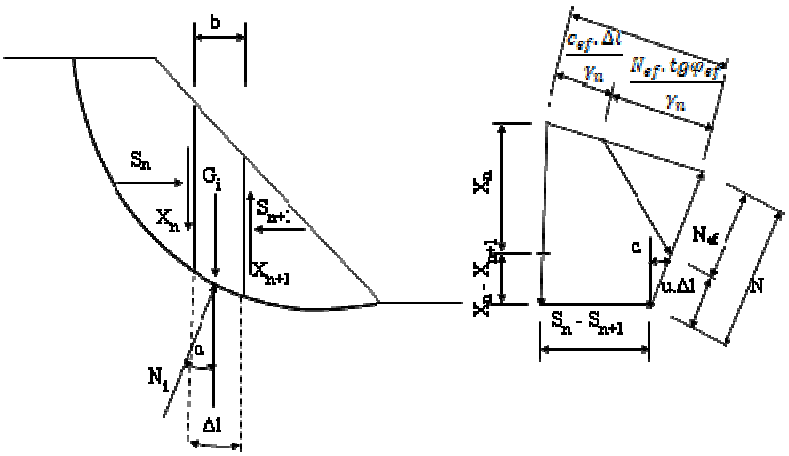

Fig. 2. Bishop Method

Sarma Method is another limit equilibrium technique. This method is based on the equilibrium condition being fulfilled for the forces and moments in the individual wedges [1]. Wedges are created by dividing the soil mass above a polygonal slip surface by planes with various inclinations (Figure 3).

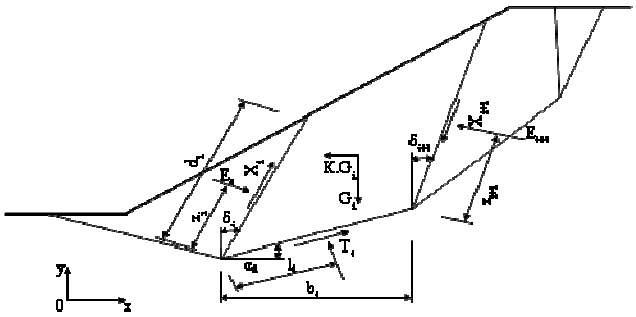

Fig. 3. Sarma Method

3. Analysis of slope stability on the road

The area of interest is located in the village Zlatno on the road II / 595. Road section is guided in a slope in the unilateral notch. In this area occurred in 2010 a landslide from 24.886 to 24.932 kilometers. The consequence of the penetration of rainwater on the right embankment slope of the road body was a landslide. Asphalt layer of roads after the landslide of the slope is broken and slid down. Landslide narrowed width of the carriageway, thereby reducing the security of vehicle passages in this section (Figure 4 and 5).

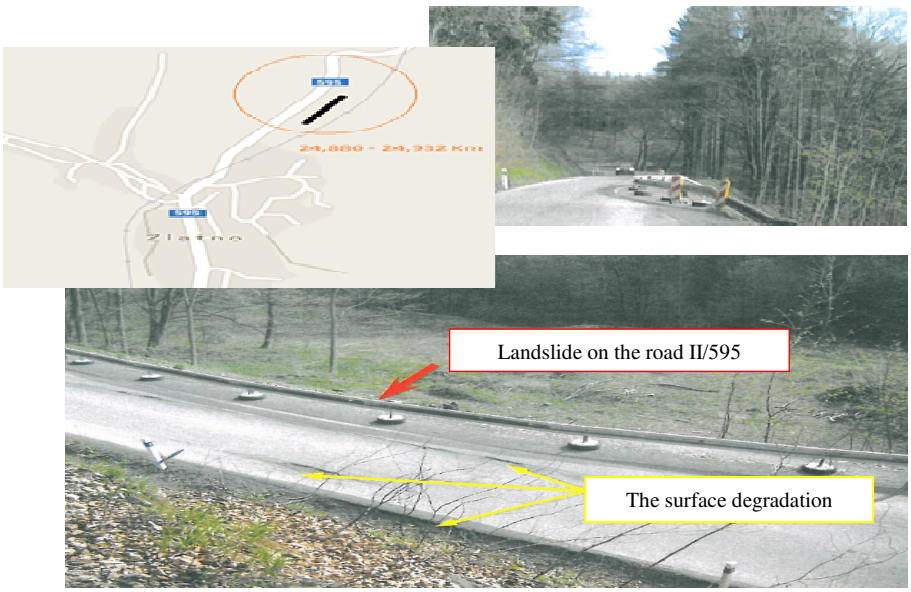

Fig. 4. Situation and photo documentation of landslide, based on [2]

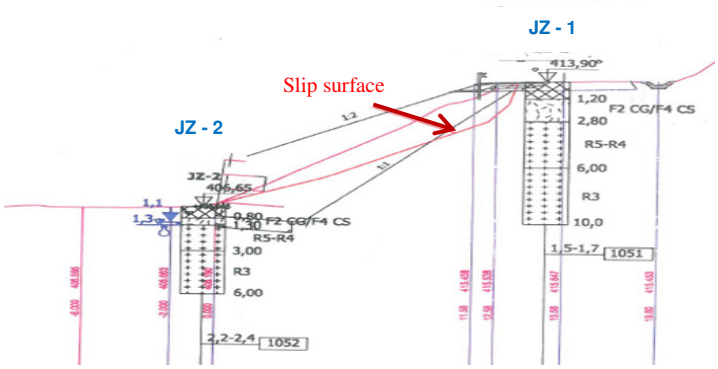

Fig. 5. The location of boreholes and geological profile of boreholes JZ-1 and JZ-2, based on [2]

The slopes of the road are made up of fine-grained soils and rocks. Subsoil is formed by Paleozoic rocks – granitoids, which are unevenly cover deluvial sediments. They are sandy clays and clayey sands with fragments of rocks. Two boreholes JZ-1 and JZ-2 have been done for geotechnical investigation [2]. Geological profiles are shown in Figure 5. Soil classification was made according to STN 72 1001 [4] and in accordance with EN 1997-1 [5]. The values of the geotechnical characteristics are given in the Table 1 and 2 [2].

Table 1. The geotechnical parameters of soils

Properties	**CG (gravelly clay) CS (sandy clay)**	**SC (clayey sand)**
Poisson's ratio υ (-)	0.35	0.35
Unit weight γ(kN.m^{-3})	19.0	18.5
Deformation modulus E_{def} (MPa)	6	9
Total stress parameters – cohesion c_u (kPa)	55	-
Total stress parameters – angle of friction φ_u (°)	0	-
Effective stress parameters – cohesion c_{ef} (kPa)	13	8
Effective stress parameters – angle of friction φ_{ef} (°)	25	27

Table 2. The geotechnical parameters of rocks

Properties	**Weathered rock layers Group R5-R4**	**Weathered rock layers Group R3**
Poisson's ratio υ (-)	0.35	0.35
Deformation modulus E_{def} (MPa)	6	9

Existing failed slopes, which can potentially be reactivated, should be analysed considering circula, as well as non-circular failure surfaces. That is a reason why Petterson, Bishop and Sarma Methods were selected for calculation and assessment of slope stability of the road. Calculation and assessment of slope stability on the road II/595 near the village Zlatno was carried out by using program "Slope stability" which is a sub-program of GEO 5 by company FINE Ltd.

The GEO 5 program is designed for the stability analysis of slopes, which suits the purpose of heterogeneous slope analyses [6]. Bishop, Petterson, and Sarma methods were employed for calculating the stability of slopes in the article. All three methods are so-called limit equilibrium techniques, i.e. based on the equilibrium principle of moments above a selected slip surface. They are derived from the existence of stress condition in the surrounding environment, while the surface where slip may occur is sought (so-called the critical slip surface). The result is a factor of safety determining the ratio between the active and passive forces. The slope stability analysis was carried out in compliance with STN EN 1997-1, Design Approach 3 [5]. According to EN 1997-1 [5] was assessed stability of slopes according to the "limit states theory". A factor of safety is defined as the ratio of the forces resisting movement (thus ensuring the slope stability) to those driving movement (thus threatening the slope stability), i.e. the ratio between the active and passive forces. In general, if the factor of safety of a slope is within the interval between 0 and 1, the slope is actively unstable. The value over 1.0 indicates that the slope is considered stable.

Assessment of slope stability on the road II/595 near the village Zlatno was made on the landslide place, in four cross-sections CS-1, CS-2, CS-3, and CS-4 (from 24.886 to 24.932 km). The load on the construction of the road was 16.8 kNm-2 and the axle load was 115 kN. Calculation of slope stability was realized in two variants. The calculated factor of safety has been compared to limit value of stability degree.

Variant I - The original condition, the dry state (i.e. before the landslide). In this variant, the groundwater level was considered, as was found by geological profile (JZ-1 a JZ-2).

Variant II – Condition after landslide, the saturated state (i.e. after the flood). In this variant was considered with maximum groundwater level, i.e. situation that caused the landslide.

In Figure 6 the slip surface for Variant I and Variant II (Petterson and Sarma Methods) can be seen. The calculated factors of safety (Fs) for these variants are shown in Table 3.

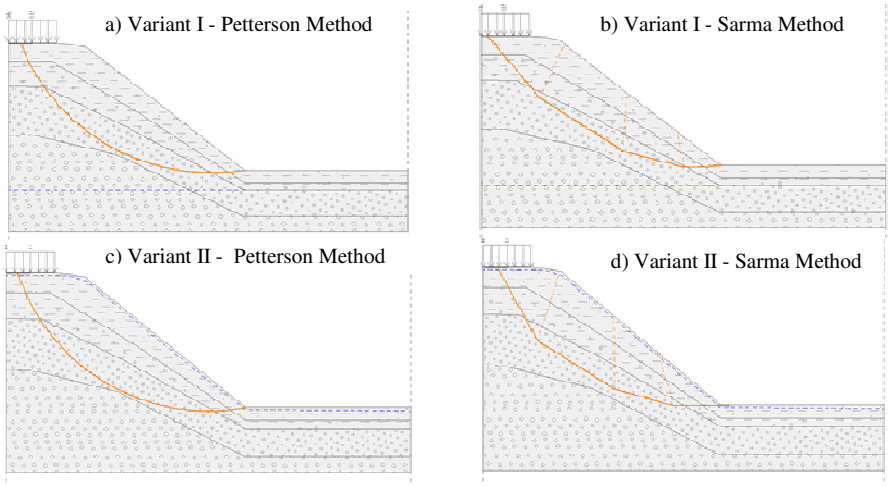

Fig. 6. Variant I and Variant II – The shape of slip surface for cross-sections CS-1

Table 3. Calculated factors of safety for Variant I and Variant II

Variant	The cross-section	Methods	Factor of safety F_s	Evaluation (F_s > 1.0)
Variant I	CS-1	Petterson	0.88	NO*
		Bishop	0.97	NO
		Sarma	**1.04**	**OK****
	CS-2	Petterson	0.97	NO
		Bishop	**1.06**	**OK**
		Sarma	**1.24**	**OK**
	CS-3	Petterson	0.89	NO
		Bishop	0.99	NO
		Sarma	**1.12**	**OK**
	CS-4	Petterson	0.86	NO
		Bishop	0.96	NO
		Sarma	**1.04**	**OK**
Variant II	CS-1	Petterson	0.60	NO
		Bishop	0.77	NO
		Sarma	0.81	NO
	CS-2	Petterson	0.65	NO
		Bishop	0.79	NO
		Sarma	0.89	NO
	CS-3	Petterson	0.61	NO
		Bishop	0.77	NO
		Sarma	0.85	NO
	CS-4	Petterson	0.58	NO
		Bishop	0.74	NO
		Sarma	0.80	NO

*NO = unstable, **OK = stable

Sarma Method is more appropriate for this calculation, because the slope is formed of rock. The calculated factors of safety by Bishop and Sarma Methods point to the fact that at any overrun load is an increased risk of landslide (Variant I). Based on the calculations and the results listed in Table 3 it can be seen that the stability of slopes did not satisfy the assessment of slope stability before the flood situation (Variant I – Petterson Method).

Due to rain and infiltration of rainwater into the slope (Variant II), there was a landslide, as confirmed by the calculated factors of safety for all cross-sections.

4. Conclusion

Calculation of slope stability of road body was realized in two variants, in which we analyzed possibilities to using conventional methods. Assessment of slope stability on the road II / 595 has been done before and after the landslide, caused by the flood (Variant I – The dry state and Variant II – The saturated state). In view of the fact that the body of the road is formed of rocks groups R3 to R5, is more appropriate for calculation of factor of safety use Sarma Method.

The calculated factors of safety by Sarma Method (Variant I), confirmed that any overrun load is an increased risk of landslide. As confirmed by the calculated factors of safety for Variant II, due to rain and infiltration of rainwater into the slope there was a landslide. Roads are considered as significant structures and therefore it is needed to pay high attention the design and assessment of these constructions. Because of their importance, security and reliability throughout their lifetime remains the top priority.

Acknowledgements: *This work was supported by the Scientific Grant Agency of the Ministry of Education of Slovak Republic and the Slovak Academy of Sciences under Project VEGA 1/0477/15.*

References

[1] Ishibashi I., Hazarika H. Soil mechanics Fundamentals, CRC Press, Taylor & Francis Group, 2010.

[2] INGEO-IGHP, s.r.o. Remediation of landslides on the road. 2011. (in slovak).

[3] Panulinová E., Harabinová S. Methods for analyzing the stability of an earthen dam slope. Advanced Material Research, Vol. 969, pp. 245–248, 2014.

[4] STN 72 1001 Classification of soils and rocks. 2010.

[5] STN-EN 1997-1. Eurocode 7. Geotechnical design, Part 1: General rules. 2005.

[6] GEO 5 software © Fine Ltd.

Przesłano do redakcji: 02.10.2017 r.
Przyjęto do druku: 27.09.2018 r.

CZASOPISMO INŻYNIERII LĄDOWEJ, ŚRODOWISKA I ARCHITEKTURY
JOURNAL OF CIVIL ENGINEERING, ENVIRONMENT AND ARCHITECTURE
JCEEA, t. XXXV, z. 65 (3/18), lipiec-wrzesień 2018, s. 127-134, DOI:10.7862/rb.2018.50

Artur BOROWIEC[1]
Leonard ZIEMIAŃSKI[2]

NUMERICAL VERIFICATION OF DAMAGE LOCALIZATION METHOD BASED ON MOVING MASS IN TRUSS STRUCTURES

The article presents examples of damage localization in numerical models of trusses based on changes in natural frequency. The changes were caused by an additional mass moving on the truss nodes. The results of the localization in several truss bars (top chord, bottom chord, diagonal bars, posts) are presented. The influence of damage size on the localization effectiveness is shown. The differential operator was used in the analyses.

Keywords: civil engineering, truss, damage, modal analysis

1. Introduction

Damage detection using modal analysis has been used in civil engineering since the 1970s [1]. Modal diagnostics is based on changes of dynamic parameters: the natural frequency, the form of natural vibrations and the damping coefficient. Most of the methods are based on the reference model, for which the values of the dynamic parameters of the structure in undamaged state are known. In [2] the comparison of vibration curves using a differential operator was applied to the damage location. In [3] an additional parameter (mass, support) was introduced to the system which allows indicating the location of the damage by analysing changes in the natural frequency relative to their position. Methods without a reference model are also being developed. Examples of the use of an additional, changing position of the mass along with the analysis of the resonant frequency derivatives allow locating the damage

[1] Corresponding author: Artur Borowiec, Rzeszow University of Technology, Department of Structural Mechanics, ul. Poznańska 2, 35-959 Rzeszów; tel. 178651617; artur.borowiec@prz.edu.pl, http://orcid.org/0000-0002-9475-3251.

[2] Leonard Ziemiański, Rzeszow University of Technology, Department of Structural Mechanics, ul. Poznańska 2, 35-959 Rzeszów; tel. 178651353; ziele@prz.edu.pl, http://orcid.org/0000-0002-4012-0002

in beams [4, 5] and plates [6]. A similar approach to distinguishing the magnitude of damage was adopted in [7]. The application of modal analysis to the localization of damage in trusses can be found in [8, 9]. The following paper presents the preliminary results of damage localization in truss models with the use of modal analysis in combination with a central differential operator without a reference model.

2. Description of numerical analyses

2.1. Numerical models

During the analyses, two numerical models of trusses with parallel chords were used. Both models have a span $L = 2{,}0\ m$ and a height $H = 0{,}2\ m$. A square cross-section with side dimensions equal to $h = 10\ mm$ has been adopted in all steel truss bars. The supports were placed in the extreme nodes of the upper chord. The finite element method models were built in the Matlab environment FEM libraries from the Calfem package.

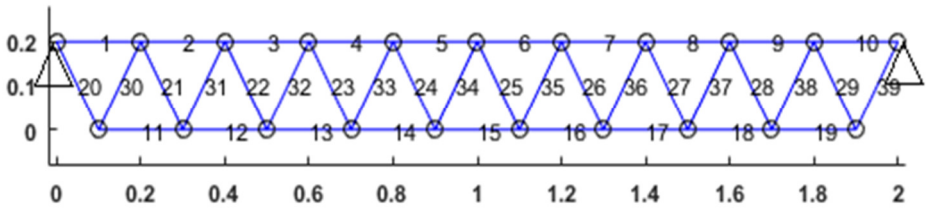

Fig. 1. Warren truss

The model of the first truss (Fig. 1) was constructed of $n_e = 39$ elements and contained $n_d = 21$ nodes. The model's geometry is Warren type "V" truss with tensioned and compressed diagonal bars without posts.

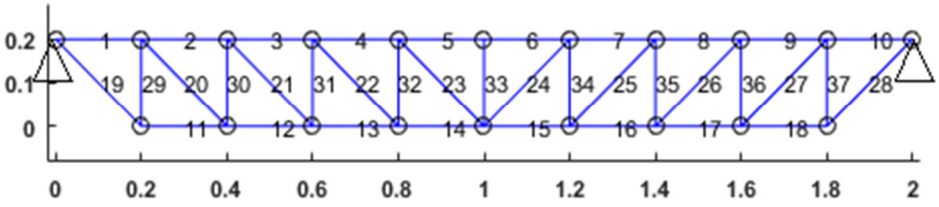

Fig. 2. Pratt truss

The second model of the truss (Fig. 2) was constructed of $n_e = 37$ elements and contained $n_d = 20$ nodes. The model's geometry is Pratt type "N" truss with tensioned diagonal bars and compressed posts.

2.2. Damage localization method

The damage was modeled by reducing the cross-section area of one of the truss bars without changing the mass of the truss. The natural frequencies $\omega_q\{l_m, l_c, h_c\}$ were calculated with the mass added successively in $l_m=1..n_d$ truss nodes, assuming the location of damage $l_c=1..n_e$ with different size of damage h_c (*1 mm-8 mm*). The eigenvalue problem was solved in the Matlab environment. The results show of changes in the first frequency ω_l performed using the second-order differential operator

$$\omega''_{l_m,1} = \frac{\omega_{l_m+1,1} - 2\omega_{l_m,1} + \omega_{l_m-1,1}}{d^2} \tag{1}$$

assuming for the trusses $d=1$. All simulation included a mass of 5% of the trusses weight. The nodes of the top chord $l_m=1, 2...11$ were taken into account.

3. Simulation results

The simulation results for the first truss were compiled for damage by 50% reduction in the cross-section area of the truss bars ($h_c=5$ *mm*). Figs. 3–5 show the changes with respect to the position of the mass on the top chord of the first frequency ω_l and the differential operator ω_l'' for the Warren truss. Figs. 3–5 present changes for different groups of truss bars: Fig. 3: top chord (el. 1–10), Fig. 4: bottom chord (el. 11–19), Fig. 5: diagonal bars (el. 20–29). In the figures with the operator, an increased value near the damaged element was shown. The most significant changes for this truss were observed for the bottom chord (Fig. 4b). For chords bars near the supports and for diagonal bars in the middle of the span, the changes were hardly visible.

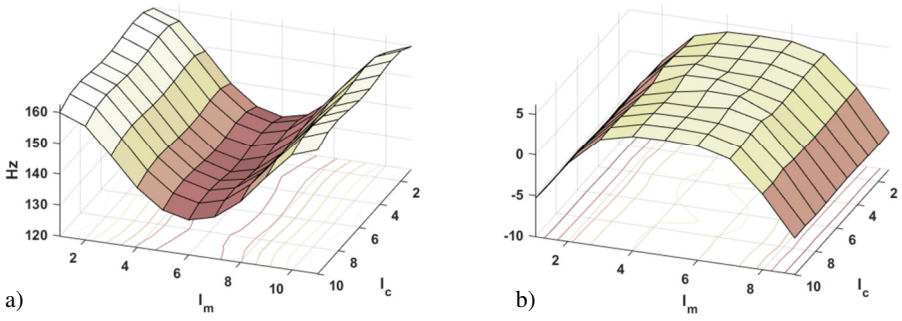

Fig. 3. The mass in the nodes of the top chord, damage in the bars of the top chord (el. 1–10) of the Warren truss: a) change ω_l b) change ω_l''

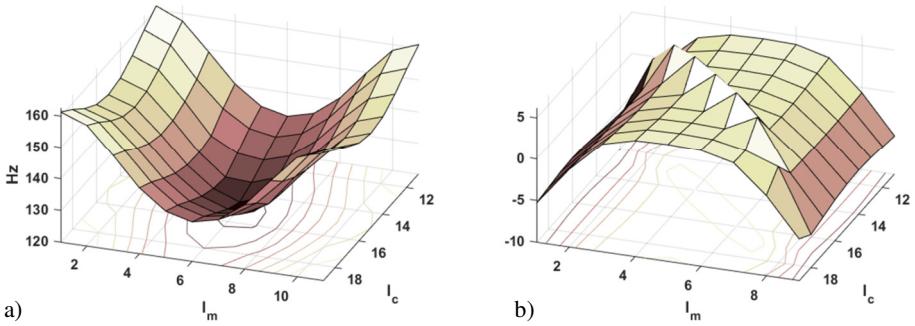

Fig. 4. The mass in the nodes of the top chord, damage in the bars of the bottom chord (el. 11–19) of the Warren truss: a) change ω_1 b) change ω_1''

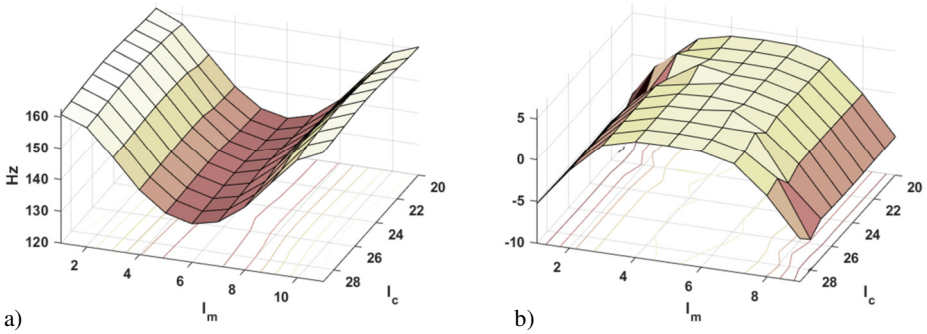

Fig. 5. The mass in the nodes of the top chord, damage in the diagonal bars (el. 20–29) of the Warren truss: a) change ω_1 b) change ω_1''

The simulation results for the second truss were compiled for damage by 50% reduction in the cross-section area of the truss bars ($h_c = 5\ mm$). Figs. 6–9 show the changes of the first frequency ω_1 with the mass position on the top chord and the change of the differential operator ω_1'' for the Pratt truss. The figures show the changes for different groups of truss bars: Fig. 6: top chord (el. 1–10), Fig. 7: bottom chord (el. 11–18), Fig. 8: diagonal bars (el. 19–28), Fig. 9: posts (el. 29–37). In the figures with the operator, an increased value near the damaged element was shown. The most significant changes for this truss were observed for the bottom chord (Fig. 7b). For all bars near the supports and the centre of the truss, the changes were hardly visible.

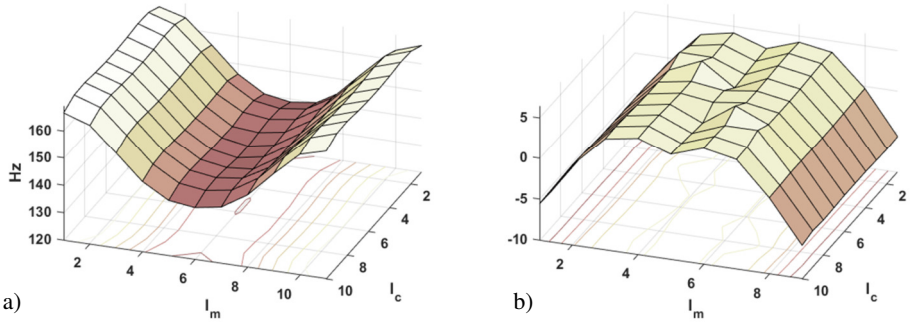

Fig. 6. The mass in the nodes of the top chord, damage in the bars of the top chord (el. 1–10) of the Pratt truss: a) change ω_l b) change ω_l''

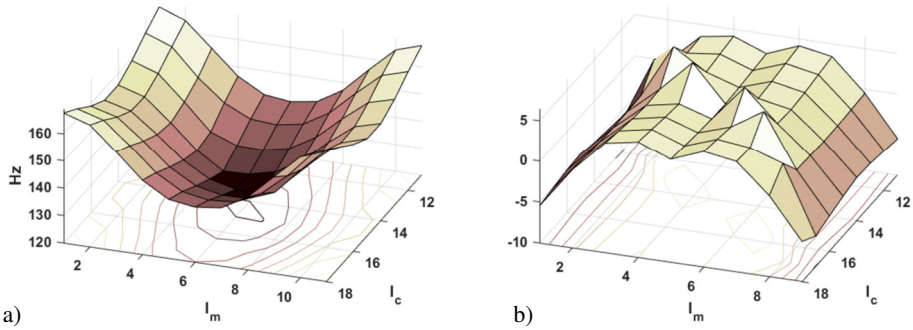

Fig. 7. The mass in the nodes of the top chord, damage in the bars of the bottom chord (el. 11–18) of the Pratt truss: a) change ω_l b) change ω_l''

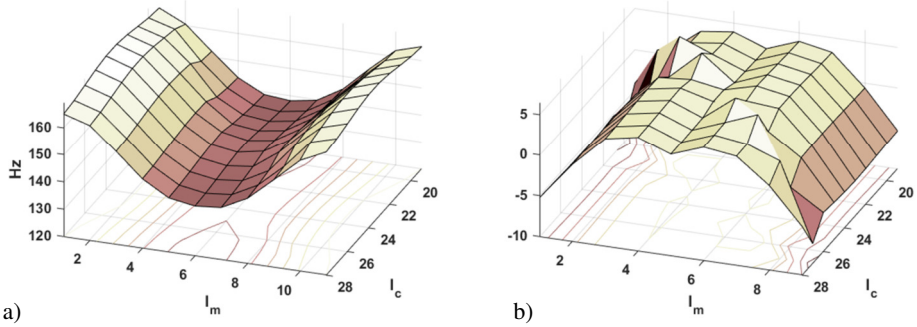

Fig. 8. The mass in the nodes of the top chord, damage in the diagonal bars (el. 19–28) of the Pratt truss: a) change ω_l b) change ω_l''

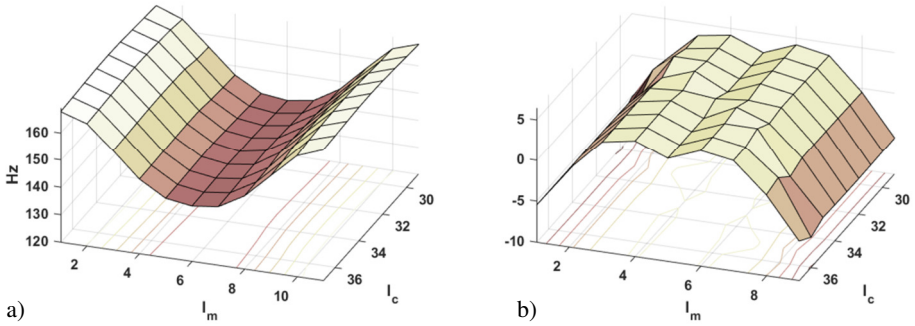

Fig. 9. The mass in the nodes of the top chord, damage in the posts (el. 29–37) of the Pratt truss: a) change ω_1 b) change ω_1''

Fig. 10 shows the impact of the damage h_c (*1 mm - 8 mm*) for both trusses in element no. 14 in the bottom chord on the value of the operator ω_1''. The figures show significant changes in the damage area as the damage increases.

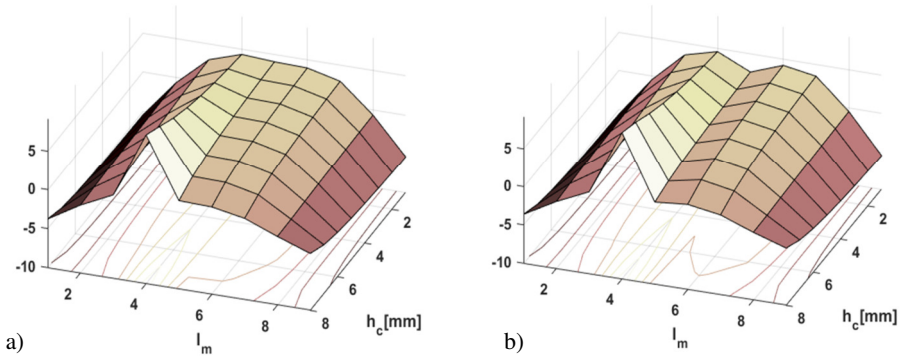

Fig. 10. The mass in the nodes of the top chord, damage in the bottom chord element no. 14, change ω_1'': a) Warren truss b) Pratt truss

Next Fig. 11 shows the impact of the damage h_c (*1 mm - 8 mm*) for both trusses in element no. 4 in the top chord on the value of the operator ω_1''. The figures show, as previously, significant changes in the damage area as the damage increases. For Warren truss (Fig. 11a) the changes were hardly visible.

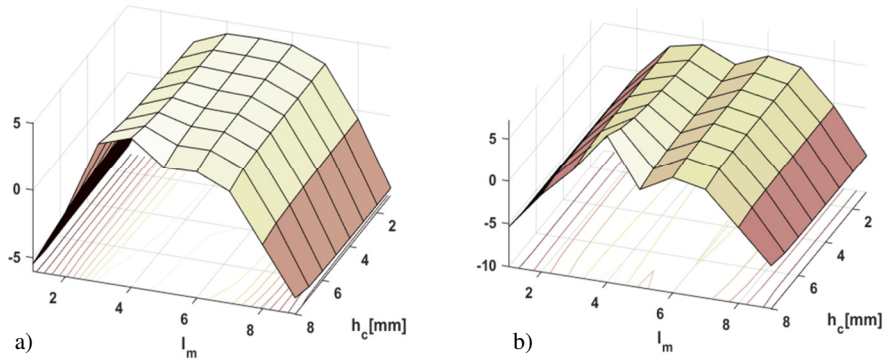

Fig. 11. The mass in the nodes of the top chord, damage in the top chord element no. 4, change ω_l'': a) Warren truss b) Pratt truss

4. Summary

The presented preliminary results of the application of the method based on the change of the natural frequency caused by moving mass allow damage localization in most truss bars. The main advantage of the presented approach is the possibility of damage localization without a reference model. A second-order differential operator was used in the work to analyse changes in natural frequencies. Hovewer, the damage was not detected in all truss elements and not for all damage sizes. In order to improve the presented method, a damage index independent of the reference model is expected in further research.

References

[1] Doebling S.W., Farrar C.R., Prime M.B., Shevitz D.W.: Damage Identification and Health Monitoring of Structural and Mechanical Systems From Changes in Their Vibration Characteristics: A Literature Review, Los Alamos National Laboratory Report LA-13070-MS, 1996.

[2] Pandey A., Biswas M., Samman M.: Damage detection from changes in curvature mode shapes. Journal of Sound and Vibration, no. 145, 1991, pp. 321–332.

[3] Dems K., Mróz Z.: Identification of damage in beam and plate structures using parameter-dependent frequency changes, Engineering Computations, 18(1/2), 2001, pp. 96–120.

[4] Zhong S., Oyadiji O., Ding K.: Response-only method for damage detection of beam-like structures using high accuracy frequencies with auxiliary mass spatial probing, Journal of Sound and Vibration, Volume 311, Issues 3–5, 2008, pp. 1075–1099.

[5] Zhong S., Oyadiji O.: Analytical predictions of natural frequencies of cracked simply supported beams with a stationary roving mass, Journal of Sound and Vibration, Volume 311, Issues 1–2, 2008, pp. 328–352.

[6] Zhang Y., Wang L., Lie S. T, Xiang Z.: Damage detection in plates structures based on frequency shift surface curvature, Journal of Sound and Vibration 332, 2013, pp. 6665–6684.

[7] Borowiec A., Ziemiański L.: Ocena stanu konstrukcji belkowych na podstawie zmiany parametrów modalnych wywołanych dodatkową masą, Zeszyty Naukowe Politechniki Rzeszowskiej, Mechanika vol. 74, 2008, pp. 9–16.

[8] Chang K.-C., Kim C.-W.: Modal-parameter identification and vibration-based damage detection of a damaged steel truss bridge, Engineering Structures, vol. 122, 2016, pp. 156–173.

[9] Siriwardane S.C, Vibration measurement-based simple technique for damage detection of truss bridges: A case study, Case Studies in Engineering Failure Analysis, vol. 4, 2015, pp. 50–58.

Przesłano do redakcji: 29.09.2018 r.
Przyjęto do druku: 30.09.2018 r.

Additional information

1. The Journal annually publishes a list of reviewers: in the last issue of the quarterly - vol. 65 (4/18) and on the website:
   www.oficyna.prz.edu.pl/pl/zeszyty-naukowe/czasopismo-inzynierii-ladowej-s/
2. The journal uses as described on its website the procedure for reviewing:
   www.oficyna.prz.edu.pl/zasady-recenzowania/
3. Information for authors available at:
   www. oficyna.prz.edu.pl/informacje-dla-autorów/
4. Review's form available at:
   www.oficyna.prz.edu.pl/pl/zeszyty-naukowe/czasopismo-inzynierii-ladowej-s/
5. Instruction for Authors, which describes in detail the structure of the article, its layout, the way of preparing illustrative material and the literature is published on the website:
   www.oficyna.prz.edu.pl/pl/instrukcja-dla-autorów/
   and
   www.oficyna.prz.edu.pl/pl/zeszyty-naukowe/czasopismo-inzynierii-ladowej-s/
6. Contact details to Editorial Office, postal and e-mail addresses for sending articles and contact details to the publisher are provided on the website:
   www.oficyna.prz.edu.pl/pl/zeszyty-naukowe/czasopismo-inzynierii-ladowej-s/

Reviewing standards, information for authors, the review form, instruction for authors and contact details to JCEEA Editors and to Publishing House are also published in the fourth number of JCEEA vol. 65 (4/18).

Circulation 120 copies. Publisher's sheet 8,46. Printer's sheet 8,50
Manuscript completed in September 2018, Printed in Decemeber 2018
Printing Publishing House, 12 Powstańców Warszawy Ave., 35-959 Rzeszow
Order no. 125/18